7-12-2010

Late Holocene Climate Variability From Northern Gulf of Mexico Sediments: Merging Inorganic and Molecular Organic Geochemical Proxies

Julie N. Richey
University of South Florida

Late Holocene Climate Variability From Northern Gulf of Mexico Sediments: Merging Inorganic and Molecular Organic Geochemical Proxies

by

Julie N. Richey

A dissertation submitted in partial fulfillment
of the requirements for the degree of
Doctor of Philosophy
College of Marine Science
University of South Florida

Co-Major Professor: Benjamin P. Flower, Ph.D.
Co-Major Professor: David J. Hollander, Ph.D.
Terrence M. Quinn, Ph.D.
Richard Z. Poore, Ph.D.
David W. Hastings, Ph.D.

Date of Approval:
July 12, 2010

Keywords: little ice age, medieval warm period, foraminifera, climate change, holocene

Table of Contents

List of Tables

List of Figures

Late Holocene Climate Variability From Northern Gulf of Mexico Sediments: Merging Inorganic and Molecular Organic Geochemical Proxies

Julie N. Richey

ABSTRACT

Accurate reconstruction of natural climate variability over the past millennium is critical for predicting responses to future climate change. In order to improve on current understanding of climate variability in the sub-tropical North Atlantic region over the past millennium, a rigorous study of Gulf of Mexico (GOM) sea surface temperature (SST) variability was conducted using both inorganic (foraminiferal Mg/Ca) and molecular organic (TEX_{86}) geochemical proxies. In addition to generating multiple high-resolution climate records, the uncertainties of the SST proxies are rigorously assessed.

There are 3 major research questions addressed: (1) What was the magnitude of GOM SST variability during the past 1,000 years, particularly during large-scale climate events such as the Little Ice Age (LIA) and the Medieval Warm Period (MWP). (2) Is the SST signal reproducible within the same sediment core, among different northern GOM basins, and using different geochemical SST proxies? (3) What are the ecological controls on the paleothermometers used to reconstruct SST variability in the GOM? Can differences in the ecology (i.e. seasonal distribution, depth habitat, etc.) of distinct paleothermometers be exploited to gain insight into changes in upper water column structure or seasonality in the GOM during the LIA and MWP?

The major findings include: (1) The magnitude of temperature variability in the GOM over the past millennium is much larger than that estimated from Northern Hemisphere temperature reconstructions. The MWP (1400-900 yrs BP) was characterized by SSTs in the GOM that were similar to the modern SST, while the LIA (400-150 yrs BP) was marked by a series of multidecadal intervals that were 2-2.5ºC cooler than modern. (2) This LIA cooling was replicated in the Mg/Ca-SST records from three different well-dated northern GOM basins (Pigmy, Garrison and Fisk Basins), as well as in two different geochemical proxies. (3) It is determined that foraminiferal test size has a significant effect on shell geochemistry. Using core-top calibration, discrepancies in the seasonal/depth habitats between different planktonic Foraminifera, and between Foraminifera and Crenarchaeota are inferred. Downcore differences are used to make inferences about changes in GOM mixed layer depth and seasonality over the past millennium.

Chapter 1

Introduction

1.1. Introductory Remarks

Global Climate Change is one of the most important problems that we face as a society today. The warming of the planet due to the increased anthropogenic input of greenhouse gasses may have large implications for the global hydrologic cycle, ocean circulation, global food production, disease and biodiversity. The Intergovernmental Panel on Climate Change (IPCC) states that global temperature increased by 0.6ºC over the course of the 20th century, and models of 21st century warming predict from 0.6ºC to 4.0ºC warming over the next century, depending on greenhouse gas emissions scenarios (IPCC, 2001). In order for the scientific community to more accurately predict the future response of Earth's climate system to anthropogenic forcing, we must improve our understanding of natural (pre-industrial) climate variability.

A reliable instrumental record of climate variability only extends back to $1850_{A.D.}$ (Jones et al., 1999), and thus proxy-based reconstructions must be relied upon to investigate climate variability further into the past. Studying the past 1,000 years of climate variability allows paleoclimatologists to explore natural modes of variability without having to account for major changes in background state (i.e. global ice volume, orbital-scale insolation changes, or tectonic-scale changes). There were also significant

hemispheric-to-global scale events such as the Little Ice Age (LIA) and the Medieval Warm Period (MWP) that occurred during the past millennium. These events act as benchmarks for determining the magnitude of natural climatic shifts during the late Holocene. A number of global and hemispheric surface temperature reconstructions covering the past millennium have been generated by merging proxy records from tree-rings, boreholes, ice cores, corals, speleothems, and sediment cores (e.g. Mann et al., 1999; Mann and Jones, 2003; Esper et al., 2002; Moberg et al., 2005), however there is still a large degree of uncertainty in these reconstructions.

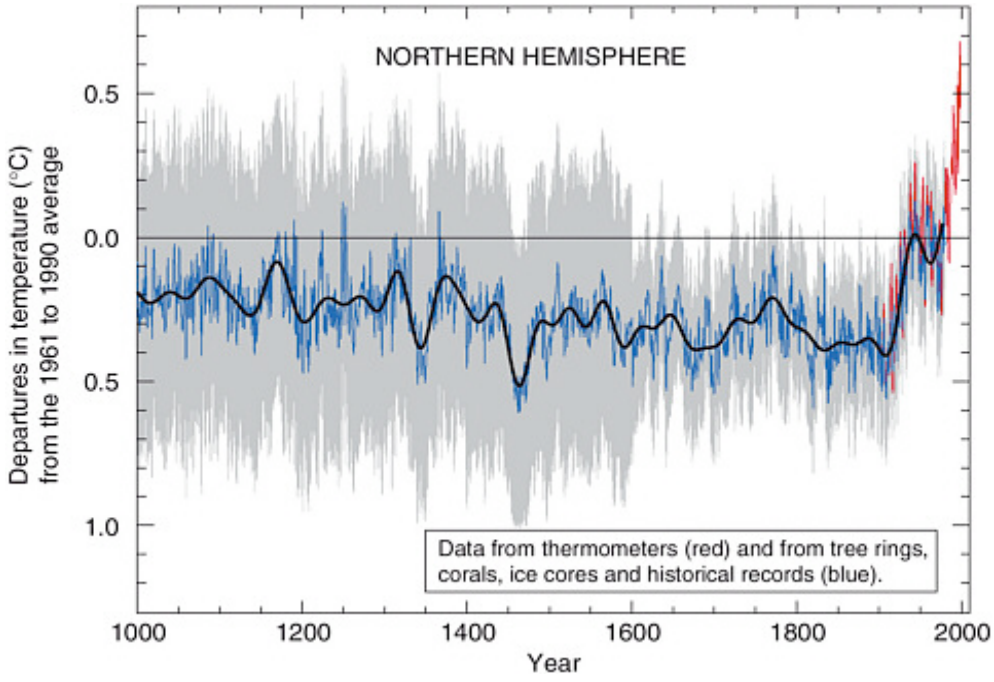

Figure 1.1. Multiproxy reconstruction of Northern Hemisphere surface temperature variations over the past millennium. Temperature reconstruction (blue), along with 50-year average (black), a measure of the statistical uncertainty associated with the reconstruction (gray), and instrumental surface temperature data for the last 150 years (red), based on the work by Mann et al. (1999).

One major source of uncertainty in large-scale climate reconstructions is sparse spatial and temporal coverage. The further back in time you go, the fewer records there

are. Many of the climate proxy records, especially ones based on archives such as corals and tree-rings, involve splicing together a succession of shorter (<200-years) time-series. The further back in time you go, the more difficult it is to find fossil archives. A second source of uncertainty is the dearth in spatial coverage. The existing large-scale climate reconstructions are primarily based on extra-tropical terrestrial records, with very few records representing the low latitudes and/or the marine environment.

The third source of uncertainty in global climate reconstructions stems from the uncertainties in the individual proxy records. Many of the climate archives are based on geochemical or biometric measurements on living and/or fossil organisms (e.g. trees, corals, Foraminifera, etc.), and the assumption is made that these organisms are passive records of their environmental conditions. The interpretation of an environmental signal in biogenic proxies can be complicated by "vital effects", which are often species-specific, and affect the geochemistry in a way that is unrelated to the climate signal contained within the geochemistry. Also, biogenic proxies may be changing their ecologies in response to changing environmental conditions, which can lead to large uncertainties in the interpretation of their climate records.

In this dissertation I addressed each of these sources of uncertainty in our collective understanding of global climate change over the past 1,000 years. First, I generated decadal-resolution sea surface temperature (SST) records from three different sites in the Gulf of Mexico. Globally, there are very few (<10) published continuous, decadal-resolution records of SST variability covering the past millennium (Figure 1.2). Improving the spatial coverage of records of ocean surface conditions during this

important time interval is essential to improving our understanding of both regional and global patterns of climate variability.

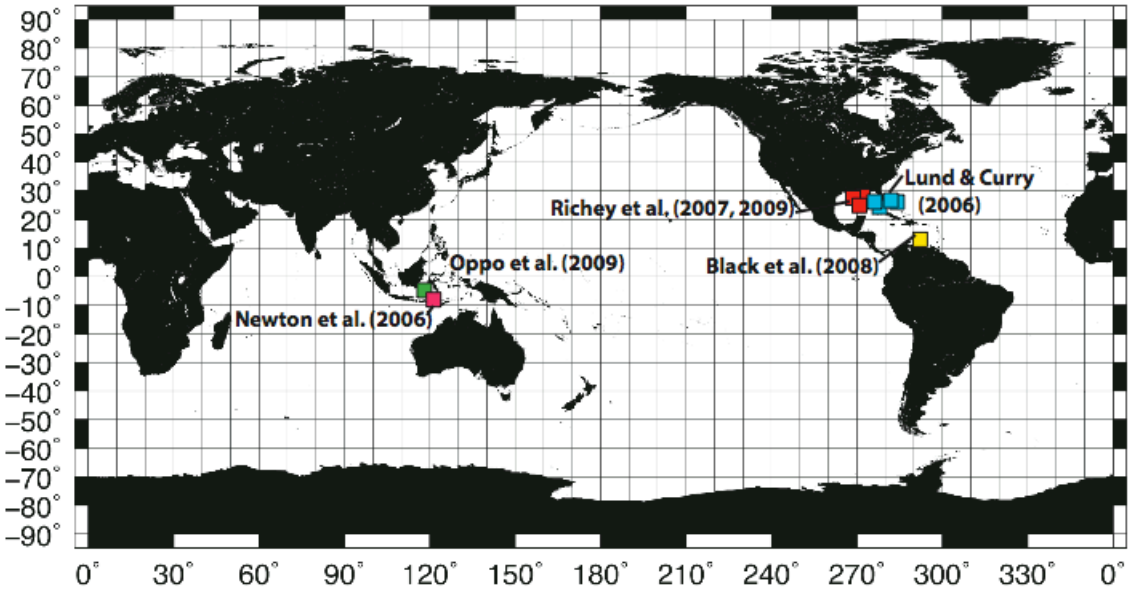

Figure 1.2. Map of sites for which there are currently published, decadal-resolution SST proxy records covering at least the past 1,000 years. Pink and green markers indicate planktonic foraminiferal Mg/Ca-SST records from the Makassar Straits (Newton et al., 2006; Oppo et al., 2009). Yellow marker indicates a Cariaco Basin planktonic foraminiferal Mg/Ca-SST record from Black et al. (2007). The blue markers indicate planktonic foraminiferal Mg/Ca-SST records from the Great Bahamas Bank and the Dry Tortugas (Lund and Curry, 2006). The red markers indicate the 3 planktonic foraminiferal Mg/Ca-SST and the TEX_{86}-SST records from the Gulf of Mexico that were generated as part of this dissertation, and published in Richey et al. (2007 and 2009)

The issue of uncertainty in SST proxy records is addressed in this dissertation in a number of ways. First, I test the reproducibility of the foraminiferal Mg/Ca-SST proxy by replicating Mg/Ca-SST records in multiple species of planktonic Foraminifera within the same sediment core. Second, I compare Mg/Ca-SST records generated from three different sites within the same region. Third, I use a multi-proxy approach, comparing SST reconstructions based on an inorganic geochemical proxy (elemental ratios in planktonic Foraminifera) and molecular organic geochemical proxy (TEX_{86} index). Finally, I rigorously assess the ecological controls on the different paleothermometers

(e.g. different species of planktonic Foraminifera and marine Crenarchaeota), thus improving our ability to interpret depth range and seasonality of the SST signal derived from each individual record.

1.2. The Little Ice Age

The Little Ice Age was a cool interval beginning roughly $1500_{A.D.}$ and lasting until $1850_{A.D.}$ that has been well documented in historical records from northern Europe and eastern North America. Anecdotal evidence, including a centuries-long theme of winter paintings in Europe, unprecedented advances of mountain glaciers upon alpine villages, and sharp increases in the price of grains due to crop failure, were all indications of extraordinarily cold winters during the 17^{th} and 18^{th} centuries. Although the most dramatic impacts of the LIA seem to be confined to the Northern Hemisphere, the LIA has been identified as a significant event in a number of tropical and Southern Hemisphere climate records. Evidence is beginning to support the idea that the LIA was a nearly global phenomenon, however the timing and magnitude of cooling varied significantly among difference regions.

In many cases, solar variability has been invoked to explain the cooling experienced during the LIA. The changes in incoming solar radiation due to changes in orbital parameters (i.e. precession of the equinoxes, eccentricity of the Earth's orbit, and tilt of the Earth's axis) were minimal over the past millennium, and thus cannot be invoked to explain the LIA cooling. The amount of solar radiation emitted by the sun does vary on shorter timescales, and has to do with the occurrence of sunspots, bright faculae, and other solar phenomena. Measurements of solar variability over the last two

11-year sunspot cycles estimate that the total solar irradiance varied by only 0.1% (Fröhlich and Lean, 2004).

The production of cosmogenic nuclides (e.g. ^{14}C and ^{10}Be) varies primarily as a function of solar activity, and thus the ^{14}C and ^{10}Be records can be used as proxies for solar variability in the late Holocene (Bard et al., 1997) (Figure 1.3). From the ^{14}C and ^{10}Be records (as well and historical sunspot counts), quasi-periodic cycles have been identified in the record of solar irradiance. For example, there is an 11-year sunspot cycle, and a 200-year cycle called the Suess Cycle. Recent minima in the Suess Cycle of solar variability: the Oort (ca. 1100 $_{A.D.}$), Wolf (ca. $1300_{A.D.}$), Spörer (ca. $1500_{A.D.}$), and Maunder (ca. $1700_{A.D.}$) minima, have been correlated with episodes of glacial advance and cooling associated with the LIA.

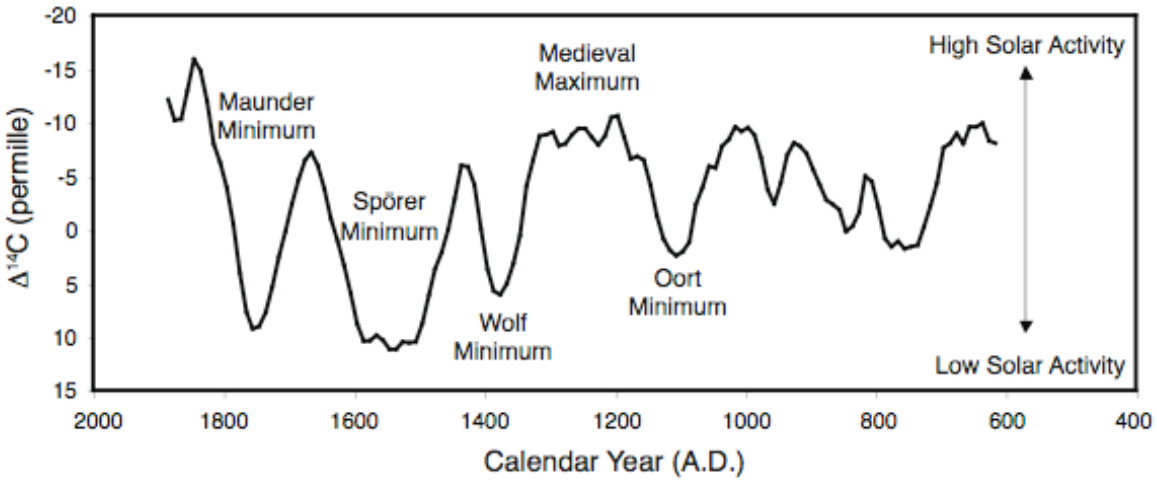

Figure 1.3. Solar Activity Record for the last 1,600 years. A decadally-averaged plot of the $\Delta^{14}C$ record is plotted for the past 1,600 years (Stuiver et al., 1998). Note that the y-axis is inverted, and increasing ^{14}C production indicated decreased solar activity.

The correlation of these strong solar minima with cooling events during the LIA is highly suggestive of a solar forcing for the LIA. However, the total reduction in solar irradiance during the Maunder Minimum was <0.6%, which is equivalent to a forcing of

~0.7 watts per square meter (W/m^2) (Bard et al., 2000). This forcing is two orders of magnitude smaller than the solar forcing associated with changes in orbital parameters and glacial-interglacial climate variability. Thus it is not likely that solar forcing alone caused the dramatic climate response during the LIA.

It has been proposed that volcanic forcing may have been an important factor in LIA cooling (Crowley, 2008). Volcanic eruptions add large amounts of ash and sulfur gasses to the atmosphere, diminishing the amount of solar radiation reaching the surface, thus causing the Earth to cool. The degree of radiative forcing from a volcanic eruption depends on the magnitude and location, as well as the composition of the ejecta (Robock, 2000).

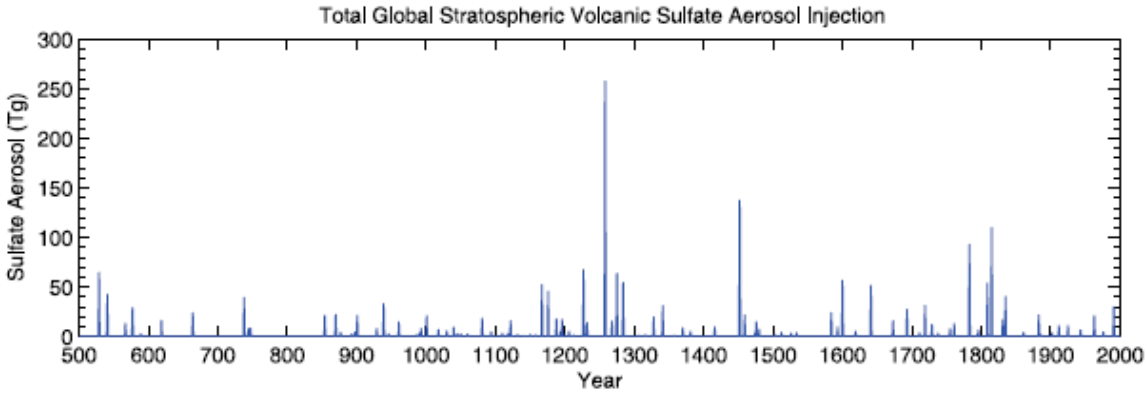

Figure 1.4. Ice core estimates of global stratospheric sulfate loading from volcanoes (A.D. 500–2000). (from Gao et al., 2008)

For example, sulfate aerosols from tropical volcanic eruptions are transported globally by high-altitude winds, thus causing widespread cooling. High latitude eruptions tend to be more spatially restricted, and have less effect on global temperature. Ejecta composed of large volcanic ash particles settles quickly, and only causes regional cooling that lasts from a few days to a few weeks. Explosive eruptions release sulfur gasses, which

combine with water vapor to form sulfate aerosols. In large eruptions, these sulfate aerosols are injected high into the atmosphere, where they can remain for years, having a longer-term cooling effect. Figure 1.4 illustrates a proxy record of sulfate loading from volcanic eruptions, reconstructed from ice cores. It appears that there were 3 pulses of unusually high volcanic activity between the 14th and 19th centuries, which may have contributed to observed LIA cooling.

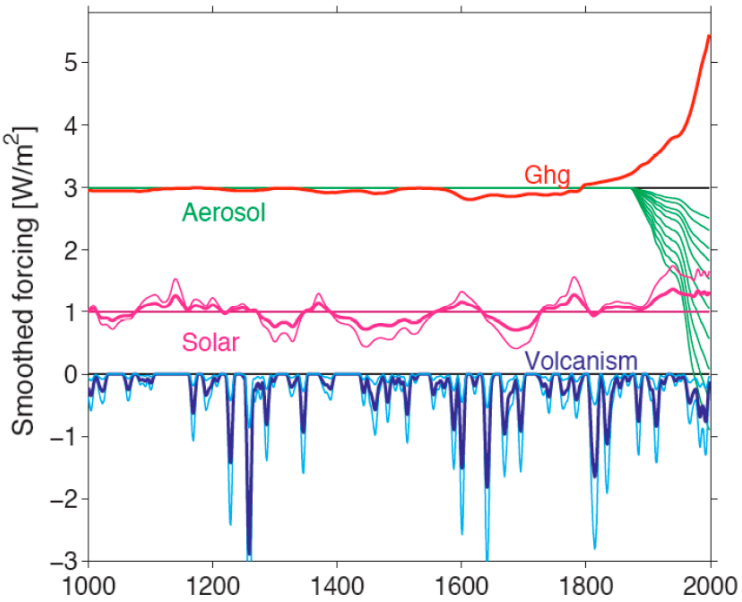

Figure 1.5. Northern Hemisphere Mean Radiative Forcing. Hegerl et al. (2006) estimate radiative forcing due to greenhouse gasses (Ghg), tropospheric aerosols, solar variability and volcanism over the past 1,000 years.

Although solar variability is often cited as the primary forcing mechanism for LIA cooling, volcanism must also be considered as a potential agent for the LIA. Hegerl et al. (2003) did a comprehensive test of this issue and found volcanism to be substantially more important than solar variability, explaining 40% of the cooling during the LIA. There has been some suggestion that the LIA and MWP were not forced by external

factors like solar variability or volcanism, but by a millennial-scale internal oscillation. Broecker (2001) hypothesized that the MWP to LIA transition was the penultimate cycle in a series of quasi-periodic oscillations called "Bond Cycles", with a periodicity of roughly 1500 years (Bond, 1997). Another potential mechanism for LIA cooling may have been a slow-down in the thermohaline circulation. Lund et al. (2006) found proxy evidence for a substantial decrease in the flow through the Florida Straits from 1200-1850_{AD}, suggesting a reduction in Gulf Stream transport during that time. A reduction in reduction in heat transport to northern Europe via the Gulf Stream may have contributed to observed LIA cooling.

1.3. The Medieval Warm Period

The so-called Medieval Warm Period (MWP) was much more heterogeneous than the LIA, but is generally described as a warm interval preceding the LIA (ca. 1000-1300_{AD}) in which global temperatures were similar to the 20^{th} century (Crowley and Lowery, 2000). A network of borehole temperature estimates suggests that global temperatures from 500-1000_{AD} were warmer than 20^{th} century temperatures (Huang et al., 1997), while large-scale climate reconstructions vary significantly in their portrayal of the MWP (e.g. Mann et al., 1999 versus Esper et al., 2002). The MWP is often used as a benchmark for pre-industrial warming, and is compared to the 20^{th} century to make arguments for whether today's warming is caused by natural climate variability, or anthropogenic input of greenhouse gasses. For this reason it is important to improve upon our understanding of the spatial and temporal patterns of climate variability during this time interval.

Evidence for the MWP is found throughout the globe, but it doesn't manifest exclusively as a warming event (for this reason, many studies now refer to this time interval as the "Medieval Climate Anomaly"). In the tropics and sub-tropics there seems to be a large hydrologic response during the MWP. Droughts in the Yucatan associated with the MWP have been connected to the termination of the Classical Mayan Civilization (Hodell et al., 2005), while unprecedented warmth allowed the Vikings to sustain successful agricultural-based settlements in Greenland. The North American Monsoon was weakened during the MWP (900-1300$_{AD}$) causing widespread drought conditions in western North America (Cook et al., 2004) (Figure 1.6). A reconstruction of Atlantic tropical cyclone activity suggests that the MWP was a time of more frequent tropical cyclones, with tropical cyclone counts similar to the 20th century (Mann et al., 2009).

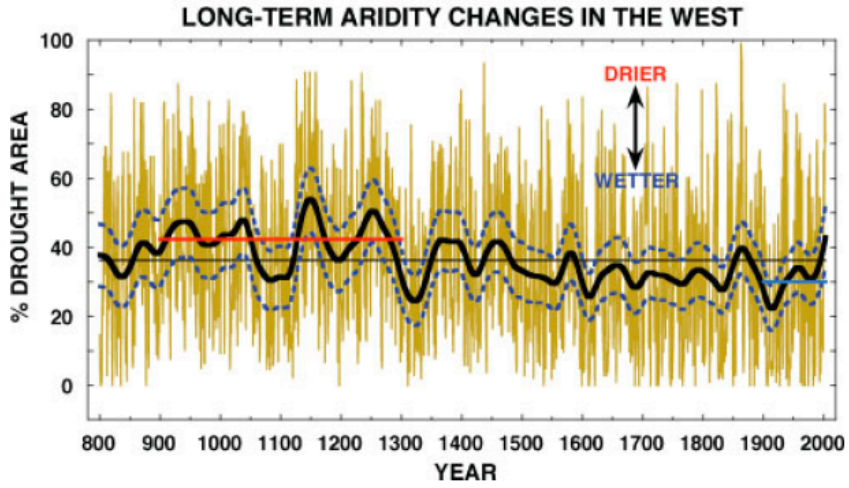

Figure 1.6. Long-term aridity changes in the Western United States. The figure shows the Drought Area Index (DAI) for the Western U.S. as reconstructed by tree rings, both annual in pale brown and 60-year low-pass filtered in black. The red and blue lines are mean DAI for the MWP (ca. 900–1300$_{AD}$) and the 20th century out to 2003, respectively. This record shows that the MWP was much more arid on average than the 20th century. Figure from Cook et al. (2010).

1.4. Reconstructing SST over the past 2,000 years

Understanding how ocean surface temperatures have varied over the past 2,000 years is critical for data-model comparisons, and accurate prediction of future climate change. Nevertheless, paleoceanographers have traditionally neglected this important time interval. There are a number of factors that make obtaining high-resolution SST records from the late Holocene difficult. Sedimentation rates are much too low in most marine depositional environments to resolve the past 2,000 years of climate variability. Marine environments with sedimentation rates high enough to resolve decadal-to-centennial scale variability (i.e. >40cm/kyr) are limited to coastal margins near major river systems, drift sites, etc. Secondly, temperature variability during the late Holocene is subtle relative to the glacial-interglacial shifts that paleoceanographers generally reconstruct. Attempting to resolve the small (<2ºC) temperature shifts of the most recent millennia is pushing the limits of existing SST proxies. In this section I will outline the advantages and limitations of existing geochemical proxies for reconstructing SST in the late Holocene.

1.4.1. Molecular Organic Proxies

With the development of new HPLC-MS (High Performance Liquid Chromatography-Mass Spectrometry) techniques (Hopmans et al., 2000) as well as techniques for compound-specific radiocarbon dating (see Eglinton and Eglinton, 2008 for a review), the field of molecular organic geochemistry is rapidly expanding in the realm of paleo-SST reconstruction. The HPLC-MS allows geochemists to easily identify, quantify and isolate large polar compounds, which cannot be effectively analyzed via

traditional gas chromatographic (GC) techniques. This has led to the recent development of a new paleothermometer, the TEX_{86} index, which is based on relative abundances of large 86-carbon polar lipids derived from marine Crenarchaeota. Compound-specific radiocarbon dating has allowed for the independent dating of molecular components of sediments, thus enabling paleoceanographers to identify discrepancies in source region as well as age offsets between organic geochemical and foraminiferal-based paleoceanographic records.

Presently there are two widely accepted molecular organic SST proxies: the TEX_{86} index and the $U_k'^{37}$ index. The TEX_{86} index is a paleothermometer based on the composition of membrane lipids called glycerol dialkyl glycerol tetraethers (GDGTs) found in marine Crenarchaeota. Schouten et al. (2002) discovered that the number of cyclopentane moieties on these GDGTs in sedimentary membrane lipids varies as a function of local mean annual SST. It is thought that Crenarchaeota adjust the number of cyclopentane moieties in these GDGT lipids with temperature to regulate membrane fluidity. The latest calibration of Kim et al. (2008), which uses a much more extensive network of core-top samples, confirms that TEX_{86} correlates with mean annual SST, globally (Figure 1.7). The $U_k'^{37}$ index is based on the ratio of di- to tri-unsaturated alkenones (Brassell et al., 1986; Prahl and Wakeham, 1987), which are 37-carbon compounds produced as membrane lipids by haptophyte algae (coccolithophorids). The index varies between 0 and 1, which corresponds to a temperature range of 0-26ºC, and is generally considered to represent mean annual SST.

Both the GDGT and alkenone lipids are contained within the fine fraction of sediments, and thus are subject to lateral transport, sometimes over large distances. The

development of compound specific radiocarbon dating has allowed for the investigation of the origin of specific molecular components of sediment. The techniques for this involve isolating individual compounds using bench chemistry, preparative capillary gas chromatography (PCGC), or preparative HPLC. Alkenones can be isolated for radiocarbon dating using a series of Si-gel columns, according to the techniques outlined in Ohkouchi et al. (2005). GDGTs have been isolated for radiocarbon dating using preparative HPLC (Shah et al., 2008). Results of radiocarbon dating of these two compound classes suggest that they have different labilities. In other words, alkenones are relatively refractory, and can survive lateral transport over long distances (Englebrecht and Sachs, 2005). GDGTs, on the other hand, are relatively labile, and do not effectively survive transport (Mollenhauer et al., 2007; Shah et al., 2008). The implications are that in some locations, the $U_k'^{37}$ signal may be neither local, nor contemporaneous with the foraminiferal record. The TEX_{86} signal, on the other hand, is much more likely to contain the signal of overlying waters, and have minimal age offset from the foraminiferal record.

The TEX_{86} proxy has both advantages and disadvantages over the $U_k'^{37}$ and foraminiferal Mg/Ca proxies. Culture studies suggest that unlike alkenones, the composition of GDGTs does not seem to be effected by crenarchaeal growth rate (Wuchter et al., 2004). The same study tests the effect of salinity on TEX_{86}, and concludes that salinity has no influence on GDGT composition, while recent studies suggest a considerable salinity effect on Mg/Ca (e.g. Ferguson et al., 2008). TEX_{86} is calibrated over a larger range of SSTs, and has been found to be an effective SST proxy in both the arctic (Sluijs et al., 2009) and the tropics (Tierney et al., 2008). TEX_{86} has

even been used to make estimates of SST as far back as the Cretaceous (Jenkyns et al., 2004). Alkenones, on the other hand are not an effective SST proxy at SSTs greater than 27ºC (Pelejero and Calvo, 2003), as concentrations of tri-unsaturated alkenone drop below detection levels.

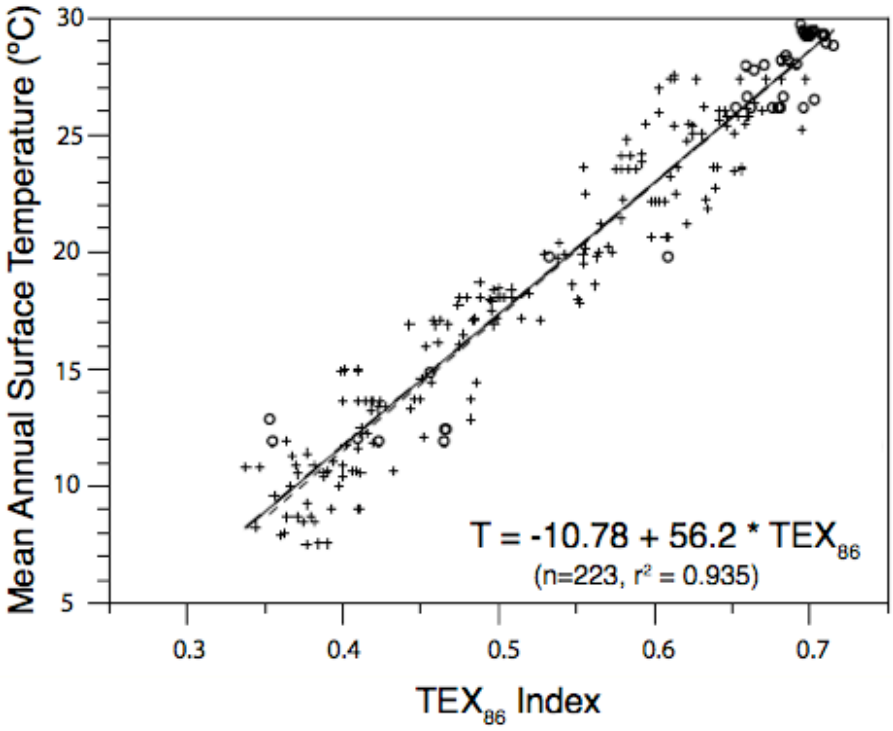

Figure 1.7. Global Core-top calibration of TEX_{86} to SST. The TEX_{86} index from 223 core-top samples, distributed globally, is calibrated to corresponding mean annual SST. Open circles represent Pacific and Indian Ocean sites, while crosses represent Atlantic Ocean sites. This results in the following equation: $SST(ºC)=-10.78 + 56.2*TEX_{86}$ from (Kim et al., 2008).

Investigating the limitations of the TEX_{86} proxy is currently an area of active research in the organic geochemistry community. One issue is the ubiquitous nature of Crenarchaeota in the marine environment. Although the TEX_{86} signal consistently reflects mean annual SSTs, live crenarchaeal communities are living and producing GDGTs throughout the water column (Karner et al., 2001), and within sub-surface

sediments (Lipp et al., 2008). There is also the issue of terrestrial GDGTs. Branched GDGTs are produced by soil bacteria, and are abundant in terrestrial organic matter (TOM). In marine depositional basins proximal to major sources of terrestrial input, the TEX_{86} could be biased by terrestrially derived GDGTs. The BIT index (branched to isoprenoid tetraether index) was developed by Hopmans et al. (2004), and is used as a proxy for TOM input. Samples with BIT values greater than 0.3 are considered suspect for bias in the TEX_{86} record (Weijers et al., 2006).

1.4.2. Foraminiferal-based proxies

The use of the stable oxygen isotope composition of planktonic Foraminifera to reconstruct paleotemperatures was pioneered in the mid-20th century by Urey (1947) and Emiliani (1954, 1955). Now the $\delta^{18}O$ of planktonic foraminifera is one of the most commonly used paleoceanographic tools (see Lea, 2003 for a review). However, the $\delta^{18}O$ of foraminiferal calcite is controlled not only by calcification temperature, but also by the oxygen isotopic composition of ambient seawater. Beginning in the mid-1990's, paleoceanographers began to use the Mg/Ca ratio of foraminiferal calcite as an SST proxy (e.g. Nürnberg et al., 1996; Rosenthal et al., 1997; Hastings et al., 1998; Lea et al., 1999; Elderfield and Ganssen, 2000). The use of Mg/Ca as an SST proxy is based on the fact that Mg^{2+} substitutes for Ca^{2+} in the calcite lattice, with an exponential temperature dependence. The exact Mg/Ca-SST calibration varies slightly among different species of Foraminifera, but general equates to a ~9% increase in Mg/Ca per 1ºC in water temperature (Anand et al., 2003).

Paired Mg/Ca and $\delta^{18}O$ measurements can be used to derive records of both temperature and the oxygen isotopic composition of seawater (Figure 1.8) if the assumption is made that the Mg/Ca of foraminiferal calcite is controlled exclusively by temperature (see discussion of caveats below). Then, changes in $\delta^{18}O$ of seawater can then be interpreted in terms of salinity variability. Thus a major advantage of paired Mg/Ca and $\delta^{18}O$ measurements on Foraminifera is the ability to generate a record of SST and salinity variability from a single archive. A number of studies over the past decade have suggested that there are additional physical parameters that can affect foraminiferal Mg/Ca, thus complicating interpretation of Mg/Ca records strictly in terms of SST. Additionally, it has been shown that post-depositional diagenetic processes can have a large impact on the elemental composition of foraminiferal calcite.

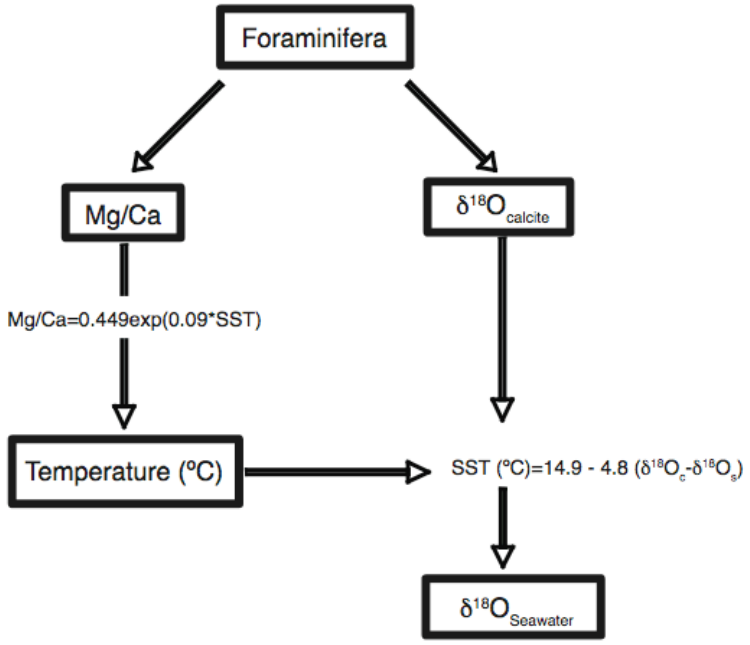

Figure 1.8. Flow Chart of Paired Mg/Ca and $\delta^{18}O$ for estimating SST and $\delta^{18}O$ of seawater. The equation for converting Mg/Ca to SST is the equation for white *G. ruber* (Anand et al., 2003). The $\delta^{18}O$ paleotemperature equation is from Bemis et al. (1998).

The Mg/Ca ratio in seawater is spatially constant and unlikely to change on timescales of less than 1 million years due to the very long residence times of both Mg and Ca in the oceans (Broecker and Peng, 1982). There are a few factors that complicate the use of Mg/Ca as a paleotemperature proxy, however. The post-mortem addition of diagenetic phases to foraminiferal calcite was recognized by Boyle (1983). Specifically, the addition of Mn-rich carbonate overgrowths (as well and Mn- and Fe-rich oxyhydroxides) has been a problem for trace metal analysis (Cd/Ca, Ba/Ca, etc.), because these phases also contain other elements that alter the original shell chemistry. One of these phases that has been demonstrated to dramatically effect shell Mg/Ca is the carbonate mineral kutnahorite. Pena et al. (2005) showed that the presence of this phase biased foraminiferal Mg/Ca to 7-36% higher values (equivalent to a 0.9-6.2ºC temperature bias). In order to remove these potentially problematic diagenetic carbonate phases, a reductive cleaning step is used (Barker et al., 2003). The reductive cleaning step can also preferentially remove Mg from the primary calcite, thus reducing shell Mg/Ca by up to 15% (Rosenthal et al., 2004). Precautions need to be taken to monitor elements associated with diagenetic alteration (i.e. Mn and Fe) when performing Mg/Ca analyses. Also, care must be taken when comparing Mg/Ca records in which different cleaning methods were used, as there may be systematic offsets in the temperature estimates due to cleaning.

Selective dissolution of high-Mg carbonate, as the foraminifera are affected by calcite-undersaturated deep waters and porewaters during sedimentation, can lead to alteration of the original Mg/Ca signal (e.g. Dekens et al., 2002). It has been noted in a number of studies that dissolution can lower foraminiferal Mg/Ca in sediments

(Rosenthal et al., 1993; Russell et al., 1994; Brown and Elderfield, 1996; Hastings et al., 1998). Waters are caustic to carbonates when the in situ concentration of carbonate ion is less than the saturation concentration of carbonate ion.

$$\text{i.e. } \Delta CO_3^{2-} = [\Delta CO_3^{2-}]_{\text{in situ}} - [\Delta CO_3^{2-}]_{\text{saturation}} \quad \text{(Berger et al., 1982)}$$

Calcite that is more enriched in Mg is more susceptible to dissolution, and high-Mg calcite can be susceptible to dissolution well above the lysocline (Brown and Elderfield, 1996). Factors that can affect the degree of dissolution include the water depth, the age of the deep waters, and the concentration of organic matter in sediments. Dekens et al. (2002) have provided a depth correction for the Mg/Ca paleotemperature calibration in the foraminifer, *Globigerinoides ruber* in order to correct for the dissolution effect on Mg/Ca.

Laboratory culture studies have shown additional physical parameters (e.g. pH, carbonate ion concentration and salinity of seawater) act as controls on Mg/Ca ratios in Foraminifera, but suggest that their influence is small in comparison with temperature (Lea et al., 1999; Nürnberg et al., 1996; Russell et al., 2004; Elderfield et al., 2006). In a laboratory culture study, Lea et al. (1999) looked at the effect of salinity on entire test Mg/Ca ratios, and found a small increase with salinity of 4±3% per psu in *Orbulina universa*. Another study of the final chambers of *Globigerinoides sacculifer* grown over a range of salinities (26-44 psu) showed increases of Mg/Ca of over 100% at higher salinity, or approximately 11% per psu (Nürnberg et al.,1996). A field study in the Mediterannean found a significant relationship between Mg/Ca and calcification salinity, in which Mg/Ca increased by 15-59% per psu (Ferguson et al., 2008). This study was conducted over a salinity range of 36-40 psu, which is significantly higher than most

open ocean settings, and may not be applicable at lower salinities.

Each of the caveats discussed in this section, for both molecular organic and foraminiferal geochemistry, are addressed in the dissertation as they are specifically related to my study sites in the Gulf of Mexico.

1.5. Dissertation Organization

This main body of this dissertation is organized into three chapters, which are written in the format of separate manuscripts for peer-reviewed journals. Figures are, for the most part, identical to those used in the publication manuscripts. Therefore there may be some redundancy with respect to certain data sets being plotted more than once. References from all 3 manuscripts are combined at the end of this dissertation.

In Chapter 2: Regionally Coherent Little Ice Age Cooling in the Atlantic Warm Pool

In this chapter I present two new Mg/Ca-SST records from the Fisk and Garrison Basins in the northern Gulf of Mexico. The aim of this study was to test the regional reproducibility of a Mg/Ca-SST record from the Pigmy Basin (GOM) that was published as part of my masters thesis (Richey et al., 2007). A large (~2ºC) cooling during the LIA was present in all three SST records, and comparison with other records within the Atlantic Warm Pool (AWP) suggest that this timing and magnitude of LIA cooling was consistent throughout the sub-tropical and tropical western Atlantic Ocean. Potential mechanisms for this regional cooling are proposed. This study was published in the journal, *Geophysical Research Letters*, in 2009:

Richey, J. N., R. Z. Poore, B. P. Flower, and T. M. Quinn, and D. J. Hollander (2009), Regionally coherent Little Ice Age cooling in the Atlantic Warm Pool, *Geophys. Res.Lett.,* 36, L21703, doi:10.1029/2009GL040445.

In Chapter 3: Merging late Holocene molecular Organic and Foraminiferal- Based Geochemical 2 Records of SST in the Gulf of Mexico

In this chapter I used a molecular organic geochemical approach (TEX_{86}) to generate an additional SST record from the Pigmy Basin, Gulf of Mexico. The TEX_{86}-SST record is remarkably similar to the Mg/Ca-SST from the same core, despite the fact that the two proxies are subject to separate diagenetic processes and are contained within different sediment fractions. The relative seasonal and depth distributions of the *Globigerinoides ruber* and marine Crenarchaeota are rigorously assessed for the northern Gulf of Mexico, and those relative differences are exploited to make inferences about changing mixed-layer depth and seasonality over the past 1,000 years. This study is currently under review at the journal, *Paleoceanography*:

Richey, J. N., D. J. Hollander, B. P. Flower and T. I. Eglinton (2010), Merging late Holocene molecular Organic and Foraminiferal- Based Geochemical 2 Records of SST in the Gulf of Mexico, *Paleoceanography*, in review.

In Chapter 4: Ecological controls on the shell geochemistry of pink and white *Globigerinoides ruber* in the northern Gulf of Mexico: Implications for paleoceanographic reconstruction

In this chapter I examine the relationship between foraminiferal test size and shell

geochemistry ($\delta^{13}C$, $\delta^{18}O$ and Mg/Ca) for the pink and white sub-species of *Globigerinoides ruber*. These data provide insights into ecological and metabolic controls on shell geochemistry, allowing for better constraints on paleoceanographic data. We conclude that there is a significant positive relationship between size and $\delta^{13}C$, which is most likely related to growth rate. A significant decrease in $\delta^{18}O$ and increase in Mg/Ca with size, suggests that larger individuals have higher calcification temperatures than smaller individuals. High-resolution down-core comparisons of Mg/Ca and $\delta^{18}O$ data for pink and white *G. ruber* are made in order to assess whether the two planktonic species have distinct seasonal distributions in the Gulf of Mexico. I conclude that the pink *G. ruber* signal is summer-weighted, while the white *G. ruber* signal represents mean annual surface conditions. The results of this study are being prepared for submission to the journal, *Marine Micropaleontology*.

Richey, J. N., R. Z. Poore, D. J. Hollander, and B. P. Flower, (2010), Ecological controls on the shell geochemistry of pink and white *Globigerinoides ruber* in the northern Gulf of Mexico: Implications for paleoceanographic reconstruction, *Marine Micropaleontology*, in preparation.

Chapter 2

Regionally Coherent Little Ice Age Cooling in the Atlantic Warm pool

2.1. Abstract

We present 2 new decadal-resolution foraminiferal Mg/Ca-SST records covering the past 6-8 centuries from the northern Gulf of Mexico (GOM). These records provide evidence for a Little Ice Age (LIA) cooling of 2-3ºC, consistent with a published Mg/Ca record from Pigmy Basin. Each of the GOM basins exhibits SST minima within the Dalton, Maunder and Spörer sunspot minima, with a general warming trend over the past 150 years. Comparison of these 3 records with existing SST proxy records from the GOM-Caribbean region show that the magnitude of LIA cooling in the Atlantic Warm Pool (AWP) was significantly larger than the mean hemispheric cooling of <1ºC. We propose that a reduction in the intensity and spatial extent of the AWP during the LIA, combined with associated changes in atmospheric circulation may account for the regional SST patterns observed in the GOM-Caribbean region during the LIA.

2.2. Introduction

Accurate reconstruction of high-resolution sea surface temperature (SST) records during time intervals of societal importance, such as the Little Ice Age (LIA), and through the 20th century, is important in determining the magnitude of pre-industrial climate variability. Given the uncertainties inherent to most SST proxies, as well as the influence of local climatology, replication of SST records is critical to understanding regional responses to climate forcings. The LIA generally spans the time interval from 1400-1850 AD, although the timing and magnitude of cooling varies widely throughout the Northern Hemisphere. Temperature reconstructions (primarily based on extratropical terrestrial proxy records) suggest that the Northern Hemisphere experienced modest cooling of 0.6-0.8ºC during the 15th-19th centuries (Mann et al., 1998, 1999; Esper et al., 2002, Moberg et al., 2005. Here we show that SST proxy records from the low-latitude North Atlantic Ocean experienced significantly larger cooling than the hemispheric average, and may be have been particularly sensitive to climate perturbations on multi-decadal to centennial timescales during the LIA.

The Atlantic Warm Pool (AWP), defined by the >28.5ºC SST isotherm, develops annually in the northern Caribbean during early summer (June) and expands into the GOM and western tropical North Atlantic through the late summer (July-October) (cf. Wang et al., 2008a). Multidecadal variability in the size of the AWP is correlated with rainfall anomalies in the Caribbean region, formation and intensification of North Atlantic hurricanes, and variability in moisture transport to the North American continent via interactions with atmospheric circulation (Wang et al., 2008a). The geographic area covered by an anomalously large AWP can be 3 times larger than an anomalously small

AWP (Wang et al., 2006), thereby altering the SST and atmospheric circulation patterns in the GOM, Caribbean and western tropical North Atlantic. A number of geochemical proxy records from corals, sclerosponges and foraminifera in the region encompassed by the AWP show a 1-3ºC cooling during the LIA (Winter et al., 2000; Watanabe et al., 2001; Nyberg et al., 2002; Haase-Schramm et al., 2003, 2005; Lund and Curry, 2006; Richey et al., 2007; Black et al., 2008; Kilbourne et al., 2008) (Figure 2.1), implying that the AWP may have been particularly sensitive to climate forcing during the LIA.

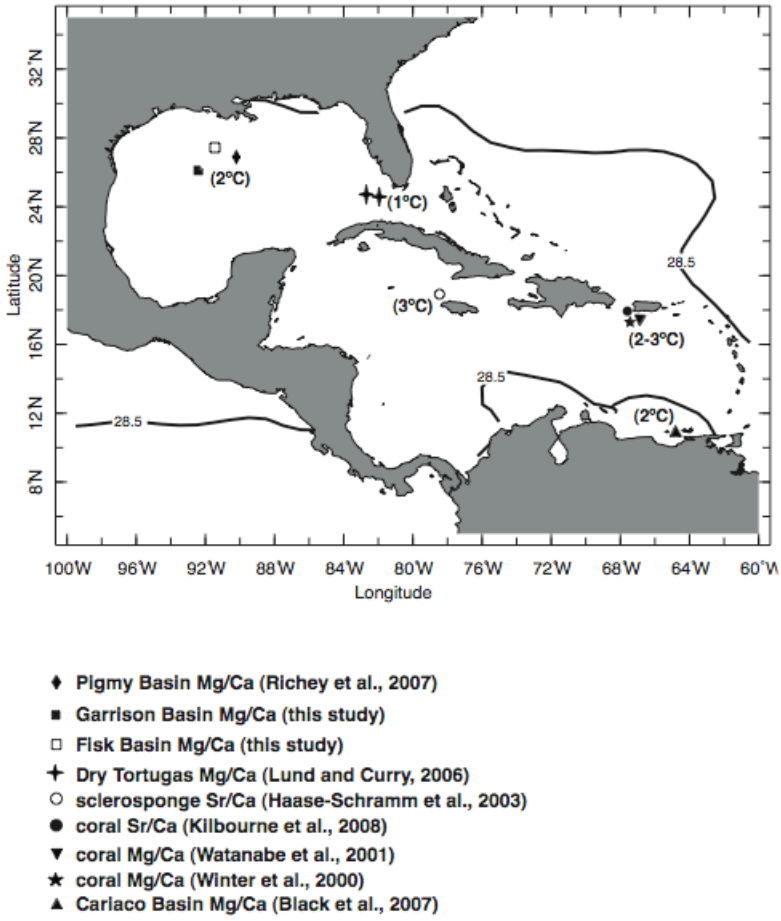

Figure 2.1. Map of proxy records in the GOM-Caribbean region exhibiting 1-3ºC cooling during the LIA. The Fisk (open square) and Garrison (closed square) basins are the 2 new Mg/Ca-SST records presented in this study. The September (maximum seasonal geographic extent) AWP (28.5ºC isotherm) is plotted using the Reynolds and Smith OISST V2.0 dataset (1ºx1º grid, averaged from 1981-2009). Mean LIA cooling is indicated in parentheses for each region.

Assessing the fidelity of these SST proxy records is especially critical for the interpretation of decadal to sub-decadal resolution, low-latitude records covering critical time intervals such as the LIA-20th century. The uncertainties inherent to foraminiferal Mg/Ca-based SST estimates can exceed the environmental signal in some cases. Factors that lead to these uncertainties include, but are not limited to, diagenetic overgrowths (e.g. Boyle 1983; Barker et al., 2003; Pena et al., 2005), salinity (e.g. Nürnberg et al., 1996; Ferguson et al., 2008), and dissolution (e.g. Dekens et al., 2003). Each of these factors has the potential to overprint the Mg/Ca signal of the downcore record, and the influence of these factors is variable, and often basin-specific. Thus, replication among a grouping of regional cores is essential to developing a coherent regional record of climate variability. In this paper we present 2 new foraminiferal Mg/Ca-SST records spanning the past 600-800 years from the northern Gulf of Mexico. These new records replicate the magnitude and pattern of SST variability recorded in a published Mg/Ca record from the Pigmy Basin (Richey et al., 2007), and further corroborate a large magnitude (1-3ºC) cooling in the GOM-Caribbean region during the LIA. We highlight the regional coherence among all published Caribbean-Gulf of Mexico SST proxy records during this time interval, and discuss potential mechanisms for this large low-latitude Atlantic cooling overprinted on the modest hemispheric cooling during the LIA.

2.3. Materials and Methods

The Fisk Basin (PE07-5I; 817 m depth; 27º33.0’ N, 92º10.1’ W) and Garrison Basin (PE07-2; 1570 m depth; 26º40.5’ N, 93º55.5’ W) box cores were collected onboard the R/V Pelican in 2007. Pigmy Basin box core (PBBC-1; 2259 m depth; 27º11.61’N,

91º24.54'W) was collected in 2002 onboard the R/V Longhorn. All of these basins are located on the continental slope in the northern Gulf of Mexico, and have a relatively high sediment accumulation rate (20-40 cm/kyr) due to large inputs of terrigenous material via the Mississippi River. For each of the box cores the sediment-water interface was recovered, and AMS ^{14}C dates with bomb radiocarbon confirm that the core-top samples include the most recently deposited sediments. We set the core-top age to 2000 AD for each of these GOM records for ease of comparison with other regional, absolutely dated records.

Radiocarbon ages (Table 2.1) were calibrated using the Calib 5.0 program with a 400-year reservoir correction. Radiocarbon AMS dates were determined using 6-8mg of mixed planktic foramnifers. The Fisk Basin age model (Figure 2.1a) was constructed by fitting a least-squares regression line through the 4 radiocarbon AMS dates and setting the intercept to 0. Radiocarbon dates below 20 cm core depth indicate much lower sediment accumulation rates prior to 800 yrs BP. Due to the uncertainties in the age model below 20 cm, we do not plot the Mg/Ca data in this paper. The linear sedimentation rate was determined to be [Cal Age (years BP)=3.7602*core-depth (mm)]. The Garrison Basin age model (Figure 2.1b) was constructed by fitting a third order polynomial through the 8 radiocarbon AMS dates [Cal Age (Yrs BP)= $-2e^{-05}x^3 + 0.022x^2 + 2.26x$; x= core-depth (mm)]. An 18% decrease in the foraminiferal weights below 13 cm in the Garrison Basin core indicates a potential problem with calcite dissolution, and thus we exclude Mg/Ca data below this core depth.

	Core Depth (mm)	^{14}C age (yrs)	error (yrs)	Cal Yrs BP
Fisk Basin	0-5	-215	30	0
	150-155	925	35	523
	160-165	1090	30	652
	200-205	1210	30	743
Garrison Basin	0-5	140	35	0
	10-15	455	25	41
	70-75	935	35	186
	120-125	1435	45	604
	200-205	2080	20	1248
	270-275	2495	35	1666
	340-345	3300	35	2695
	390-395	3640	30	3064

Table 2.1. Radiocarbon dates. 6 AMS radiocarbon dates are shown for Fisk Basin and 4 dates for Garrison Basin. The error column indicates the analytical error on the ^{14}C age. The radiocarbon ages were converted to calendar ears using the CALIB 5.0 program, with a 400-year reservoir correction.

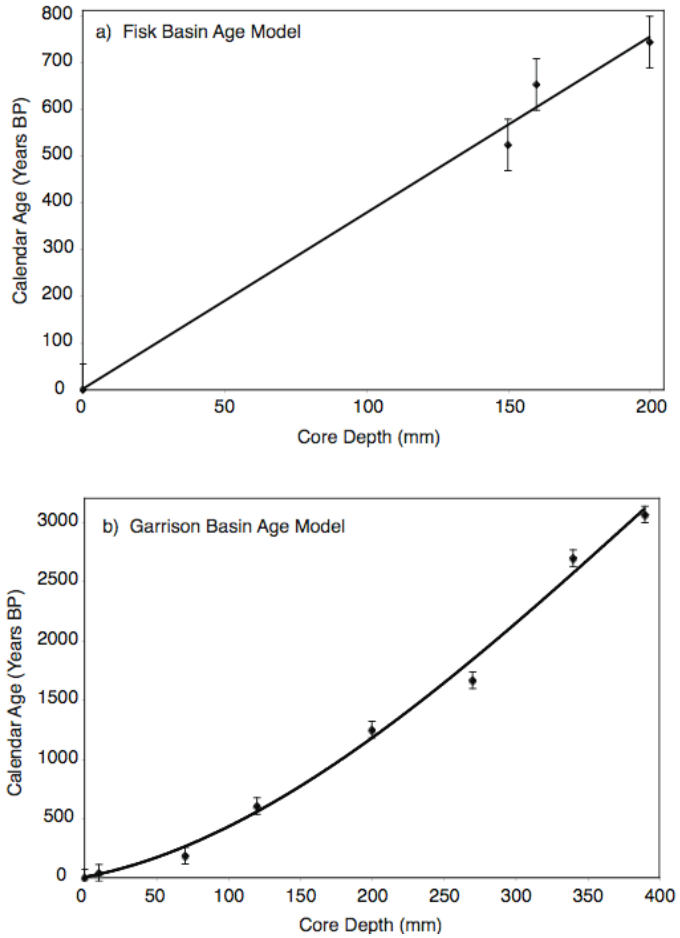

Figure 2.1. Age models. a) Fisk Basin age model and b) Garrison Basin age model. For the Fisk Basin, a least squares regression is fit through the 4 AMS radiocarbon dates. For the Garrison Basin a second order polynomial is fit through the 7 AMS radiocarbon dates.

For all down-core elemental analyses ≥60 foraminifera were picked from the 250-300mm size fraction of *Globigerinoides ruber* (white). Foraminifera were lightly crushed and underwent a cleaning process that includes multiple clay removal steps, an oxidative step to remove organic material, and an acid leaching step to remove adsorbed metals (Barker et al., 2003). A reductive cleaning step was not performed on these samples. Elemental analyses were performed on a Perkin Elmer Optima 4300 dual view inductively coupled plasma-optical emission spectrometer (ICP-OES) at the College of Marine Science, University of South Florida. In all cases where there are replicate Mg/Ca analyses, replicates are based on aliquots of ≥60 foraminifera that have been crushed, cleaned and analyzed separately.

2.4. Gulf of Mexico Mg/Ca records

In order to test the reproducibility of the Pigmy Basin Mg/Ca record (Richey et al., 2007), we generated Mg/Ca records in 2 additional Gulf of Mexico basins: Garrison Basin (box core PE07-2) and Fisk Basin (box core PE07-5I). The upper 13 cm of the Garrison Basin box core covers the past ~600 yrs (age control provided by 4 AMS radiocarbon date, see supplemental materials). An 18% decrease in the foraminiferal weights below 13 cm indicates potential problems with calcite dissolution, and thus we exclude Mg/Ca data below this core depth. The core-top Mg/Ca value is 4.43 mmol/mol (±0.16 mmol/mol), based on 2 replicate measurements, and corresponds to an SST of 25.4ºC (using [Mg/Ca=0.449*exp(0.09*SST)], from Anand et al., 2003), the modern annual average for the Gulf of Mexico (Levitus, 2003). This is equivalent to the core-top Mg/Ca value of 4.43 (±0.03 mmol/mol) that was generated from replicate measurements

of 3 different sub-cores from the Pigmy Basin box core (Richey et al., 2007). The mean precision for replicate analyses of the Garrison Basin downcore record is ±0.14 mmol/mol (±0.3ºC), with 60% of the samples run in duplicate. The major features of this record include 3 distinct SST minima (ca. 1450-1550, 1700-1750, and 1900 AD), that are ~2ºC cooler than the core-top SST. These minima appear to correspond with the Spörer, Maunder, and Dalton sunspot minima, respectively (Figure 2.3).

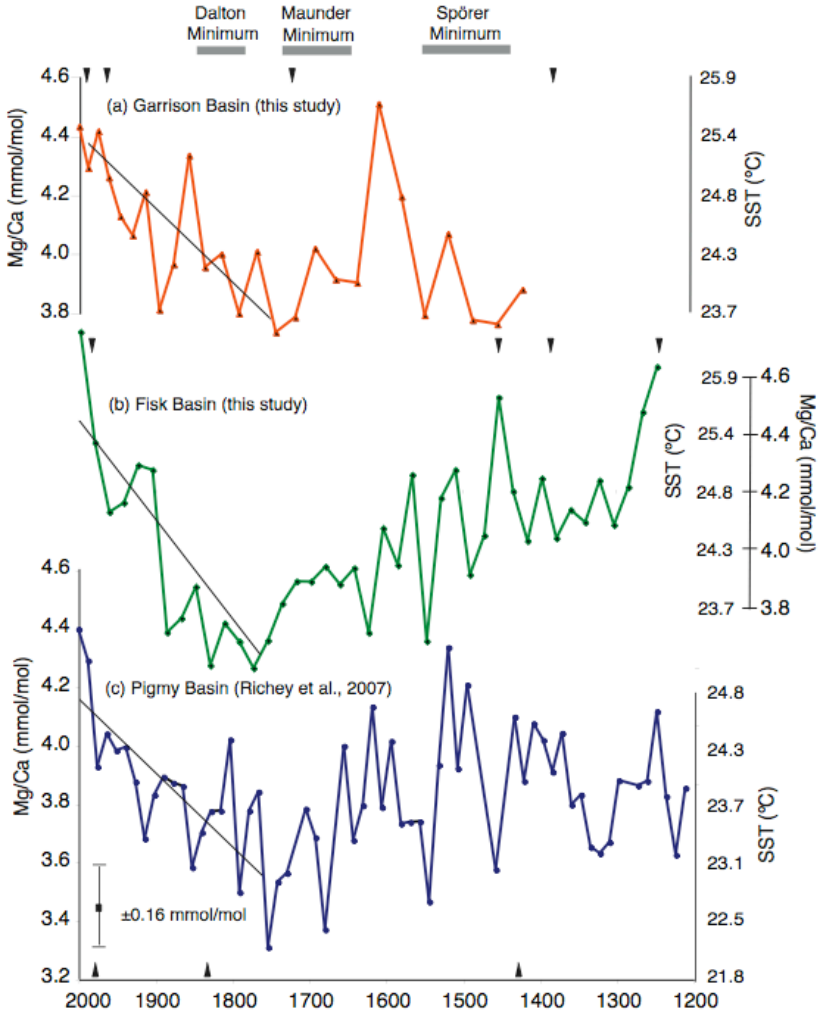

Figure 2.3. Gulf of Mexico Mg/Ca Records. (a.) Garrison Basin (b.) Fisk Basin and (c.) Pigmy Basin (from Richey et al., 2007) are plotted on the same Mg/Ca scale, with age control points indicated by arrows. Corresponding SST scale is given on a secondary y-axis, using the relationship [Mg/Ca=0.449*exp(0.09*SST], from Anand et al. (2003). Lines are plotted on each curve representing the linear warming trend over the past 250 years.

The upper 20 cm of the Fisk Basin box core span the past ~800 years (age control provided by 4 AMS radiocarbon dates). Radiocarbon dates below 20 cm core depth indicate much lower sediment accumulation rates prior to 800 yrs BP. Due to the uncertainties in the age model below 20 cm, we focus on the uppermost 20 cm of the box core, which has a sedimentation rate of ~26.5cm/kyr (sampling resolution of ~18 yrs per 0.5 cm sample). The core-top Mg/Ca value is 4.75 mmol/mol (±0.17 mmol/mol), based on 3 measurements, which corresponds to an SST of 26.2ºC (±0.4ºC), and is slightly higher (by 0.8±0.4ºC) than the core-top Mg/Ca-SST for Pigmy and Garrison Basins. The Fisk Basin Mg/Ca record shows a similar pattern of variability to the other 2 Gulf of Mexico records over the past 6 centuries, with SST minima ca. 1550 and 1750-1850 AD that are ~3ºC cooler than the core-top SST (Figure 2.3).

LIA cooling in all 3 GOM Mg/Ca records is preceded by an interval of warmth in which Mg/Ca is as high or higher than the mean core-top value of 4.4 mmol/mol. The timing of the warm interval in the Pigmy and Fisk basins is similar (ca. 1500 and 1450 AD, respectively), while it is slightly later in Garrison Basin (~1600 AD). All 3 basins reach maximum cooling ca. 1750 AD. The linear warming trend from maximum LIA cooling (1750 AD) to the core-top is similar in the Pigmy and Garrison basins (~0.007ºC/yr), while the slope of the warming trend is slightly steeper in Fisk Basin (Figure 2.3). In actuality however, given the uncertainty of the age models and Mg/Ca-SST estimates, the timing of the onset as well as the magnitude of LIA cooling is consistent among these 3 GOM sites.

2.5. Regional Comparisons

We have generated a 600-year stacked ΔSST record for the northern GOM based on the Fisk, Garrison and Pigmy Basin Mg/Ca-SST records (Fig. 2.4d). In order to generate the stacked ΔSST record, the mean was removed from each record for the period in which there is overlap between the 3 records (from 2000-1420 AD), (i.e. ΔSST is the SST relative to the 580-year mean). The ΔSST records were re-sampled at a constant ΔT of 20 years, and then the mean of the 3 re-sampled ΔSST records was calculated to generate the GOM ΔSST stack. The uncertainty in the stack is ±0.4ºC (indicated by the error bar in Figure 2.4d.). This stack represents the multi-centennial trend that is common to the 3 independent GOM SST records, and is used here to draw regional comparisons.

We compare the GOM ΔSST stack to a 250-year continuous coral Sr/Ca-SST record from the species *Montastraea faveolata* from La Parguera, Puerto Rico (Kilbourne et al., 2008). Both records (plotted their own independent timescale, and calibration to SST) show that it was ~2ºC cooler ca. 1750 AD than modern, and they also can both be described by a linear warming trend of 0.007ºC/yr from the LIA toward the present (Figure 2.4, a and d). There are 2 additional coral-based SST records from Puerto Rico that compare brief time intervals during the LIA to late 20th century SSTs. Winter et al. (2000) infer that LIA SSTs were 2-3ºC cooler than modern, while Watanabe et al. (2001) suggest that LIA SSTs were 2ºC cooler than modern (from $\delta^{18}O$ and Mg/Ca data in *M. faveolata*, respectively). In summary, these 3 different Puerto Rico coral-based geochemical proxies agree that early 18th century SSTs were 2-3ºC cooler than modern.

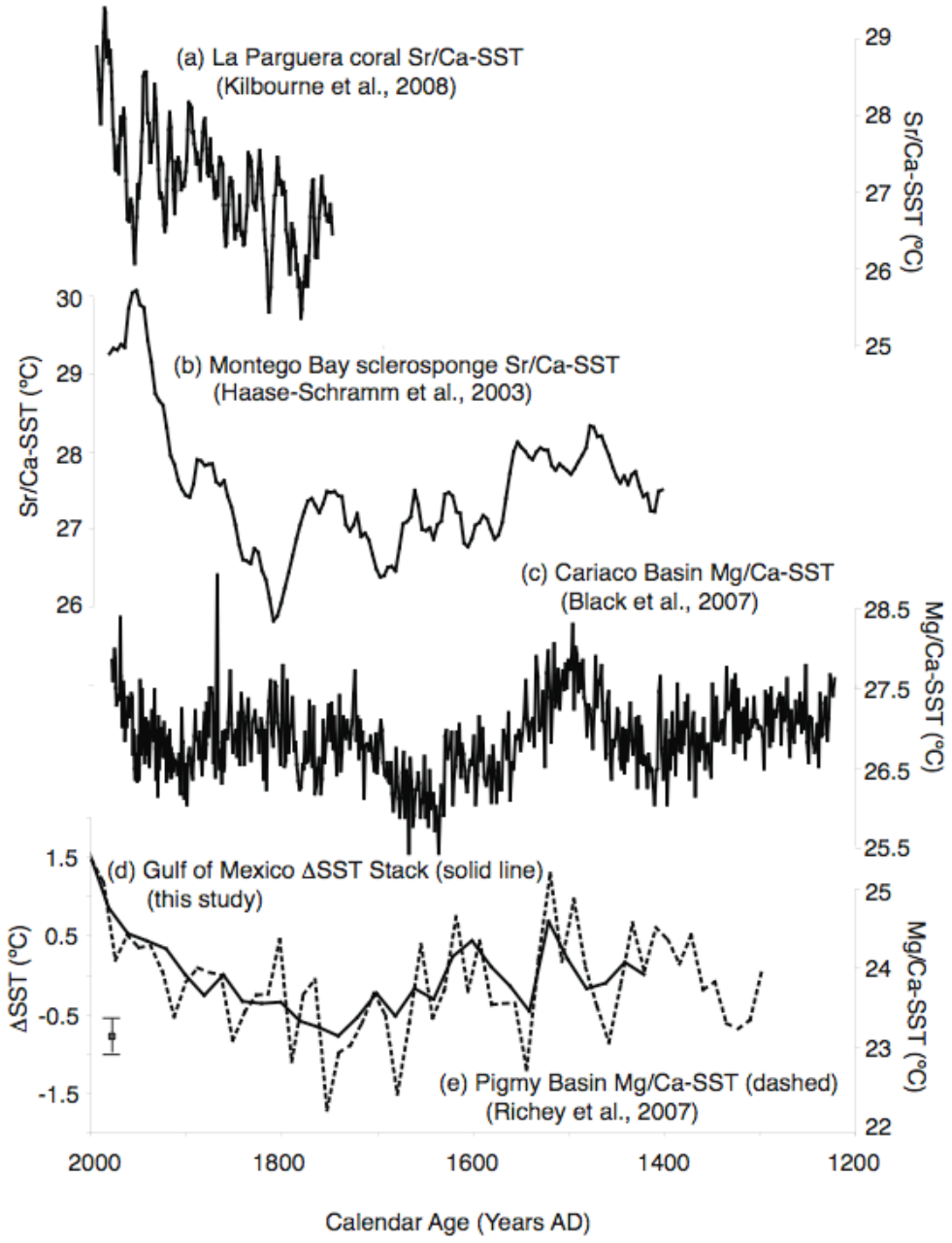

Figure 2.4. AWP Regional SST Comparison. (a) La Parguera, Puerto Rico coral Sr/Ca-SST (Kilbourne et al., 2008). The coral Sr/Ca is calibrated to SST using the equation [Sr/Ca= -0.047*T+10.3726], and the plot is a 5-year running mean. (b) Montego Bay, Jamaica sclerosponge Sr/Ca-SST (Haase-Schramm et al., 2003). The sclerosponge Sr/Ca data was calibrated to SST using the equation [Sr/Ca=-0.102*T+12.5] from Rosenheim et al. (2004). The record was re-sampled at a constant ΔT of 4 years, and then smoothed using a 5-point running mean (c) Cariaco Basin *G. bulloides* Mg/Ca-SST calibrated to SST using the equation Mg/Ca=0.0.368exp(0.092*T), (d) Gulf of Mexico ΔSST stack (solid line) and (e) Pigmy Basin, GOM foraminiferal Mg/Ca-SST (dashed line)(Richey et al., 2007). Each record is plotted on its own independent timescale, and SST is scaled identically in each panel. The error bar in panel (d) indicates the uncertainty in the GOM ΔSST stack of ±0.4ºC.

A Sr/Ca-SST record spanning the past 650 years from a Jamaican sclerosponge shows mean LIA conditions that were ~3ºC cooler than modern (Haase-Schramm et al., 2003). Although the magnitude of cooling inferred from this sclerosponge record is slightly larger than that observed in other circum-Caribbean SST records, the general pattern of variability is very similar to other regional records (Figure 2.4b).

A Cariaco Basin foraminiferal Mg/Ca-SST record shows a similar pattern of centennial-scale variability to the GOM Mg/Ca-SST records over the past 8 centuries (Black et al., 2007). Both show a period of warmth ca. 1500 AD., during which SSTs are similar to core-top SSTs, followed by a period of significant cooling during the LIA, and a rapid warming over the past 100 years (Figure 2.4c). The amplitude of SST variability reported in Black et al. (2007) is muted relative to GOM SST variability; however, the use of an alternate Mg/Ca-SST calibration equation yields an SST record that exhibits a ~2ºC LIA cooling, and an amplitude of variability that is similar to that of the GOM SST records.

The similarities between the SST proxy records that span the GOM-Caribbean region, in spite of the uncertainties in both the Mg/Ca and Sr/Ca temperature proxies, suggests that the trends recorded in the northern GOM over that past 6 centuries are representative of a regional climate signal.

2.6. Discussion

There are important implications of a regionally coherent >2ºC cooling in the Gulf of Mexico-Caribbean region during the LIA. Northern Hemisphere temperature reconstructions, which are based predominantly on mid- to high-latitude records, show a

<1ºC hemispheric cooling (Mann et al., 1998, 1999; Esper et al., 2002; Moberg et al., 2005). Model results using both medium and high solar radiative forcing estimate Northern Hemisphere LIA cooling of <1ºC (Ammann et al., 2007). Simulated Northern Hemisphere temperature response to volcanic forcing shows cooling of 0.2-0.5ºC, and is in good agreement with Northern Hemisphere temperature reconstructions (Gao et al., 2008). While model simulations and temperature reconstructions suggest a <1ºC LIA cooling for the Northern Hemisphere, proxy records estimate that cooling in the high northern latitudes is on the order of 1-3ºC (Overpeck et al., 1997). Based on the concept of polar amplification, one would predict much more subtle temperature changes in the subtropical Atlantic Ocean than at the high northern latitudes. We suggest, based on the weight of evidence, that there was a large cooling (1-3ºC) in the GOM-Caribbean region during the LIA (ca. 150-400 yrs BP), indicating that this particular region of the sub-tropical Atlantic Ocean was especially sensitive to climate perturbations during this time interval.

Timing of local SST minima in existing high-resolution continuous records from the GOM-Caribbean correspond roughly to minima in solar insolation associated with sunspot minima (The Dalton, Maunder and Spörer Minima). The reduction in solar irradiance (0.25-0.65%) attributed to these sunspot minima indicates a very small change in radiative forcing (Bard et al., 2000). A model simulation by Ammann et al. (2007) shows that the low-latitude North Atlantic has a relatively low sensitivity to solar forcing (<0.05ºC/watt m^{-2}) compared with the mid to high latitudes. Modeled surface air temperature response to irradiance changes, similar to the decrease in irradiance associated with the Maunder Minimum, show a ΔT of ~0.3ºC in the GOM-Caribbean

region (Shindell et al., 2006), which is much smaller than the observed SST variability from proxy records in this region during these solar minima. Thus direct solar forcing alone is not likely responsible for the large LIA cooling in the low latitude North Atlantic, but perhaps positive feedbacks (e.g. intensification of the subtropical high) amplified cooling during periods of reduced solar irradiance.

The observed LIA cooling in the Caribbean and northern GOM may have been driven by changes in the size of the AWP, which can vary by ±50% (Wang et al., 2008b) and the SST anomaly within the AWP can vary by ±0.6ºC (Wang et al., 2006) on multidecadal timescales. During the LIA, it is possible that there was a dramatic reduction in the geographic extent and intensity of the AWP, thus reducing summer SSTs in regions on the periphery of the AWP (e.g. Puerto Rico and the northern GOM) for prolonged time intervals. Model results of Wang et al. (2008a) suggest that an anomalously small AWP, coupled with associated changes in atmospheric circulation can lead to an increase in the mid-summer drought in the Central America/Yucatan region, and an increase in moisture transport from the GOM to the North American continent via a strengthening of the Caribbean low-level jet (CLLJ) and the Great Plains low-level jet (GPLLJ). Proxy records of hydrologic variability suggest that this was the likely regional climate scenario during the LIA. A GOM record of terrigenous input (via the Mississippi River) suggests wetter conditions in North American during the LIA (Flannery et al., 2008). Records from the Yucatan Peninsula suggest drier conditions during the LIA (Hodell et al., 2005), while bulk $d^{18}O$ from the Blue Hole in Belize suggest drier and/or cooler conditions in Central America (Gischler et al., 2008). An increase in salinity (inferred from an increase in the $d^{18}O$ of seawater) in the GOM (Richey et al., 2007) and

Florida Current (Lund and Curry, 2006) during the LIA further supports increased evaporation minus precipitation in the GOM-Caribbean.

The LIA cooling in the low-latitude North Atlantic is consistent with an increase in the north-south sea-level pressure (SLP) gradient associated with the positive phase of the North Atlantic Oscillation (NAO). Increased levels of Na^+ and K^+ in a glaciochemical series from the GISP2 ice core suggest multiple intervals of increased north Atlantic storminess during the LIA (Meeker and Mayewski, 2002), which suggests an increase in the pressure gradient between the Icelandic Low and the North Atlantic subtropical high (Maasch et al., 2005). This positive NOA-like pattern is characterized by an increase in North Atlantic trade wind strength, and a cooling in northern hemisphere tropical and subtropical SSTs (Marshall et al., 2001). A centennial-scale strengthening of the trade winds is consistent with evidence for cooler and drier conditions observed throughout the Gulf of Mexico-Caribbean region. Although a recent reconstruction of the NAO suggests a shift to weaker NAO conditions during the LIA (Trouet et al., 2009), evidence from the subtropical North Atlantic is consistent with a persistent, enhanced positive NAO pattern of SLP and SST during the LIA.

2.7. Conclusions

Despite uncertainties in foraminiferal Mg/Ca-SST proxy data and radiocarbon dating, the 3 late Holocene Mg/Ca-SST records generated from the northern Gulf of Mexico show very similar variability over the past 6 centuries, corroborating observations from throughout the Gulf of Mexico-Caribbean region that there was a prominent Little Ice Age cooling of 1-3ºC. This suggests that the tropical-subtropical

North Atlantic may be more dynamic than previously thought during the late Holocene. A reduction of the AWP, coupled with reorganization of atmospheric circulation patterns during the Little Ice Age, may explain the observed cooling in this region. Additional high quality SST proxy records from the subtropical North Atlantic Ocean are needed to establish the spatial extent and timing of this Little Ice Age cooling. Additional terrestrial proxy records of regional hydrologic variability will aid in understanding the ocean-atmosphere dynamics during this climatically important interval. Models including solar and volcanic forcings during the LIA have not been able produce a >1ºC cooling in the GOM-Caribbean region, thus more work needs to be done to better understand the regional climate dynamics that could lead the observed cooling.

Chapter 3

Merging late Holocene molecular Organic and Foraminiferal-based Geochemical Records of SST in the Gulf of Mexico

3.1. Abstract

A molecular organic geochemical proxy (TEX_{86}) for sea surface temperature (SST) is compared with a Foraminifera-based SST proxy (Mg/Ca) in a decadal-resolution marine sedimentary record spanning the last 1,000 years from the Gulf of Mexico (GOM). We assess the relative strengths of the organic and inorganic paleoceanographic techniques for reconstructing high-resolution SST variability during recent climate events, including the Little Ice Age (LIA) and the Medieval Warm Period (MWP). SST estimates based on the molecular organic proxy TEX_{86} show a similar magnitude and pattern of SST variability to foraminiferal Mg/Ca-SST estimates, but with some important differences. For instance, both proxies show a significant cooling (1.5-2.5ºC) of GOM SSTs during the LIA. During the MWP, however, Mg/Ca-SSTs are similar to near-modern SSTs, while TEX_{86} indicates SSTs that were significantly cooler than core-top. Using the respective SST calibrations for each proxy results in TEX_{86}-SST estimates that are 2 to 4°C warmer than Mg/Ca-SST throughout the 1,000-year record. We interpret the TEX_{86}-SST as a summer-weighted SST signal from the upper mixed layer, whereas the Mg/Ca-SST better reflects the mean annual SST. Differences in the SST estimates between the two proxies are interpreted in the context of varying seasonality and/or changing water column temperature gradients.

3.2. Introduction

Accurate reconstruction of the spatial and temporal patterns of sea surface temperature (SST) variability in the low latitude oceans is critical to understanding the range of natural climate variability over the past millennium. While the low latitude oceans are a major source of heat and moisture to the mid-and high latitudes, global and hemispheric climate reconstructions are predominantly based on extra-tropical terrestrial proxy records (c.f. National Research Council, 2006). There are few locations in the low latitude oceans from which continuous decadal resolution SST proxy records covering the past 1,000 years have been published (Lund and Curry, 2006; Newton et al., 2006; Richey et al., 2007; Black et al., 2008; and Oppo et al., 2009). These SST reconstructions, although widely distributed geographically, all show significant SST fluctuations (1-2ºC) over the past 1,000 years.

Paleoclimate records from the Atlantic Warm Pool (AWP), which includes much of the western tropical/sub-tropical Atlantic Ocean, provide further evidence for significant climate fluctuations over the past 6 centuries (c.f. Richey et al., 2009). The AWP is defined by the >28.5ºC SST isotherm, and encompasses the northern Caribbean, GOM and western tropical North Atlantic during the summer (cf. Wang et al., 2008). Multi-decadal variability in the size/intensity of the AWP is correlated with rainfall anomalies in the Caribbean region, formation and intensification of North Atlantic hurricanes, and variability in moisture transport to the North American continent via interactions with atmospheric circulation (Wang et al., 2008).

A number of geochemical proxy records from the region encompassed by the AWP provide evidence for a large (2-3ºC) cooling during the LIA (ca. 400-150 yrs BP)

(Winter et al., 2000; Watanabe et al., 2001; Nyberg et al., 2002; Haase-Schramm et al., 2003; Richey et al., 2007; Black et al., 2007; Kilbourne et al., 2008; Richey et al., 2009). However, two additional SST proxy records from within the AWP show a subtler LIA cooling (~1ºC): A Mg/Ca-SST record from a sediment core from the Great Bahamas Bank (Lund and Curry, 2006), and a coral growth rate-based SST record from the Bahamas (Saenger et al., 2009). Additional multi-proxy studies are needed to determine whether the discrepancies observed are real regional differences in the climate response during the LIA, or whether there are site- and proxy-specific factors that are influencing the SST records.

Presently, there are three widely used SST proxies derived from marine sedimentary archives: $U^{K'}_{37}$, TEX_{86}, and foraminiferal Mg/Ca. The $U^{K'}_{37}$ index, an organic geochemical SST proxy based on the ratio of long-chain diunsaturated to triunsaturated alkenones (Brassell et al., 1986), is not ideal in low latitude marine settings where SSTs exceed 28ºC. The $U^{K'}_{37}$ index approaches 1.0 at temperatures > 28ºC (Prahl and Wakeham, 1987) due to insufficient production of the triunsaturated alkenones. Although Jasper and Gagosian (1989) generated a low resolution 100 kyr $U^{K'}_{37}$ –SST record from Pigmy Basin sediments, there are insufficient alkenone concentrations in late Holocene sediments to provide an SST record of the past 1,000 years.

A novel molecular organic SST proxy, TEX_{86} (the TetraEther IndeX of tetraethers with 86 carbon atoms), is based on the relative abundance of isoprenoid glycerol dialkyl glycerol tetraethers (GDGTs) with varying numbers of cyclopentane moieties (Schouten et al., 2002). GDGTs are membrane lipids biosynthesized by marine Crenarchaeota, and the number of cyclopentane moieties in these crenarchaeotal membrane lipids has been

observed to increase with increasing growth temperature (Wuchter et al., 2004). Although Crenarchaeota are ubiquitous throughout the water column (Karner et al., 2001) and have been found living deep within sub-surface sediments (Lipp et al., 2008), TEX_{86} has been shown to correlate linearly with mean annual SST (Schouten et al., 2002, Kim et al., 2008) throughout the global oceans. Mesocosm studies suggest that salinity and nutrients are not significant factors in TEX_{86} measurements (Wuchter et al., 2004). It has been shown that terrestrial organic matter often contains isoprenoid GDGTs (Weijers et al., 2006), and thus TEX_{86}-SST estimates may be biased in marine settings with large terrestrial input. However, the contribution of terrestrial relative to marine GDGTs can be monitored downcore via the BIT (Branched to Isoprenoid Tetraether) index (Hopmans et al., 2004).

Foraminiferal Mg/Ca has been widely accepted as an SST proxy, however factors such as diagenetic overgrowths (e.g. Boyle, 1983; Barker et al., 2003; Pena et al., 2005), salinity (e.g. Nürnberg et al., 1996; Ferguson et al., 2008) and dissolution (e.g. Dekens et al., 2003) have been shown to influence Mg/Ca of foraminiferal calcite. In this study we present the first direct comparison of foraminiferal Mg/Ca with a molecular organic (TEX_{86}) SST proxy, from co-occurring sediments in a decadally-resolved 1,000-year long sedimentary record from the Gulf of Mexico. Using a multi-proxy approach we can better constrain the effects of the local ecology and other oceanographic factors on each paleothermometer. Coupling of the two SST proxies expands our ability to assess SST conditions, and thus will provide a more complete picture of regional ocean climate variability (e.g. seasonality, vertical temperature gradients) during the late Holocene.

3.3. Study Location

The location of our study is the Pigmy Basin, an intraslope basin located in the northern Gulf of Mexico (27º11.61 N, 91º24.54 W, water depth 2259 m), ~200 km south of the Mississippi River mouth (Figure 3.1). The Mg/Ca and TEX_{86} records discussed in this study are derived from two different sub-cores (PBBC-1E and PBBC-1F, respectively) isolated from a single box core recovered from the Pigmy Basin in 2003 aboard the RV Longhorn. Sedimentation rates during the late Holocene are relatively high (43 cm/kyr) as a result of the large volume of terrigenous material delivered via the Mississippi River. The high sedimentation rate combined with a 0.5 cm sampling interval allow for detailed study of multi-decadal to centennial scale climate variability of the past millennium.

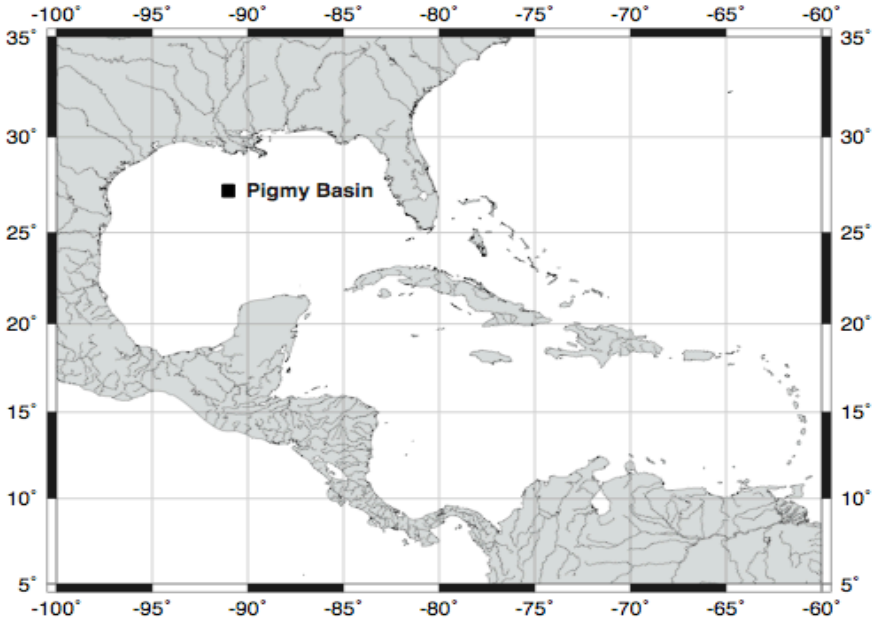

Figure 3.1. Map of the Gulf of Mexico. Location of the Pigmy Basin (27º11.61'N, 91º24.54'W, 2259 meters water depth) is indicated by marker.

An age model was constructed for sub-core PBBC-1E based on 7 accelerator mass spectrometer radiocarbon dates on planktonic Foraminifera (Richey et al., 2007). Calibrated calendar ages (calibrated using the CALIB 5.0 program with a 400 year reservoir correction [Stuiver et al., 1998]) were plotted against core depth, and a least squares linear regression (r^2=0.995) indicates a sedimentation rate of 43 cm/kyr. The core-top radiocarbon date indicates post-1950 deposition, and therefore we infer a near-modern core-top. The age model for PBBC-1E was projected onto sub-core PBBC-1F (i.e. the core-top age was set to 0 yrs BP, and a 12.3 yr interval was assigned to each 0.5 cm sample). The discrepancy between the lengths of the two sub-cores (PBBC-1E is 59 cm long and PBBC-1F is 44 cm long) is due to their relative positions within the box core. The shovel of the box core is curved such that cores taken in the center of the box core are longer than core taken on the sides of the box core.

3.4. Methods

3.4.1. Extraction and Isolation of GDGT Lipids

Core PBBC-1F was sampled at 0.5 cm intervals and freeze-dried. Samples were solvent extracted with a DIONEX Accelerated Solvent Extractor (ASE 200) using a solvent mixture of 9:1 dichloromethane (DCM) to methanol (MeOH) at the College of Marine Science, University of South Florida. The resulting total lipid extract (TLE) then underwent a base hydrolysis (in 0.5M KOH in MeOH), and was separated into an acid and neutral fraction via liquid-liquid extraction under neutral and acidic conditions, respectively. The neutral fraction was then separated into an apolar, ketone and polar

fraction via silica pipette column chromatography using hexane, 3:2 (vol:vol) hexane/DCM, and 1:1 (vol:vol) DCM/MeOH, respectively.

3.4.1. TEX_{86} and BIT Analysis

The polar fraction, containing the GDGTs, was dissolved in a 99:1 (vol:vol) mixture of hexane:propanol, then filtered through 0.45μm PFTE filters. Analyses of GDGTs for TEX_{86} and BIT index determination were performed by high pressure liquid chromatography-mass spectrometry (HPLC-MS) at the Woods Hole Oceanographic Institution. Samples were analyzed on an Agilent 1200 series LC/MSD SL operating in positive APCI mode, with an autoinjector and Chemstation software. A Prevail Cyano column (150 x 2.1 mm, 3 μm-from Grace Davison Discovery Sciences) was used with 99:1 hexane:isopropanol (vol:vol) as an eluent. After the first 5 min, the eluent increased by a linear gradient up to 1.8% isopropanol (vol) over the next 45 min at a flow rate of 0.2 mL/min. Scanning was performed in single ion monitoring (SIM).

The TEX_{86} indices were calculated according to the following equations:

$$TEX_{86} = ([II]+[III]+[IV'])/[I]+[II]+[III]+[IV']) \text{ (from Schouten et al., 2002)}$$

$$BIT = ([V]+[VI]+[VII])/([V]+[VI]+[VII]+[IV]) \text{ (from Hopmans et al., 2004)}$$

where the roman numerals refer to the GDGT structures shown in Figure 3.2. The TEX_{86} index was then converted to SST according to the following equation from Kim et al., (2008):

$$T = -10.78 + 56.2*TEX_{86}$$

Each of the 88 GDGT samples in this study was analyzed in triplicate. The average standard deviation for TEX_{86} among triplicate analyses is ±0.007, which corresponds to

±0.4ºC using the calibration equation of Kim et al. (2008). For the BIT index, the average standard deviation among triplicates is ±0.006.

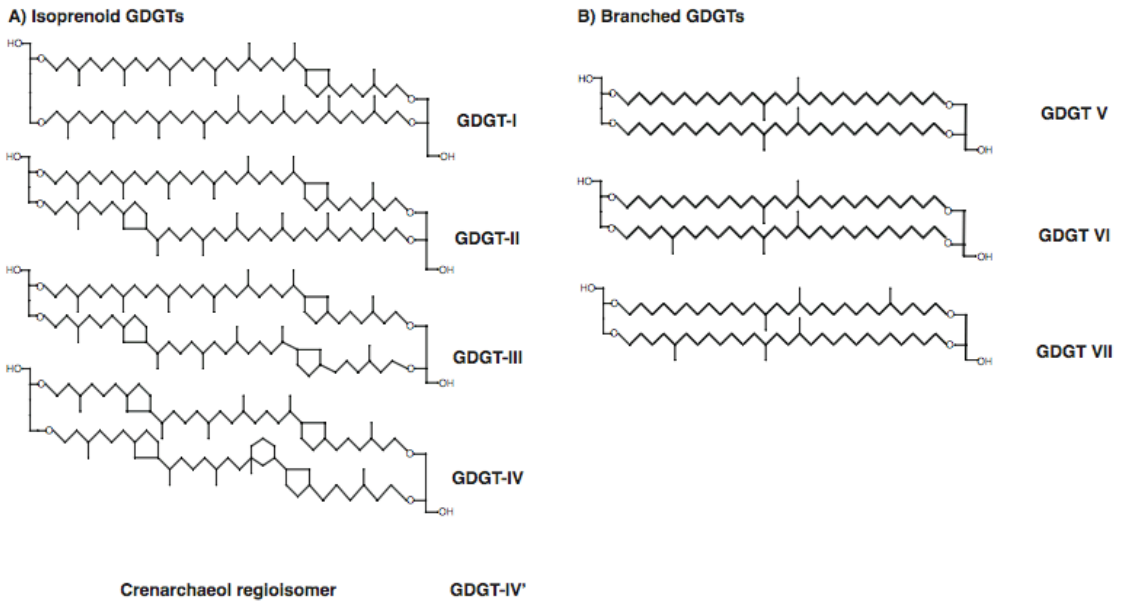

Figure 3.2. Molecular structures of GDGTs. A) isoprenoid and B) branched glycerol dialkyl glycerol tetraethers (GDGTs) used in the TEX_{86} (Schouten et al., 2002) and BIT (Hopmans et al., 2004) indices.

3.5. TEX_{86}-SST record from Pigmy Basin

The TEX_{86} record from the Pigmy Basin indicates significant SST fluctuations over the past 1,000 years (Figure 3.3a). The TEX_{86} varies between 0.65 and 0.70 (25.8-28.5ºC) and there is a general warming trend over the length of the record, with the core-top recording the warmest TEX_{86}-SST (28.5ºC) of the past millennium. The time interval 1,100-600 yrs BP is relatively stable with a mean TEX_{86}-SST of 27ºC, with the exception of a century-long SST excursion (1,000-900 yrs BP) in which temperatures were 1ºC cooler. This period is followed by a rapid transition to ~1ºC warmer SSTs ca. 600 yrs BP. The LIA (400-150 yrs BP) is marked by a 0.5ºC drop in mean SSTs from the

preceding two centuries (600-400 yrs BP), and followed by a rapid 1.5ºC warming into the 20th century.

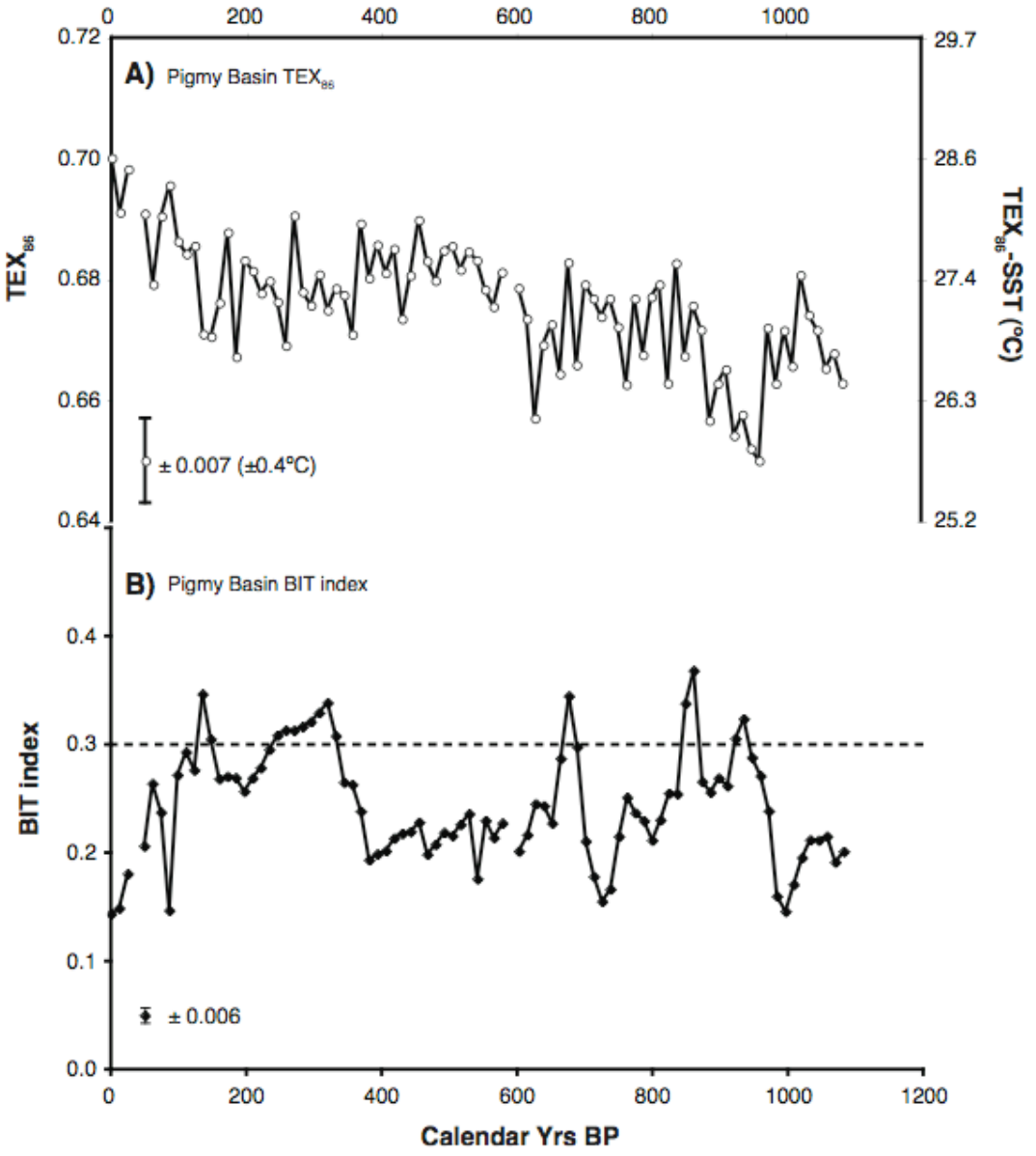

Figure 3.3. GDGT based proxy records for a Pigmy Basin box core (PBBC-1F). A) TEX_{86} record with corresponding temperature scale, calibrated using the equation: $T=-10.78 + 56.2*TEX_{86}$ from Kim et al. (2008). The pooled standard deviation of triplicate TEX_{86} measurements is indicated (±0.007) which corresponds to ±0.4ºC. B) BIT index for PBBC-1F. The pooled standard deviation among triplicate analyses is ±0.006. The dashed lined indicates the threshold BIT value of 0.3, above which input of terrestrial organic matter may influence TEX_{86} (Weijers et al., 2006).

3.6. Influence of terrestrial input on Pigmy Basin TEX_{86}

In marine marginal settings proximal to major fluvial systems such as the Mississippi River, there is concern that the TEX_{86}-SST proxy may be influenced by delivery of isoprenoid GDGTs derived from terrestrial sources. The Branched and Isoprenoid Tetraether (BIT) index, based on the relative abundance of terrestrially derived branched tetraether lipids (GDGT V, VI, and VII) versus the marine-derived crenarchaeol (GDGT IV), can be used to monitor the relative contribution of terrestrial organic matter (TOM) to sediments (Hopmans et al., 2004). Weijers et al. (2006) found that in marine sediments with a large contribution of terrestrially derived organic matter, TEX_{86} values tended to be biased toward warmer temperatures. Using a two end member mixing model (GDGT distribution in African soils versus GDGT distribution in marine sediments of the Niger deep sea fan), Weijers et al. (2006) predicted a +1ºC temperature bias in the TEX_{86}-SST of sediments with BIT values of 0.2-0.3, and the influence of TOM on TEX_{86} temperature estimates was found to increase non-linearly at BIT values > 0.3. However, this specific temperature bias depends heavily upon the composition and source of TOM, and therefore is not necessarily applicable to other marine basins.

In the Pigmy Basin (core PBBC-1F) the BIT index varies between 0.14 and 0.40 (mean=0.25) over the past 1000 years (Figure 3.3b), which lies between the values observed for coastal and open marine environments (Hopmans et al., 2004). In order to quantify the potential bias to the TEX_{86}-SST record introduced by the moderately elevated BIT index in Pigmy Basin sediments, the GDGT composition of TOM delivered to the GOM via the Mississippi River would have to be characterized. Although we cannot directly assess to what degree, if any, terrestrially derived GDGTs are influencing

the TEX_{86} measurements, we adopt the working hypothesis that downcore variability in TOM input does not significantly affect downcore TEX_{86} variability. Figure 3.3 shows a comparison of the downcore records of both the BIT and TEX_{86} indices from Pigmy Basin, and illustrates that the two indices do not covary (the correlation between the TEX_{86} and BIT indices is r = 0.2, which is small, but significantly different from 0, at the 90% confidence level). The lack of correlation is further illustrated in a cross-plot of the BIT index versus TEX_{86}-SSTfrom the Pigmy Basin (r^2 = 0.04) (Figure 3.4). We conclude that, while there is a possibility that the absolute SST may be biased, the pattern of TEX_{86} variability over the past 1,000 years in the Pigmy Basin is not systematically influenced by changes in terrestrially derived GDGT input.

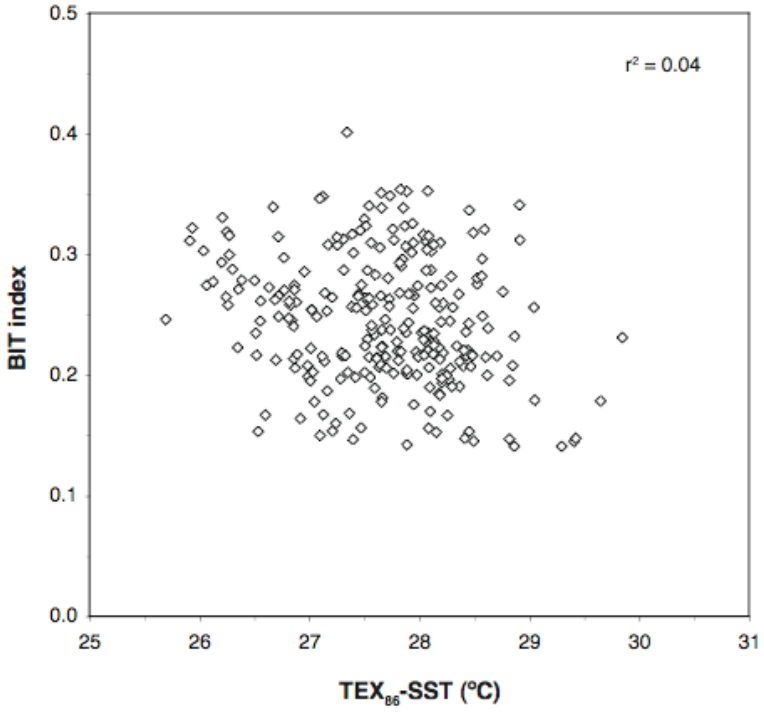

Figure 3.4. Cross plot between BIT index and TEX86-SST for Pigmy Basin box core (PBBC-1F).There is no significant correlation between TEX86 and BIT indices (r^2=0.04).

3.7. Inferring depth and seasonality for TEX_{86} signal in the GOM

The global core-top calibration of Kim et al. (2008) indicates that TEX_{86} best reflects mean annual SST of the upper mixed layer (0-30 m). Although Crenarchaeota are living and biosynthesizing GDGTs throughout the water column, Wuchter et al. (2006) showed that the TEX_{86} signal recorded in deep sediment trap samples (> 500 m) still reflects surface temperatures, rather than water temperatures resulting from deep water-column GDGT production. This is most likely due to the effective packaging and export of GDGT-containing crenarchaeal cells from the upper water column in fecal pellets via zooplankton grazing. Due to lack of a packaging process and mechanism of transport to sediments, deep-water crenarchaeotal production likely has an insignificant effect on TEX_{86} SST estimates (Wuchter et al., 2005).

The core-top TEX_{86} value of 0.70 (±0.008) in the Pigmy Basin corresponds to an SST of 28.5ºC (±0.5ºC), which is ~3ºC warmer than the mean annual SST for the GOM (25.4ºC), and equivalent to the mean summer (June-Sept.) SST for the GOM mixed layer (Levitus, 2004) (Figure 3.5a). This suggests that the TEX_{86} record in the Pigmy Basin is a heavily summer-weighted signal, and that crenarchaeotal production and/or export via zooplankton grazing must be significantly higher during the summer in the Gulf of Mexico. This is contrary to the observation of Wuchter et al. (2005) that GDGTs occurred in higher abundances during the winter and spring in a number of marine settings, including the subtropical and tropical Atlantic sites, BATS (Bermuda Atlantic Time-series Study) and in the Cariaco Basin. In contrast, Shah et al. (2008) found in Bermuda Rise core-top sediments that TEX_{86} indicated SSTs ~2ºC warmer than those estimated from co-occurring foraminiferal $\delta^{18}O$, a fact consistent with our findings in the

Pigmy Basin. At present there are no data from the GOM on seasonal changes in crenarchaeotal production.

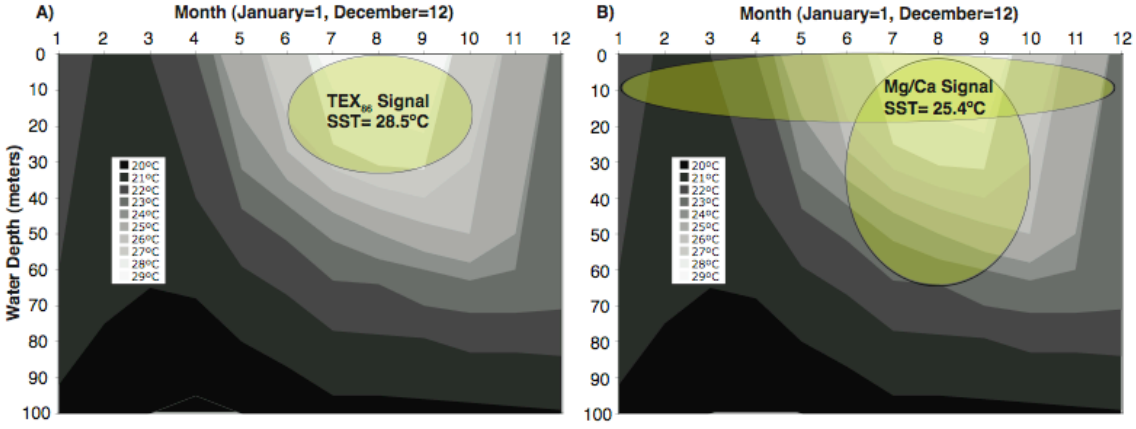

Figure 3.5. **Annual cycle of water temperature variability in the upper 100 meters of the water column**. Data are monthly averages from the climatic means for the Gulf of Mexico (Levitus, 2004). A) The circled region indicates the dominant depth and seasonal range of the TEX_{86} signal, based on the core-top TEX_{86}-SST of 28.5ºC. B) The circled regions indicate the two possible distributions of *G. ruber* in the Gulf of Mexico. The modern SST (25.4ºC) recorded by *G. ruber* indicates that they are living in the upper mixed layer (0-30 meters) throughout the year, or they are limited to the summer months (Jun-Sept), but living over a greater depth range (0-75 meters).

3.8. Comparison of Pigmy Basin TEX_{86}-SST to Mg/Ca-SST Record

Comparison of two or more different paleotemperature proxy records from co-occurring sediments often reveals strikingly different climate histories. This can be attributed to a number of physical, biological and chemical factors, including separate transport mechanisms to the sediment, different ecologies of the signal carrying organisms, and susceptibility to separate diagenetic processes of the different sediment components. It has been well documented that organic compounds, which are attached to fine-grained particles, can be laterally transported long distances (e.g. Ohkouchi et al., 2002; Mollenhauer et al., 2005) causing age and temperature offsets between molecular

organic proxies (e.g. $U^{K'}_{37}$ and TEX_{86}) and planktonic Foraminifera-based proxies. Compound-specific radiocarbon dating suggests that GDGTs may be more labile than alkenones, and thus don't survive transport over long distances under oxic conditions as well as alkenones (Mollenhauer et al., 2007; Shah et al., 2008). Thus GDGTs are more likely to contain a local signal that is contemporaneous with the foraminiferal signal.

Each paleo-SST proxy is based on the geochemistry of a planktonic organism, each of which has a different depth and seasonal distribution. These depth and seasonal distributions for a signal carrier can vary depending on geography and local controls on productivity. For example, Huguet et al. (2006) find a 2.5ºC difference between the estimates of LGM to present warming between $U^{K'}_{37}$-SST and TEX_{86}-SST in the Arabian Sea. They attribute these discrepancies to differences in seasonality between the crenarchaeota and haptophyte algae, which are the planktic source of the TEX_{86} and $U^{K'}_{37}$ signals, respectively. Castañeda et al. (2010) found that $U^{K'}_{37}$ and TEX_{86}-based SST estimates in the eastern Mediterranean were similar during the LGM, but TEX_{86}-SSTs were generally 1-2ºC warmer than $U^{K'}_{37}$-SSTs during the Holocene. They also attribute this discrepancy to changing seasonality of crenarcaeota and haptophyte blooms during the last deglaciation.

The TEX_{86}-based SST record generated from the Pigmy Basin (core PBBC-1F) shows similar patterns of variability to the Mg/Ca-based SST record (core PBBC-1E) previously published by Richey et al. (2007) from the same box core, but with important differences. Due to the potential implications of offsets in absolute SST calibration between the two different paleotemperature proxies (TEX_{86} and Mg/Ca), similarities in the decadal to centennial-scale patterns of variability are discussed first. Figure 3.6

shows the down core SST variability in both records plotted as a temperature anomaly relative to their respective core-top SSTs. Both the Mg/Ca and TEX_{86}-based SST records indicate that SSTs ca. 500 yrs BP were ~1ºC cooler than core-top SSTs. The Mg/Ca record shows that the mean temperature during the LIA (ca. 400-150 yrs BP) was 2.0ºC (±0.6ºC) cooler than today, and the TEX_{86} record indicates a LIA mean that was 1.2ºC (±0.6ºC) cooler than today. From 850-600 yrs BP both records indicate SSTs that were ~1.5ºC cooler than their modern core-top SSTs. The major discrepancies between the 2 records are 1) The LIA is not the coolest interval during the past millennium as recorded by TEX_{86}, and 2) The period prior to 900 yrs BP was similar to the core-top SST as recorded by foraminiferal Mg/Ca, but cooler in the TEX_{86} record.

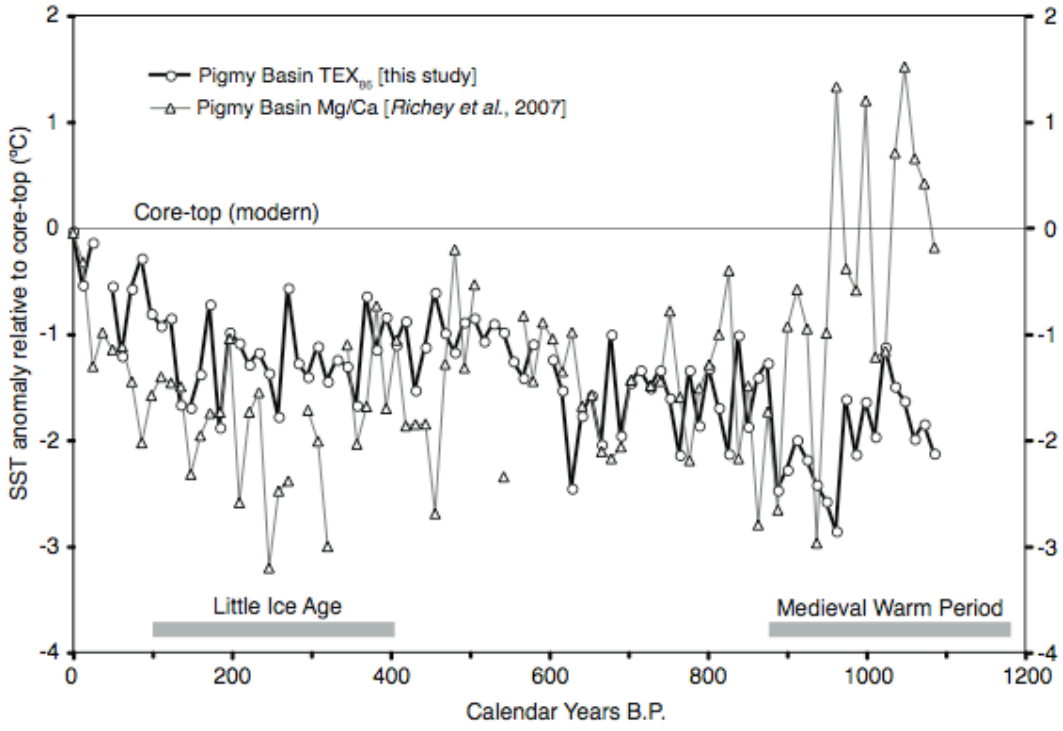

Figure 3.6. TEX86 and Mg/Ca records plotted as anomalies relative to their respective calibrated core-top temperatures. Individual data points are shown with open circles (TEX_{86}) and open triangles (Mg/Ca). Both records are derived from separate subcores with in the same Pigmy Basin box core. Sub-core PBBC-1F (TEX_{86}) is 15 cm shorter than PBBC-1E (Mg/Ca), due to position within the box core.

3.9. Inferring Depth and Seasonality for *G. ruber* in the GOM

The white variety of the planktonic foraminifer, *Globigerinoides ruber*, is abundant throughout the tropical and subtropical oceans, and is constrained to the euphotic zone by its photoautotrophic dinoflagellate symbionts. The seasonal and depth distribution of *G. ruber* (white) has been reported from sediment trap (e.g. Deuser, 1987; Tedesco et al., 2003; Tedesco et al., 2009) and plankton tow studies (e.g. Tolderlund and Bé, 1971; Fairbanks et al., 1980; Bé, 1982) in a number of different locations proximal to the Gulf of Mexico. The modern depth preference of *G. ruber* (white) has been documented in a number of Sargasso Sea plankton tows studies, but there are limited data specific to the Gulf of Mexico. Fairbanks et al. (1980) found that *G. ruber* (white) was common throughout the upper 100 meters of the water column in a November 1975 plankton tow study, while a series of monthly plankton tows in the Sargasso Sea indicated that *G. ruber* (white) was most abundant in the uppermost 10 meters of the water column (Tolderlund and Bé, 1971). Bé (1982) confirmed the presence of *G. ruber* (white) throughout the upper 50 meters of the water column in the western Gulf of Mexico.

The Mg/Ca of *G. ruber* (white) is typically interpreted as a mean annual mixed layer signal in the Gulf of Mexico (e.g. Flower et al., 2004; LoDico et al., 2006; Richey et al., 2007). Flux data from a sediment trap study in the Sargasso Sea indicate that *G. ruber* are present throughout the annual cycle, with peak fluxes in early spring and late summer (Deuser, 1987). A one-year sediment trap study in the northern Gulf of Mexico indicates that *G. ruber* (white) is present throughout the year, with small peaks in flux in early spring and late summer (Tedesco et al., 2009).

The Mg/Ca record in the Pigmy Basin was generated from a well-constrained size fraction (250-300μm) of the white variety of *G. ruber* (Richey et al., 2007). A mean Mg/Ca core-top value of 4.43 mmol/mol (±0.03) for the Pigmy Basin was determined from replicate analyses of core-top (0–0.5 cm) samples from 7 GOM core-tops. This robust core-top value corresponds to an SST of 25.4ºC (Mg/Ca = 0.449 * exp(0.09 * SST) (from Anand et al., 2003), which is the modern mean annual SST for the GOM (Levitus et al*.,* 2004).

Unlike the TEX_{86} signal, which is well constrained as a surface summer signal, the core-top Mg/Ca-SST of 25.4ºC can be produced by a number of different scenarios (Figure 3.5b). 1) The *G. ruber* (white) depth habitat is limited to the uppermost 30 meters of the water column and flux to the sediments is equally weighted throughout the year. 2) The flux of *G. ruber* (white) is summer-weighted, but *G. ruber* (white) has a greater range (0-75 meters) in the water column. In either case, increases (decreases) in SST, as recorded by the Mg/Ca of *G. ruber*, may be influenced by warmer (colder) winters or deeper (shallower) mixed layers.

3.10. Mg/Ca-SST to TEX_{86}-SST gradients

Previous studies have interpreted the difference in paleo-temperature records between species of Foraminifera with known differences in seasonal and depth distribution (Williams et al., 2009). Using the assumptions we have made about the depth and seasonal distribution of GDGTs versus *G. ruber* (white) in the GOM, we can exploit the differences between the two SST records to make inferences about changing upper water column structure and/or seasonality over the past millennium. To do this we

take the difference (ΔT) between the TEX_{86} and Mg/Ca-based SST records using their respective paleotemperature calibrations (Figure 3.7). The results of this exercise are plotted in Figure 3.7, and suggest that the greatest difference between the TEX_{86} and Mg/Ca SST occurs between 200 and 300 yrs BP, during the maximum LIA cooling.

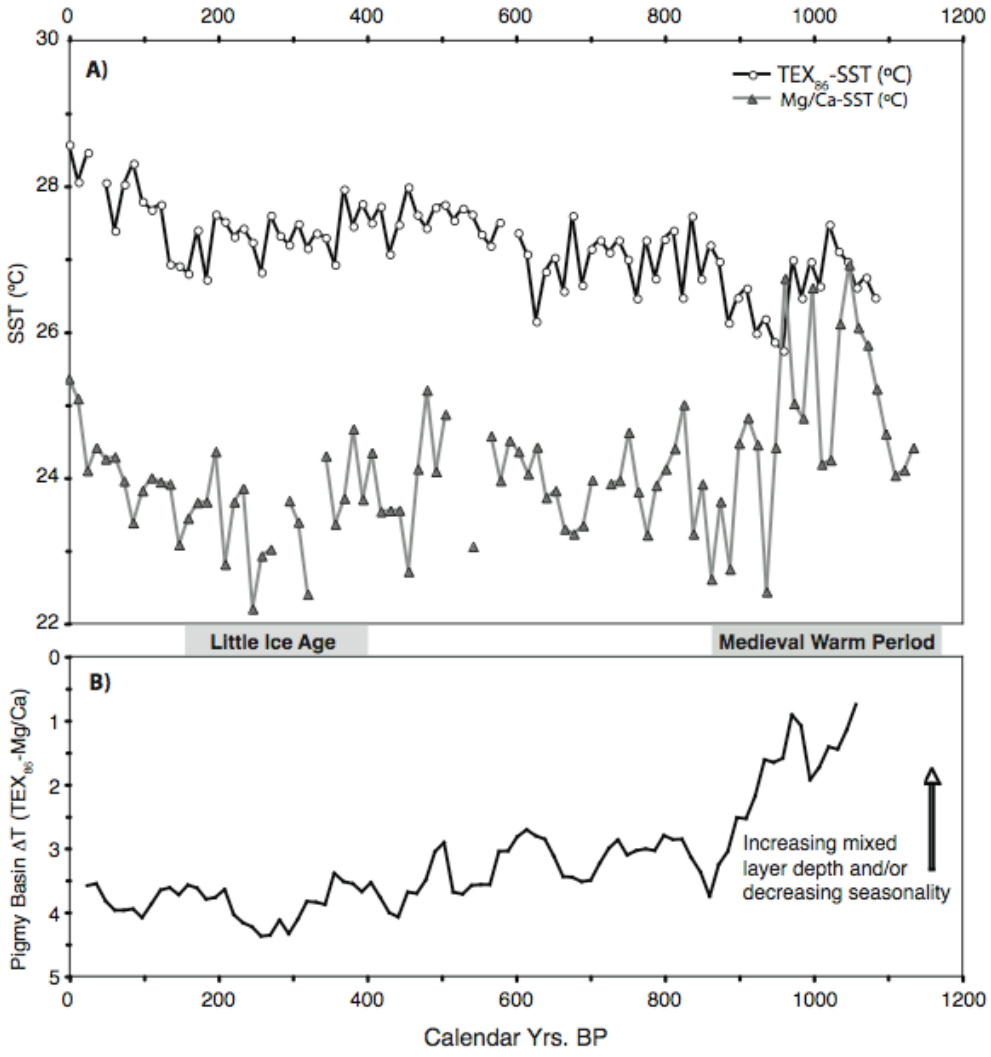

Figure 3.7. The ΔT (TEX_{86}-Mg/Ca) for the Pigmy Basin, Gulf of Mexico. A) The SST records derived from TEX_{86} (open circles) and Mg/Ca (closed circles), calibrated to SST using their independent paleotemperature equations. B) The ΔT (TEX_{86}-Mg/Ca) for the Pigmy Basin, Gulf of Mexico. The largest ΔT (>4ºC) occurs during the LIA, while minimum ΔT (<1ºC) occurs during the MWP. Note that when uncertainties associated with respective calibrations to SST and analytical errors associated with both proxies are compounded, the error of the ΔT record is ± 2ºC.

The maximum is controlled by greater cooling of Mg/Ca-SST. This implies that the LIA cooling observed in the GOM may have been dominated by enhanced winter cooling relative to summer cooling, or shoaling of the thermocline (shallow mixed layer). The minimum difference between the TEX_{86} and Mg/Ca-SST records occurs 1100-900 yrs BP, during the MWP. This implies that during this time there was a significant decrease in seasonality and/or increase in mixed layer depth.

Without seasonally resolved flux data for Crenarchaeota or *G. ruber* specific to the Gulf of Mexico, we cannot evaluate whether the differences between TEX_{86} and Mg/Ca SST estimates result from differences in seasonal or depth distribution. Figure 3.8(a-d) depicts the different scenarios by which the ΔT between the two proxies could change over time. Figures 3.8a and 3.8c depict the theoretical LIA scenarios, in which there was an especially shallow mixed layer (causing a steep thermal gradient in the upper 100 meters of the water column) or increased seasonality. In either of these scenarios we would expect the ΔT between TEX_{86} and Mg/Ca temperatures to be greater. The converse is shown in Figures 3.8b and 3.8d, where the mixed layer is deeper (causing a decreased thermal gradient in the upper water column), or decreased seasonality. In these scenarios, a smaller ΔT between TEX_{86} and Mg/Ca temperatures would be expected. It must also be recognized that the seasonal or depth preferences of either signal carrier may be influenced by some other environmental factor over the past 1,000 years, such as changes in nutrient input or salinity.

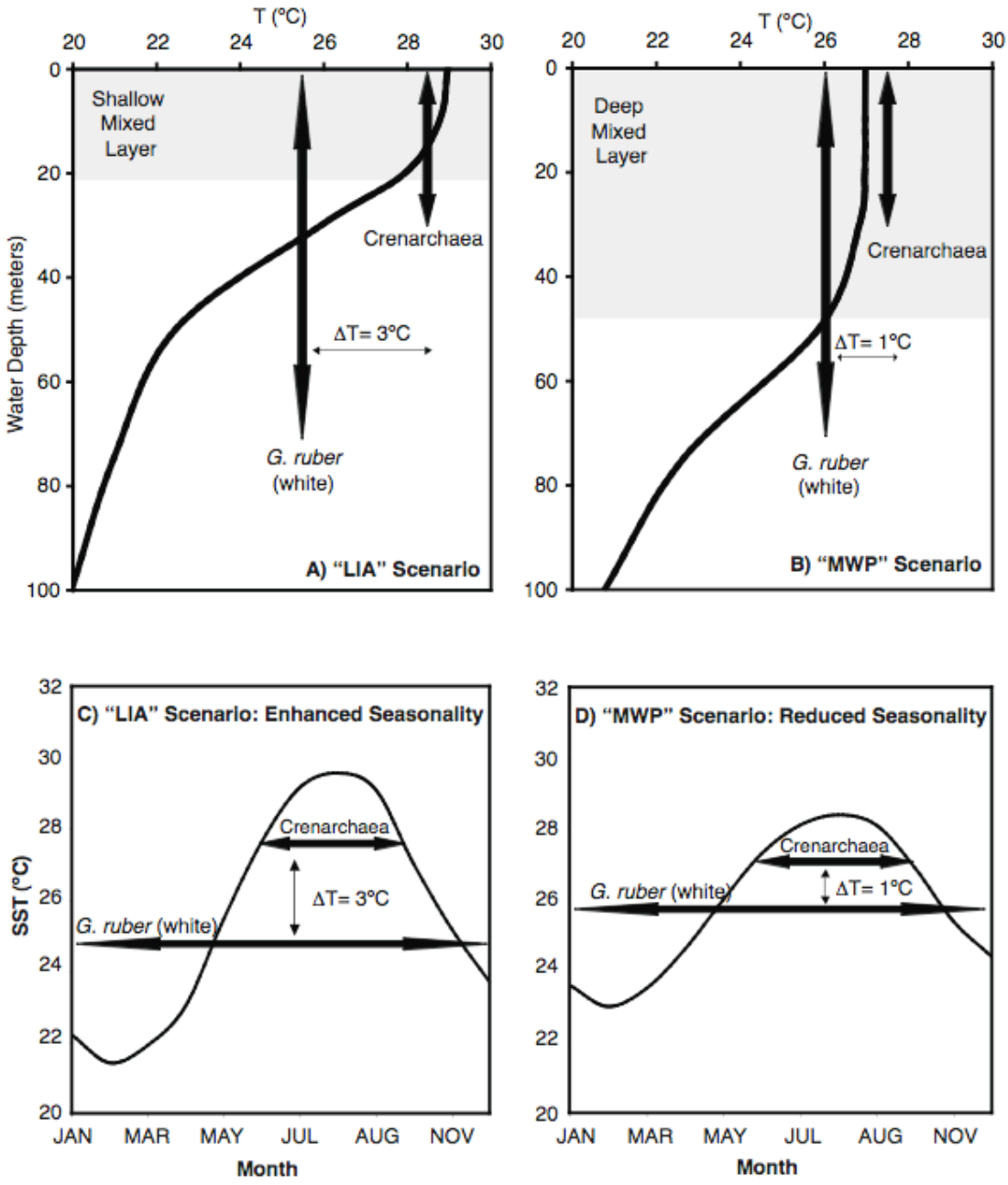

Figure 3.8. Illustrations of Mixed Layer and Seasonality Hypotheses. An illustration of the working hypotheses that A & B) the changes in ΔT (TEX_{86}-Mg/Ca) over time may be indicative of changes in the thermal gradient in the upper water column in the Gulf of Mexico and/or C & D) changes in ΔT over time may be indicative of changes in the seasonality in the Gulf of Mexico. The "LIA scenario", in which we observe the greatest ΔT, is illustrated by a steeper thermal gradient (or shallow mixed layer) in panel A, or by a greater seasonal range of SST in the Gulf of Mexico in panel C. The "MWP scenario", in which we observe the smallest ΔT, is illustrated by a reduced thermal gradient (or deeper mixed layer) in panel B, or by a reduced seasonal range in the Gulf of Mexico in panel D. Both scenarios require the assumption that the Mg/Ca and TEX_{86} signals maintain their relative depth and/or seasonal distributions throughout the past millennium.

3.11. Potential Implications for the ΔT record

The changes in ΔT between the TEX_{86} and Mg/Ca SST records in the Pigmy Basin can be interpreted in terms of changes in the amplitude of the seasonal SST cycle and/or changes in mixed layer depth. Either scenario, 1) a deepening of the mixed layer, or 2) a decreased seasonal SST variability with reduced winter cooling, would result in increased heat storage in the upper ocean on an annual basis. The Gulf of Mexico is in the path of, or the birthplace for a large number of Atlantic tropical cyclones, and thus it follows that a persistent annual build-up of heat in the upper water column may have been a factor in enhancing tropical cyclone activity in the past.

The MWP (ca. 1100-900 yrs BP) is marked by the minimum ΔT for the past 1,000 years in the Pigmy Basin, suggesting a centennial scale period in which more heat was being stored in the upper ocean. Greater heat storage in the GOM via a warm mixed layer that is thicker and/or more seasonally persistent is consistent with reconstructions of greater tropical cyclone frequency in the Atlantic basin during the MWP (Figure 3.9) (Mann et al., 2009). Maximum ΔT in the Pigmy Basin record is observed during the LIA, suggesting a period of enhanced seasonality and/or a decreased mixed layer depth. This observation is also consistent with a minimum in reconstructed tropical cyclone frequency during the LIA by Mann et al. (2009).

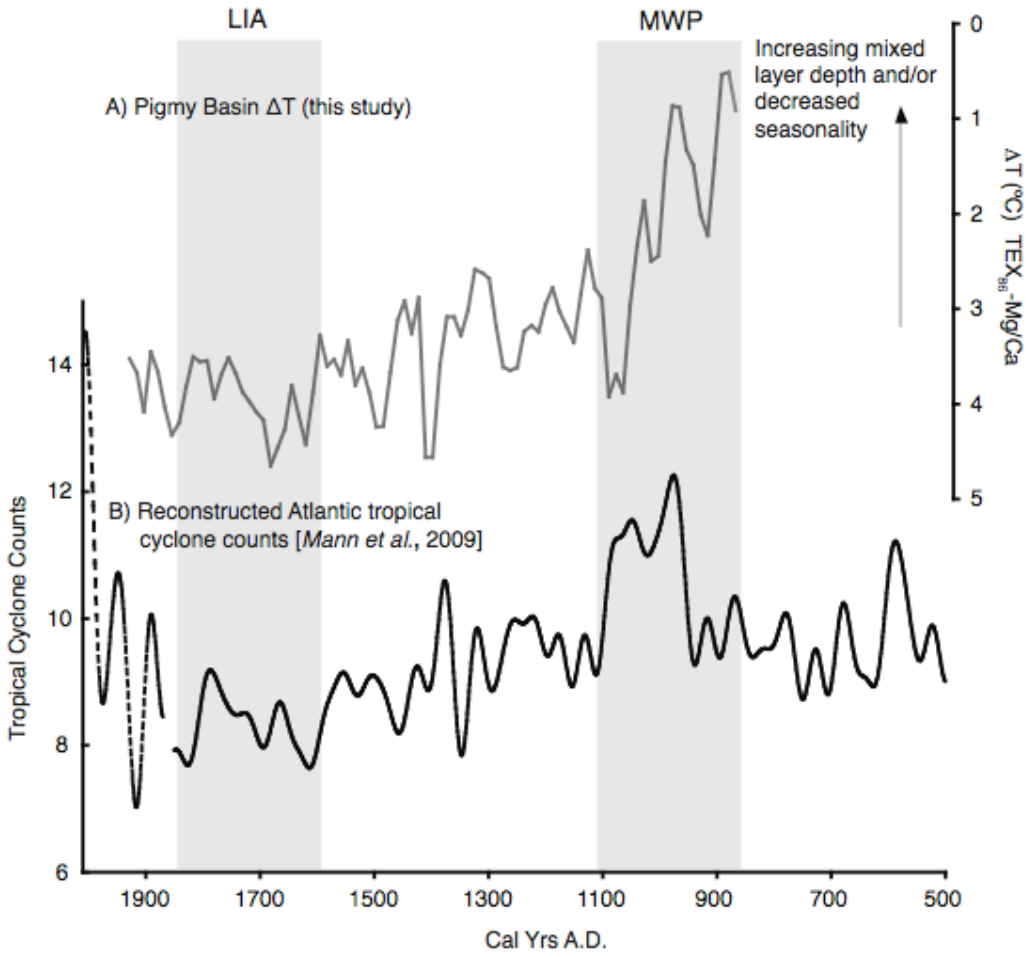

Figure 3.9. Comparison of Pigmy Basin ΔT (TEX_{86}-Mg/Ca) with a reconstruction of tropical cyclone counts. A) Grey curve is a 3-point running mean of the ΔT record from the Pigmy Basin. We interpret decreasing ΔT in terms of increasing mixed layer depth and/or decreased seasonality. B) The dashed line is a multidecadal-smoothed record of Atlantic tropical cyclone counts over the past 150 years. The solid black line is the proxy reconstructed Atlantic tropical cyclone counts based on statistical model from *Mann et al*. [2009]. The LIA is indicated by the shaded bar and highlights a minimum in reconstructed tropical cyclone counts, and a maximum ΔT. The MWP, indicated with a shaded bar, can be characterized by a maximum in reconstructed tropical cyclone counts and a minimum in ΔT.

3.12. Conclusions

We present the first comparison of a decadal resolution TEX_{86}-based SST record with a foraminiferal Mg/Ca-based SST record for the past 1,000 years from marine sediments. There are similarities in the magnitude and pattern of SST variability recorded

by TEX_{86} and Mg/Ca in co-occurring sediments of the Pigmy basin box core, especially over the past four centuries, including a substantially cooler LIA (by 1.5-2.5ºC). There are however, significant differences in the two SST records that can most likely be attributed to changes in the seasonal and/or depth distribution of crenarchaeota versus *G. ruber* (white). The core-top TEX_{86}-SST indicates that TEX_{86} in the Gulf of Mexico is a summer weighted, upper mixed layer signal, while the Mg/Ca-SST indicates that *G. ruber* are most likely living throughout the year, and/or deeper in the water column. The difference (ΔT) between the two proxy records indicates changes in seasonality and/or mixed layer depth over the past millennium with the LIA characterized by enhanced seasonality and/or a shallow mixed layer whereas the MWP was recognized by a decrease in the seasonal temperature gradient and/or a deeper mixed layer. The increased ability to store heat in the GOM surface waters during the MWP may be a link to understanding historical changes in past Atlantic tropical cyclone activity.

Chapter 4

Ecological controls on the shell geochemistry of pink and white *Globigerinoides ruber* in the northern Gulf of Mexico: Implications for paleoceanographic reconstruction

4.1. Abstract

We assess ecological controls on shell geochemistry for two of the most commonly used planktonic foraminifers for paleoceanographic reconstruction in the subtropical Atlantic Ocean: the pink and white varieties of *Globigerinoides ruber*. We evaluate the relationship between foraminiferal test size and shell geochemistry ($\delta^{13}C$, $\delta^{18}O$ and Mg/Ca) using temporally well-constrained core-top samples from the Pigmy and Garrison Basins, in the northern Gulf of Mexico. The core-top samples are from the uppermost 0.5cm of the respective box cores, and represent ~10-30 years of sedimentary deposition. For each size fraction, multiple separate analyses (2-10 aliquots) of 60 foraminifera were analyzed. Data show a significant positive relationship between Mg/Ca and test size, with a range of 1.1 mmol/mol (~2.5ºC) from the smallest (150-212μm) to largest (>500μm) size fractions of *G. ruber* (pink), but no significant relationship in *G. ruber* (white). There is a depletion in $\delta^{18}O$ of 0.26‰ per 100μm increase in test size for both pink and white *G. ruber*. The increase in Mg/Ca and decrease in $\delta^{18}O$ is consistent with an increase in calcification temperature of 0.66ºC per 100mm increase in test size. Overall, these results stress the necessity for using a consistent size fraction. In addition, we compare downcore records of $\delta^{18}O$ and Mg/Ca from both pink and white *G. ruber*, and make inferences about the relative seasonal distribution and depth habitat of the 2 varieties.

4.2. Introduction

Improving understanding of the biological, chemical and physical factors that contribute to uncertainty in foraminiferal geochemical proxies is critical to the interpretation of paleoceanographic records. The uncertainties inherent to Mg/Ca-based SST estimates can exceed the environmental signal in some cases, especially in low latitude records covering the past few millennia, when SST variability was likely small (<2ºC) relative to glacial-interglacial changes. Some sources of uncertainty in Mg/Ca-SST estimates include, but are not limited to diagenesis (e.g. Boyle 1983; Barker et al., 2003; Pena et al., 2005), salinity (e.g. Nürnberg et al., 1996; Ferguson et al., 2008; Kisakürek et al., 2008), shell heterogeneity (e.g. Eggins et al., 2004; Sadekov et al., 2008) and dissolution (e.g. Dekens et al., 2003). Each of these factors has the potential to overprint the Mg/Ca signal of the downcore record, and the influence of these factors is variable, and often basin-specific.

One issue that has been explored to some degree is the effect of foraminiferal test size on Mg/Ca (Elderfield et al., 2002; Ni et al., 2007). Elderfield et al. (2002) illustrated that there is a positive correlation between Mg/Ca and test size in a number of species of planktonic foraminifera; however it is difficult to quantify the relationship in that study due to the small number of individuals analyzed for each size fraction (~20), and insufficient temporal constraint in their sediment sample (their sample represented ~800 yrs (Elderfield et al., 2002)). Ni et al. (2007) found no relationship between test size and Mg/Ca in the white variety of *Globigerinoides ruber*, but their sample also represented multiple centuries of deposition, and they had few replicate analyses.

In this study we improve upon previous studies by presenting a temporally well-constrained data set to investigate the relationship between test size and Mg/Ca in the white and pink varieties of *G. ruber*. The 0.5cm zero-age dated core-top samples from the two high accumulation rate (40cm/kyr) basins (Pigmy and Garrison basins) in the Gulf of Mexico (GOM) represent the most recent few decades, and between 2 and 10 aliquots of 60 individual Foraminifera were analyzed for each size fraction of pink and white *G. ruber*. We propose an internally consistent explanation of the changes in three geochemical parameters with size ($\delta^{13}C$, $\delta^{18}O$ and Mg/Ca), as well as for observed offsets in the geochemistry of the pink and white varieties of *G. ruber*.

The pink and white varieties of *G. ruber* are the two most abundant foraminifers in modern GOM sediments, and when combined, make up >45% of the total assemblage, respectively (Brunner, 1979; Kennett et al., 1985; Dowsett et al., 2003). The two are morphologically very similar, are both hosts to dinoflagellate photosymbionts, and accordingly reside within the euphotic zone. Despite their similarities, we observe differences in their shell geochemistry. We compare downcore geochemical records of pink and white *G. ruber* in a high-resolution, recent sedimentary series in order to assess their relative depth and seasonal distributions.

4.3. Materials and Methods

The samples used for the size fraction study are from the core-top (top 0.5 cm) of the Pigmy Basin box core (PBBC-1; 27º11.61'N, 91º24.54'W; 2259 meters water depth), and the Garrison Basin box core (PE07-2; 26º40.5' N, 93º55.5' W; 1570 meters water depth). Each of these basins is an intraslope basin in the northern Gulf of Mexico, and

has a relatively high sediment accumulation rate (20-40 cm/kyr) due to the input of terrigenous material from the Mississippi River. For each of the box cores the sediment-water interface was recovered, and therefore the core-top samples incorporate the most recently deposited sediments. Radiocarbon dates from a mixed assemblage of planktonic foraminifera, for each of the core-top samples, reflect a modern age (< 0 after reservoir correction; Richey et al., 2007, 2009). Size fractions where separated by sieving, and between 2 and 10 different aliquots of ≥60 foraminifera were analyzed for each size fraction of both pink and white *G. ruber*.

Downcore analyses were performed on the 250-300μm size fraction of pink and white *G. ruber* from the same subcore of the Pigmy Basin box core, PBBC-1. The age model for PBBC-1, as well as the oxygen isotope and Mg/Ca records from the white variety of *G. ruber*, was previously published by Richey et al. (2007). Age control is based on 7 accelerator mass spectrometer (AMS) radiocarbon dates. The sampling interval of 0.5 cm combined with the linear sedimentation rate of 43 cm/kyr yields a sampling resolution of ~12 years.

For all elemental analyses ≥60 Foraminifera were picked from each size fraction of *Globigerinoides ruber* (white and pink). Foraminifera were lightly crushed and underwent a cleaning process that includes multiple clay removal steps, an oxidative step to remove organic material, and an acid leaching step to remove adsorbed metals (Barker et al., 2003). A reductive cleaning step was not performed on these samples. Elemental analyses were performed on a Perkin Elmer Optima 4300 dual view inductively coupled plasma-optical emission spectrometer (ICP-OES) at the College of Marine Science, University of South Florida (CMS, USF). In all cases where there are replicate Mg/Ca

analyses, replicates are based on separate aliquots of ≥60 foraminifera that have been crushed, cleaned and analyzed separately. Oxygen and carbon isotope ratios were measured on a ThermoFinnigan Delta Plus XL light stable isotope ratio mass spectrometer (SIRMS) at the CMS, USF. The $\delta^{18}O_{calcite}$ and $\delta^{13}C_{calcite}$ are reported on the VPDB scale.

4.4. Results

4.4.1. Relationship between test size and carbon isotopic composition

The positive relationship between the $\delta^{13}C$ and foraminiferal test size has been well established in number of studies using a variety of different planktonic foraminifera species across a range of oceanographic settings (e.g. Berger et al., 1978; Curry and Matthews, 1981; Oppo and Fairbanks, 1989; Ravelo and Fairbanks, 1995; Elderfield et al., 2002). Berger et al. (1978) proposed that foraminiferal $\delta^{13}C$ increases with test size as a function of ontogeny, due to the fact that metabolic rates are highest in the early ontogenetic stages (i.e. smallest individuals), and therefore are the most depleted relative to equilibrium.

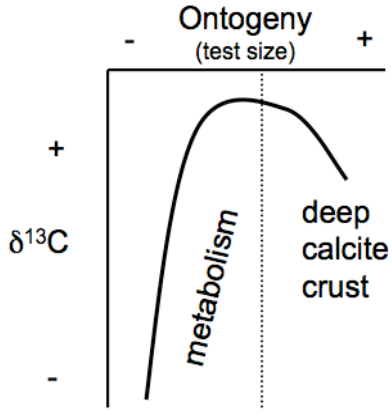

Figure 4.1. Illustration of the relationship between $\delta^{13}C$ and ontogeny in Foraminifera. This illustration was redrawn from Berger et al. (1978).

As the foraminiferan matures, the metabolic rate slows and the carbon isotopic composition of the test becomes less depleted relative to the $\delta^{13}C$ of seawater $\sum CO_2$. The formation of a deep calcite crust by mature planktonic Foraminifera accounts for the observed depletion in the largest individuals (Figure 4.1).

It has also been proposed that the increase in $\delta^{13}C$ with increasing size can be attributed to symbiont photosynthesis (Oppo and Fairbanks, 1989; Spero and Lea, 1993). Symbionts preferentially utilize ^{12}C during photosynthesis, leaving the carbon pool in the calcification microenvironment enriched with respect to ^{13}C (Spero and Williams, 1988). Photosynthetic activity increases as a function of increasing light level (Spero and Lea, 1993), and the increase in symbiotic density with advancing ontogeny (Spero and Parker, 1985). A culture study in which *O. universa* and *G. sacculifer* were grown under variable light levels revealed that the $\delta^{13}C$ of the Foraminifera was controlled by symbiont photosynthesis, rather than ontogeny. However, the observation of increasing $\delta^{13}C$ with increasing test size in non-symbiont bearing foraminifera (e.g. Ravelo and Fairbanks, 1995; Elderfield et al., 2002) suggests that symbiont photosynthesis is not the sole contributing factor to the $\delta^{13}C$-size relationship.

Our observation of the relationship between $\delta^{13}C$ and test size in white and pink *G. ruber* is consistent with previous studies. For *G. ruber* (pink) the $\delta^{13}C$ ranges from 0.5‰ in the smallest size class (150-212μm), to 2.0‰ in the largest size class (425-500μm). *G. ruber* (white) ranges from 0.3‰ in the smallest size class (150-212μm) to 1.3‰ in the largest size class (355-425μm) (Figure 4.2.a). The rate of change per increase in size slows as the forams get larger, which is consistent with a smaller

fractionation with decreasing metabolic rate. The pink variety of *G. ruber* is consistently ~0.4‰ more enriched than the white variety. The overall range in $\delta^{13}C$ from the smallest to largest individuals exceeds the downcore $\delta^{13}C$ variability over the past 1500 years in both white and pink *G. ruber*, thus emphasizing the importance of using a narrow size range for all downcore paleoceanographic studies.

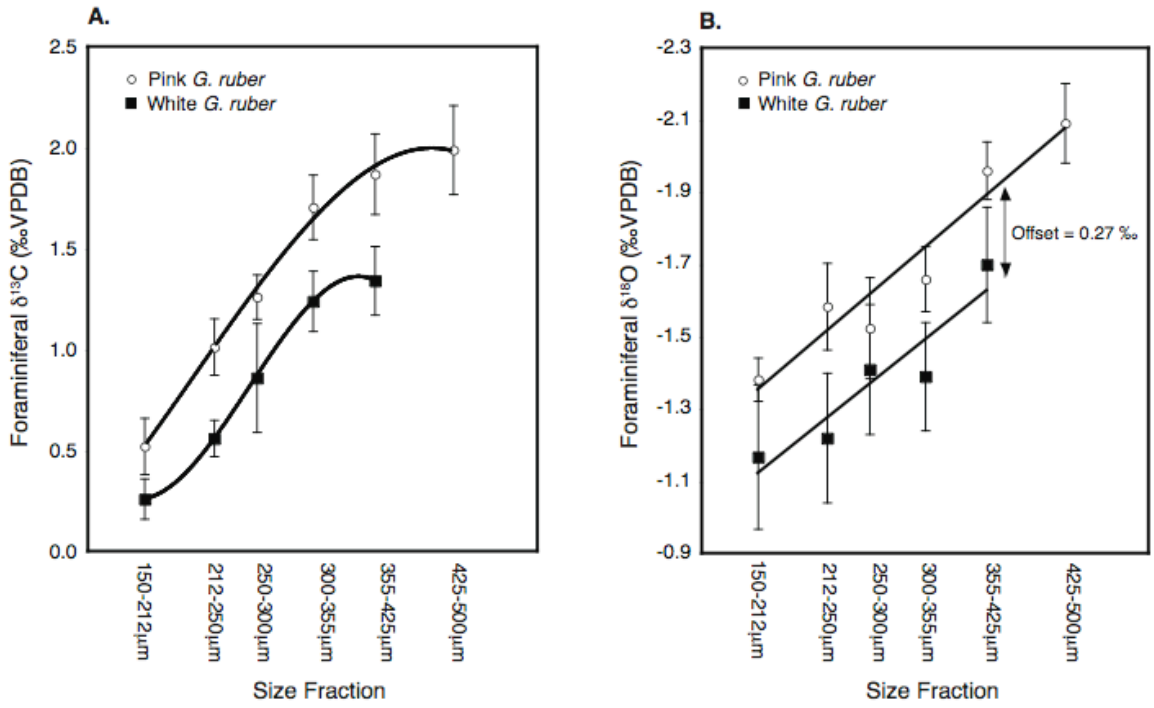

Figure 4.2. Relationship between foraminiferal test size and $\delta^{13}C$ and $\delta^{18}O$. A) The carbon isotopic composition is plotted against test size for pink (open circle) and white (square) *G. ruber*. A 3º order polynomial is fit through both data sets. B) The oxygen isotopic composition is plotted against test size for pink (open circle) and white (square) *G. ruber*. A linear least squares regression line is fit through both data sets, and they both have the same slope. The mean offset between pink and white *G. ruber* in $\delta^{18}O$ is 0.27‰. Error bars represent the standard deviation among all replicate measurements for each size fraction.

4.4.2. Relationship between test size and oxygen isotopic composition

A number of studies have investigated the relationship between $\delta^{18}O$ and size in planktonic foraminifera, however, unlike with $\delta^{13}C$, the relationship does not seem to be

systematic. Elderfield et al. (2002) found that there was a general decrease in $\delta^{18}O$ in three species of planktonic foraminifera (*Orbulina universa*, *Neogloboquadrina dutertrei*, and white *G. ruber*), but 14 other planktonic species analyzed showed either the opposite relationship, or no significant relationship at all. Ravelo and Fairbanks (1992, 1995) observed a significant decrease in $\delta^{18}O$ of *G. ruber* (white) with increasing test size, but no relationship in *G. ruber* (pink). Curry and Matthews (1981), however, looked at the relationship between $\delta^{18}O$ and test size in *G. ruber* (white), and found no significant relationship. In a culture study, Spero and Lea (1993) concluded that ontogeny did not have an effect on the shell $\delta^{18}O$ of *G. sacculifer*, but they observed a significant depletion in $\delta^{18}O$ with increasing light levels for the symbiont-bearing *O. universa* and *G. sacculifer*.

Size Fraction (μm)	n	$\delta^{18}O$ (permille)	STDEV	$\delta^{13}C$ (permille)	STDEV
150-212	4	-1.38	0.06	0.52	0.14
212-250	7	-1.58	0.12	1.01	0.14
250-300	9	-1.52	0.14	1.26	0.11
300-355	7	-1.66	0.09	1.70	0.16
355-425	8	-1.96	0.08	1.87	0.20
425-500	6	-2.09	0.11	1.99	0.22

Table 4.1. Oxygen and Carbon isotopic data for *G. ruber* (pink). Data in this table represent the mean values for all measurements in each size fraction. "n" is the total number of measurements for each size fraction, and each measurement is based on ≥60 individual Foraminifera. STDEV represents the standard deviation among replicate measurements for each size fraction.

Size Fraction (μm)	n	$\delta^{18}O$ (permille)	STDEV	$\delta^{13}C$ (permille)	STDEV
150-212	5	-1.17	0.20	0.26	0.10
212-250	7	-1.22	0.18	0.56	0.05
250-300	8	-1.41	0.18	0.86	0.27
300-355	7	-1.39	0.15	1.24	0.15
355-425	3	-1.70	0.16	1.34	0.17

Table 4.2. Oxygen and Carbon isotopic data for *G. ruber* (white). Data in this table represent the mean values for all measurements in each size fraction. "n" is the total number of measurements for each size fraction, and each measurement is based on ≥60 individual Foraminifera. STDEV represents the standard deviation among replicate measurements for each size fraction.

Our results indicate that $\delta^{18}O$ decreases with increasing test size in both white and pink *G. ruber* (Figure 4.2.b). In the white variety the $\delta^{18}O$ of foraminiferal calcite decreases from -1.1‰ from the smallest individuals (150-212μm) to -1.6‰ in the largest individuals (355-425μm), while pinks range from -1.4‰ in the smallest size class (150-212μm) to -2.0‰ in the largest size class (425-500μm). A least-squares linear regression through the mean $\delta^{18}O$ values for each size fraction indicates a significant negative correlation between $\delta^{18}O$ and size for both pink and white *G. ruber* (r^2= 0.94 and 0.84, respectively). The slopes of the relationships are nearly identical for pink and white *G. ruber*, and indicate a 0.26‰ decrease in $\delta^{18}O$ per 100μm increase in size. There is a consistent offset between pink and white *G. ruber* in which the pink variety is depleted by ~0.27‰ relative to the white.

4.4.3. Relationship between foraminiferal test size and Mg/Ca

In *G. ruber* (pink) there is a significant increase in Mg/Ca with increasing test size from 150μm to >500μm (Figure 4.3.a). The overall range in Mg/Ca from the smallest size (150-212μm) to the largest size (>500μm) is 1.1 mmol/mol. This corresponds to an

SST difference of 2.5ºC from the smallest to largest size fraction based on the Mg/Ca paleotemperature equation for *G. ruber* (pink):

(1) Mg/Ca=0.38exp(0.09*T) from Anand et al. (2003)

A temperature range of 2.5ºC exceeds the range of SST variability expected for most late Holocene records. The increase in Mg/Ca with test size appears to be linear, with a positive slope of 0.27 mmol/mol (0.66ºC) per 100μm increase in test size. The Mg/Ca values for the 250-300μm and 300-355μm size fractions are not significantly different from each other, and have Mg/Ca values (mean=4.3±0.02mmol/mol) that correspond to the modern summer-weighted (April-October) SST for the Gulf of Mexico (27.0ºC), when calibrated using equation (1).

This exercise was repeated for a second depth interval (320-325mm, 650 yrs B.P.) in the Pigmy Basin box core (PBBC-1) in order to test whether the relationship between test size and Mg/Ca is stationary through time. The interval ca. 650 yrs B.P. was 2ºC colder than the modern core-top in the downcore record, as indicated by the Mg/Ca-SST from the 250-300μm size fraction of *G. ruber* (white) (Richey et al., 2007). Figure 4.3.b illustrates a nearly identical slope of the size-Mg/Ca relationship for the both the modern core-top sample and for the sample at 650 yrs B.P., indicating that the increase in Mg/Ca with test size is a robust relationship, even under different climatic conditions. The fact that each size fraction from the interval 650 yrs B.P. is consistently offset ~2ºC cooler than the corresponding size from the modern core-top SST, further corroborates the 2ºC cooling observed in the downcore record. It is also worth noting that there were no *G. ruber* (pink) in the >500μm size fraction for the 650 yrs B.P. sample, while there were

more than 60 individuals in the >500μm size fraction in the core-top sample. This supports the hypothesis that Foraminifera grow larger under warmer conditions.

Size Fraction (μm)	*n*	Mg/Ca (mmol/mol)	STDEV	SST (°C)
150-212	5	4.00	0.32	26.1
212-250	5	4.19	0.19	26.7
250-300	10	4.35	0.23	27.1
300-355	7	4.37	0.19	27.1
355-425	7	4.57	0.30	27.6
425-500	6	4.83	0.27	28.2
>500	1	4.92	n/a	28.5

Table 4.3. Mg/Ca data versus size for *G. ruber* (pink). The data listed in this table represent the midpoint of n measurements made for each size fraction, where n is the number of replicate measurements for each size fraction. STDEV is the standard deviation among the n replicate measurements. The SSTs listed are calibrated using the equation for *G. ruber* (pink), Mg/Ca=0.38exp(0.09*SST) (Anand et al., 2003).

Size Fraction (μm)	*n*	Mg/Ca (mmol/mol)	STDEV	SST (°C)
150-212	5	4.36	0.10	25.2
212-250	6	4.29	0.27	25.1
250-300	8	4.32	0.16	25.2
300-355	5	4.30	0.22	25.1
355-425	2	4.73	0.19	26.2

Table 4.4. Mg/Ca data versus size for *G. ruber* (white). The data listed in this table represent the midpoint of n measurements made for each size fraction, where n is the number of replicate measurements for each size fraction. STDEV is the standard deviation among the n replicate measurements. The SSTs listed are calibrated using the equation for *G. ruber* (white), Mg/Ca=0.449exp(0.09*SST) (Anand et al., 2003).

The relationship between test size and Mg/Ca is not as clear in the white variety of *G. ruber*. In our samples, *G. ruber* (white) is not abundant enough in the >425μm size fractions to make a Mg/Ca measurement. The four size fractions between 150 μm and 355 μm (150-212μm, 212-250μm, 250-300μm and 300-355μm) have the same Mg/Ca value of 4.32mmol/mol (within the analytical error) (Figure 4.3.a). The Mg/Ca value of

the largest size fraction, 355-425 μm, does increase significantly, by 0.41 mmol/mol, consistent with the increase in Mg/Ca for this size fraction in pink *G. ruber*. Each of the size fractions between 212μm and 425μm in *G. ruber* (white) falls, within 1σ error, on the trend line relating Mg/Ca to test size for *G. ruber* (pink). However, looking at the test size vs. Mg/Ca data for just the *G. ruber* (white) data, there is no significant relationship between Mg/Ca and size.

4.5. Discussion of Size Fraction Data

Unlike the positive test size-$\delta^{13}C$ relationship that has been observed for nearly all species of planktonic Foraminifera investigated (e.g. Curry and Williams, 1981; Ravelo and Fairbanks, 1995; Elderfield et al., 2002), the relationship between test size and the Mg/Ca and $\delta^{18}O$ parameters varies between positive, negative and no relationship for a variety of planktonic Foraminifera (e.g. Curry and Matthews, 1981, Elderfield et al., 2002; Ni et al., 2007). Spero and Lea (1993) concluded from analysis of individual chambers that ontogeny has no significant effect on shell $\delta^{18}O$ in two species of symbiont-bearing planktonic Foraminifera (*O. universa* and *G. sacculifer*), therefore changes in metabolic rate are not likely to be the cause of $\delta^{18}O$-size relationships. Likewise, in a study of intra-test Mg/Ca variability in *Globigerinoides ruber*, Sadekov et al. (2008) found no significant differences in the mean Mg/Ca values of the different chambers within a single test. This finding suggests that changing metabolic rates as a foraminiferan grows does not have a significant effect on shell Mg/Ca.

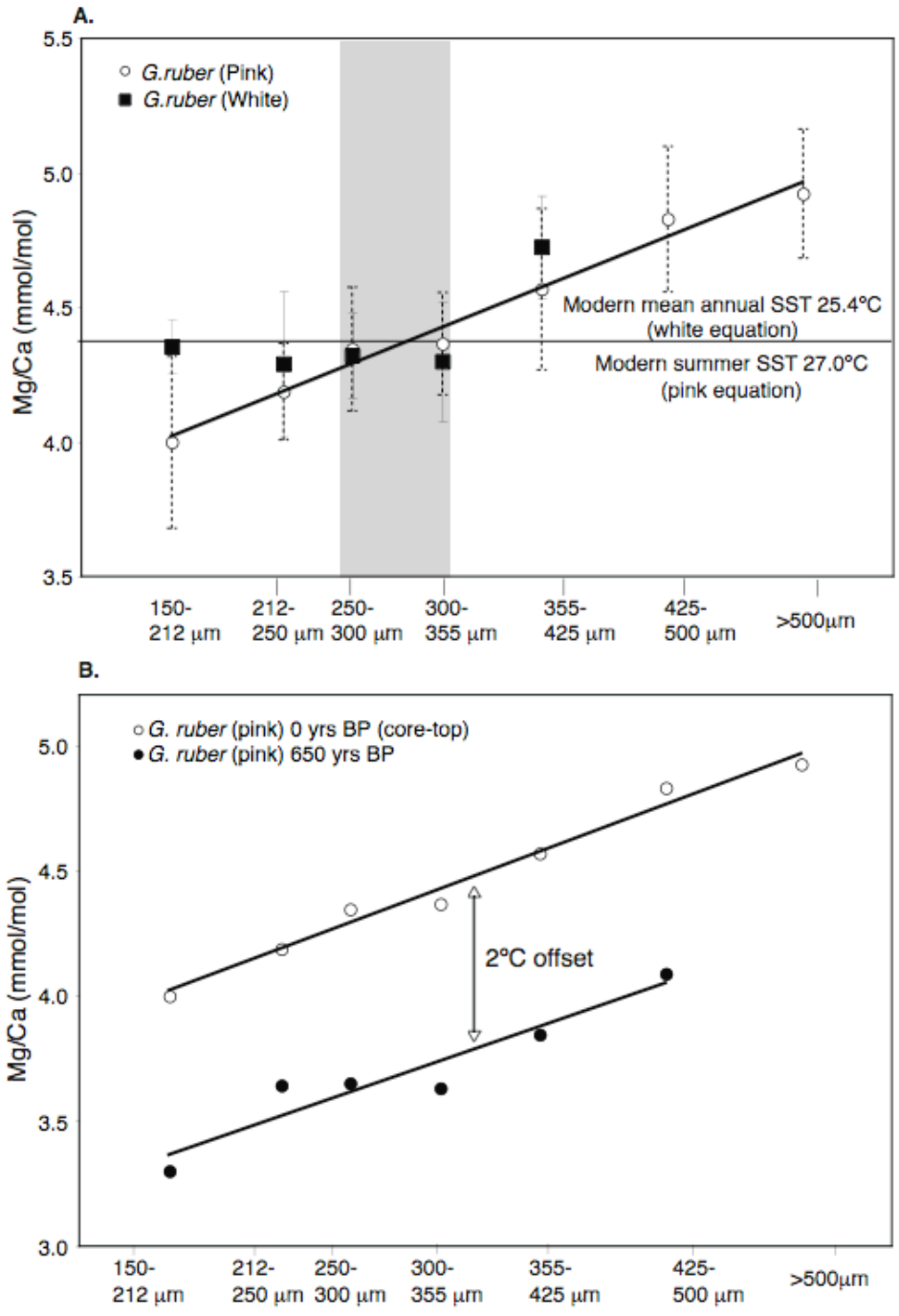

Figure 4.3. Relationship between Mg/Ca and test size. A) Mg/Ca is plotted against test size for pink (open circles) and white (black squares) *G. ruber*. Error bars represent standard deviation among replicate measurements. A linear least squares regression is plotted through the data for *G. ruber* (pink). There is no significant relationship in *G. ruber* (white), but the values for *G. ruber* (white) are not significantly different from the values for *G. ruber* (pink). B) Size versus Mg/Ca for *G. ruber* (pink) is plotted from two different depths in the Pigmy Basin box core. The slope of the relationship is identical in the two different samples, and there is a 2ºC offset, which is consistent with the downcore Mg/Ca that suggests that SST was 2ºC cooler 650 yrs BP.

We hypothesize that changes in Mg/Ca and $\delta^{18}O$ with test size observed for *G. ruber* in this study reflect differences in calcification temperature among the different size fractions. The increase in Mg/Ca and decrease in $\delta^{18}O$ with increasing test size is consistent with larger individuals calcifying in warmer waters than smaller individuals. In a culture experiment Spero and Lea (1993) demonstrated that the two symbiont-bearing foraminifers, *O. universa* and *G. sacculifer*, grow significantly larger under "high light" culture conditions than "low light" culture conditions. They also found that foraminiferal $\delta^{18}O$ decreased with increasing light-levels, most likely as a result of increased symbiont photosynthesis. In the marine environment, the highest-light conditions are found at shallow depths in the water column or during the summer season, so it follows that size fractions in *G. ruber* may vary in their depth/seasonal distribution in the GOM.

We established that the increase in Mg/Ca with size was equivalent to a 0.66ºC increase in calcification temperature per 100μm increase in test size, with a total range of 2.5ºC among the size fractions of *G. ruber* (section 4.4.3.). The vertical temperature gradient in the upper 50 meters of the water column in the GOM is ~4ºC, and the seasonal range in mixed layer (0-30 meters) temperature is ~7ºC (Figure 4.5). Therefore, if we adopt the working hypothesis that the Mg/Ca change we observe with test size is a function of calcification temperature, it is reasonable to assume that the range in calcification temperatures observed could result from differences in depth and/or seasonal distribution of the different sized Foraminifera.

In order to assess whether the change in Mg/Ca-based calcification temperature with size is consistent with $\delta^{18}O$-based calcification temperatures,, we use the following paleotemperature equation to convert $\delta^{18}O$ to temperature,

$$T=16.5-4.80* (\delta^{18}O_c- \delta^{18}O_{sw}) \qquad (2)$$

Where T is temperature (ºC), $\delta^{18}O_c$ is the measured $\delta^{18}O$ of foraminiferal calcite, and $\delta^{18}O_w$ is the oxygen isotopic composition of seawater (converted from the VSMOW scale to VPDB by subtracting 0.27‰). Equation (2) is the paleotemperature equation developed for *Orbulina universa* under "high-light" culture conditions by Bemis et al. (1998), and has been determined to be appropriate for use in *G. ruber* (Thunell et al., 1999). If we assume a constant $\delta^{18}O_w$ of 0.7‰ for the Gulf of Mexico mixed layer, the increase in $\delta^{18}O$-calcification temperature with size is equal to a 1.3ºC increase in temperature for each 100μm increase in test size for both pink and white *G. ruber*. This is twice as large as the temperature change with test size predicted from Mg/Ca in this study. However, if we assume a decrease in $\delta^{18}O_w$ of 0.06‰ with each larger test size (i.e. we assume a $\delta^{18}O_w$ of 0.7‰ for the 150-212μm size fraction, decreasing to 0.37‰ for the 425-500μm size fraction), then the estimated increase in calcification temperature with increasing size is equivalent using both Mg/Ca and $\delta^{18}O$ paleotemperature equations. This change in $\delta^{18}O$ over the range of sizes is equivalent to the change in $\delta^{18}O$ expected over the upper 50 meters of the water column, or over the annual cycle in the Gulf of Mexico.

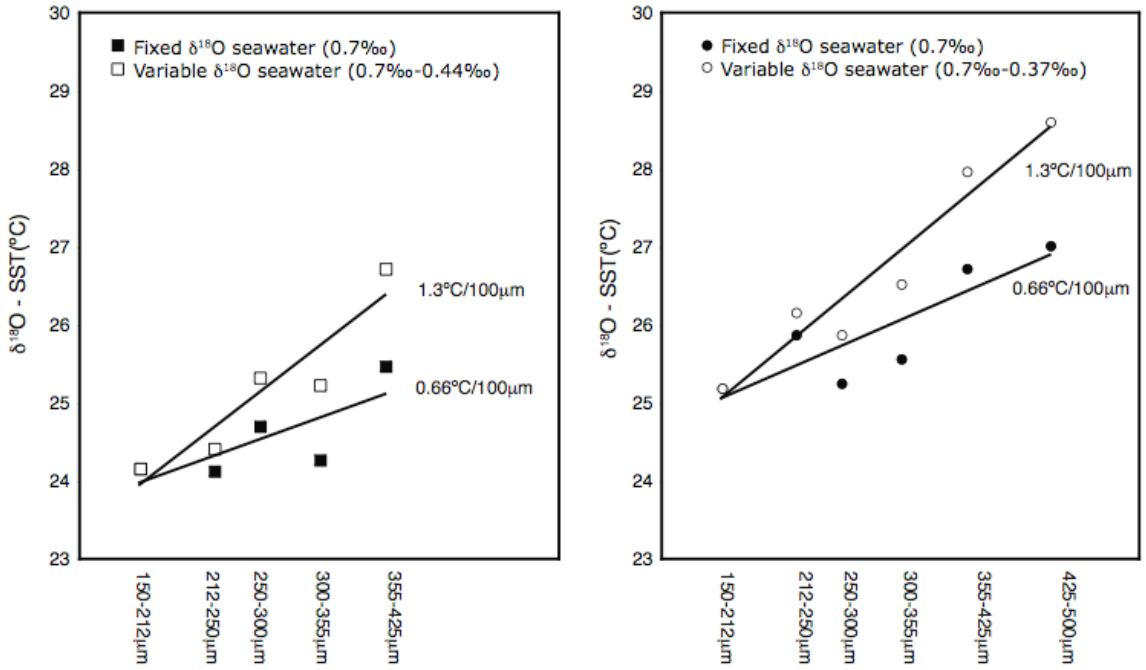

Figure 4.4. Conversion of $\delta^{18}O_{calcite}$ to calcification temperature. A) $\delta^{18}O_c$ data for *G. ruber* (white) is converted to calcification temperature using the paleotemperature equation for *Orbulina universa* "high-light" from Bemis et al. (1998): T=16.5-4.80* ($d^{18}O_c$- $d^{18}O_{sw}$). The $\delta^{18}O_c$ data are converted to SST using a fixed $\delta^{18}O_{sw}$ value of 0.7‰ for each size fraction (open squares), and using a variable $\delta^{18}O_{sw}$ (solid squares). For the variable $\delta^{18}O_{sw}$, a value of 0.7‰ is assigned to the smallest size fraction (150-212mm) and the $\delta^{18}O_{sw}$ is decreased by 0.07‰ for each subsequent size fraction. B) The same calculation is performed for *G. ruber* (pink). When the $\delta^{18}O_{sw}$ is fixed at 0.7‰, the resulting change in calcification temperature with size is 1.3ºC increase per 100µm increase in size. When the variable $\delta^{18}O_{sw}$ is used, the result is a change in calcification temperature of 0.66ºC per 100µm increase in size.

Since $\delta^{18}O_c$ is a function of both calcification temperature and the oxygen isotopic composition of ambient seawater, we convert $\delta^{18}O_c$ to calcification temperature again, but this time assuming a decrease of 0.07‰ in $\delta^{18}O_w$ for each larger size fraction (i.e. the 150-212µm size fraction calcifies in seawater with a $\delta^{18}O$ of 0.7‰, while the 212-250µm size fraction calcifies in 0.63‰ seawater, and so on). With this assumed change in $\delta^{18}O_w$, the increase in calcification temperature is equal to 0.66ºC per 100mm increase in test size. This is equivalent to the increase in calcification temperature with size estimated by Mg/Ca in this study.

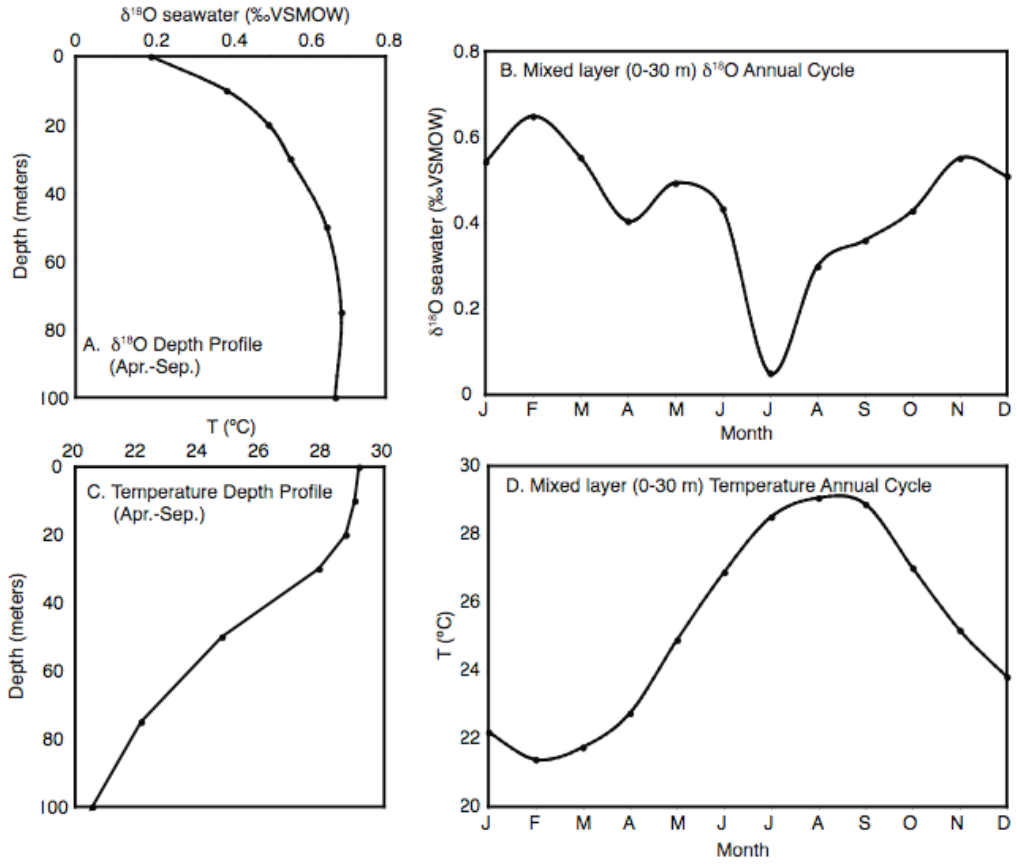

Figure 4.5. Vertical profiles and seasonal cycles of temperature and $\delta^{18}O_{sw}$ variability in the GOM. A) Summer-weighted (April-September) vertical profile of $\delta^{18}O_{sw}$ inferred from salinity data in the GOM. B) Seasonal cycle of mixed layer (upper 30 meters) $\delta^{18}O_{sw}$ inferred from salinity in the GOM. The $\delta^{18}O_{sw}$ was calculated from salinity data from the Levitus (2004) data set, using the equation: $\delta^{18}O_{sw}$= 0.557*salinity-19.98. C) Summer-weighted (Apr.-Sep.) vertical temperature profile for the GOM. D) Seasonal cycle of mixed layer (upper 30 meters) temperature for the GOM. Temperature data are also from the Levitus (2004) data set.

4.6. Comparison of downcore geochemical records for pink and white *G. ruber*

Relative offsets in the Mg/Ca and $\delta^{18}O$ of pink and white *G. ruber* have been exploited in downcore records to make inferences about changing seasonality in the past (e.g. Williams et al., 2009). This is based on the premise that *G. ruber* (white) reflects mean annual sea-surface conditions, while the geochemical signal from *G. ruber* (pink) is summer-weighted. We compare near-modern core-top data with Gulf of Mexico climatologic data to make inferences about depth/seasonal habitat preferences for pink

and white *G. ruber*. Comparison of the downcore oxygen isotopic and Mg/Ca records of pink and white *G. ruber* from a high resolution sedimentary record spanning the past 1500 years provides additional insights into the differences between the two sub-species of *G. ruber*.

White and pink *G. ruber* are the two most abundant species of planktonic Foraminifera in the Gulf of Mexico assemblages, comprising >45% of the total assemblage in core-top sediments (Kennett, 1985). Both live in tropical to sub-tropical surface waters, and are confined to the euphotic zone by their photoautotropic dinoflagellate symbionts. Sediment trap data from twenty global sites suggest the optimum SST range for *G. ruber* (white) is 22-31°C, while *G. ruber* (pink) has a more limited ideal range of 23-30°C (Žarić et al., 2005). Plankton tow data from the Sargasso Sea reveal that white and pink *G. ruber* are most commonly found in SSTs ranging from 18-26°C, with highest concentrations seen at 23-27°C. The pink variety is found at even warmer temperatures up to 28°C (Bé and Hamlin, 1967).

Modern depth preferences of planktic Foraminifera such as *G. ruber* have been studied extensively in the Sargasso Sea, yet little work has focused on GOM. Plankton tow results taken in November 1975 in the Sargasso Sea suggest that white *G. ruber* is commonly present in the top 100 m while the pink variety is found at low concentrations up to 200 meters (Fairbanks et al., 1980). Monthly plankton tows also from the Sargasso Sea showed that white and pink *G. ruber* were most abundant in the top 10 meters (Tolderlund and Bé, 1971). A single tow in April 1980 in the western GOM revealed that the *G. ruber* (white) is present from 0-50 meters water depth, while the less abundant pink *G. ruber* is found slightly deeper from 25-50 meters (Bé, 1982).

From the limited sediment trap data available for the subtropical Atlantic Ocean, white and pink *G. ruber* appear to have distinct seasonal distributions. Sediment-trap data from the Sargasso Sea indicate that *G. ruber* (white) is present in high abundance throughout the year (with fluxes >50 tests m^{-2} day^{-1} during all months) (Deuser et al., 1981; Deuser, 1987; Deuser and Ross, 1989), suggesting that *G. ruber* (white) is representative of mean annual sea-surface conditions in the sediment record. Data indicate that *G. ruber* (pink) exhibits peak abundances from April-October (with fluxes of >5 tests m^{-2} day^{-1}), and fluxes drop to nearly 0 during the winter (December-April). A recent sediment trap study in the GOM (January-December 2008) (Tedesco et al., 2009) shows that white *G. ruber* (white) is present throughout the year (although in much lower abundances than in corresponding core-top sediments). The flux of *G. ruber* (pink) in the GOM sediment trap study is broadly consistent with the Sargasso Sea data, such that fluxes are low (near zero) during the coldest months (December-April), while maximum fluxes occur during the summer months (July-September).

4.6.1. Comparison of white and pink Mg/Ca records

A Mg/Ca record was generated from the 250-300μm size fraction of *G. ruber* (pink) for comparison with the previously published Mg/Ca record from white *G. ruber* (Richey et al., 2007) from the Pigmy Basin. The raw downcore Mg/Ca values, as well as the overall pattern of variability are nearly identical (±0.23 mmol/mol) for both pink and white *G. ruber* records. Centennial scale features, such as a 1.1 mmol/mol increase in Mg/Ca from ca. 300 yrs B.P. to the 20th century, are present in both records. Additionally, the abrupt transition from elevated Mg/Ca values that occurs ca. 950 yrs

B.P., as well as the 3 multi-decadal intervals of elevated Mg/Ca that occur between 1000 and 1400 yrs B.P., are present in both the pink and white *G. ruber* records. This indicates that the original Mg/Ca record from white *G. ruber* is highly reproducible from a second surface dwelling species from the same box core.

Anand et al. (2003) determined that the temperature dependence (i.e. the exponential constant of the Mg/Ca paleotemperature equation) was approaching 9% increase in Mg/Ca per 1ºC for nearly all planktonic foraminifers in their study. However the pre-exponential constants were determined to be different among species. Therefore, using the respective Mg/Ca paleotemperature equations for pink and white *G. ruber* results in a downcore SST record in which the variability is the same, but the *G. ruber* (pink) is consistently 1.8ºC warmer than the *G. ruber* (white) record (Figure 4.6.a). If the assumption is made that there is a real difference in the distribution coefficient for Mg/Ca between white and pink *G. ruber*, the results suggest that *G. ruber* (pink) is consistently calcifying at significantly warmer SSTs than *G. ruber* (white) over the past 1400 years. This may be attributed to a seasonal distribution for *G. ruber* (pink) that is weighted toward warmer months of the year, or *G. ruber* (pink) may be living at a shallower depth in the water column than *G. ruber* (white).

In order to test whether a consistent 1.8ºC offset between the white and pink *G. ruber* downcore records can be attributed to differences in seasonal distribution, we compared the core-top Mg/Ca-SST of pink and white *G. ruber* with monthly instrumental data for the Gulf of Mexico. The mean annual SST for the Gulf of Mexico is 25.4ºC, while the mean summer SST (April-October) is 27.0ºC (Levitus, 2004). The downcore Mg/Ca records for pink and white *G. ruber* vary in step, with *G. ruber* (pink) consistently

recording 1.8ºC warmer SSTs when their respective paleotemperature equations are used. Therefore, this interpretation of differing seasonal distribution leads to the inference that the climatic variations observed in this 1400-year record indicate mean state changes, and not changes in seasonality.

Alternatively, the 1.8ºC offset between white and pink *G. ruber* could be explained by a difference in mean depth habitat. The mean temperature gradient across the upper 50 meters of the water column from April-October (when the upper 50 meters of the water column in the northern Gulf of Mexico are not fully mixed) is ~4ºC (Levitus, 2003). Therefore it is plausible that *G. ruber* (pink) could be consistently calcifying at shallower depths than *G. ruber* (white), thus producing a downcore Mg/Ca-SST record that is weighted 1.8ºC warmer. Our conclusion from this exercise is that it is possible to explain a consistent 1.8ºC offset by either differences in preferred season or depth habitat.

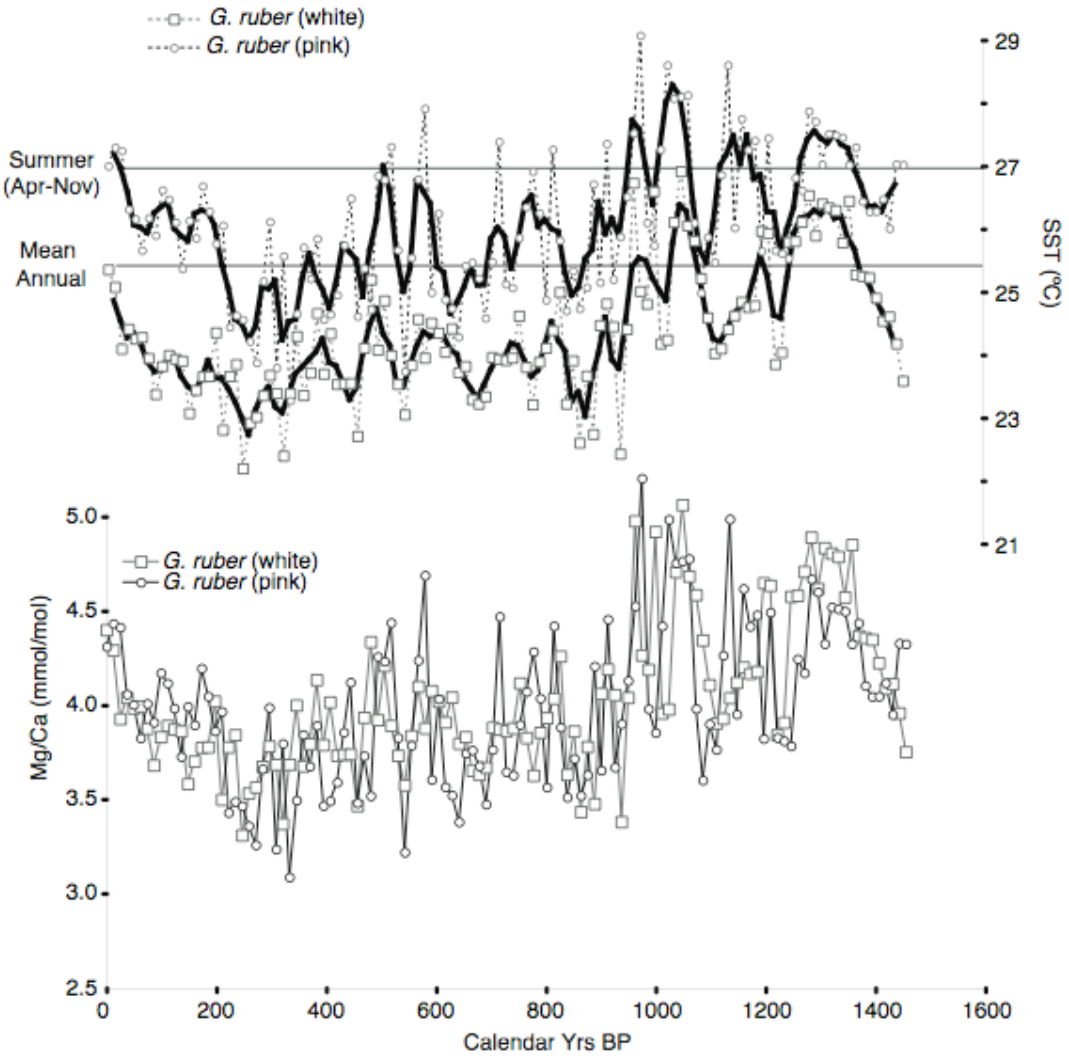

Figure 4.6. Downcore comparison of Mg/Ca records for white and pink *G. ruber*. A) Pink and white *G. ruber* Mg/Ca records are calibrated using their respective paleotemperature equations [Mg/Ca= 0.38exp(0.09*SST), and Mg/Ca=0.449exp(0.09*SST) from Anand et al., (2003)]. The mean summer (Apr-Nov) SST and mean annual SST are indicated. B) Raw Mg/Ca records for pink and white *G. ruber* are plotted.

4.6.2. Comparison of downcore $\delta^{18}O$ data

The $\delta^{18}O$ of foraminiferal calcite is a function of both calcification temperature, and the oxygen isotopic composition of ambient seawater. Unlike the raw Mg/Ca records of pink and white *G. ruber*, the $\delta^{18}O_{calcite}$ records do not covary. The major difference between the two $\delta^{18}O_{calcite}$ records occurs when there are excursions to more enriched $\delta^{18}O_{calcite}$ in white *G. ruber* record. During these excursions of increased $\delta^{18}O_{calcite}$ in white *G. ruber*, (ca. 1000 yrs B.P., 600 yrs BP, etc.) the pink *G. ruber* $\delta^{18}O_{calcite}$ record actually records a depletion in $\delta^{18}O_{calcite}$ (Figure 4.7). When the $\delta^{18}O_{calcite}$ record of *G. ruber* (white) is converted to a $\delta^{18}O_{seawater}$ record by removing the temperature effect on the $\delta^{18}O_{calcite}$ record (using equation 2) those excursions to more enriched $\delta^{18}O_{calcite}$ are dominated by increases in the $\delta^{18}O_{seawater.}$ The first $\delta^{18}O_{seawater}$ excursion occurs during a warm period (as recorded by the Mg/Ca-SST of both pink and white *G. ruber*), while the second excursion occurs during an SST minimum in the Mg/Ca records. Interestingly the % abundance of both pink and white *G. ruber* drop to their lowest over the 1500-year record (to <5% and <10%, respectively) during these inferred high-salinity excursions. This is consistent with other studies in the Gulf of Mexico that show large drops in *G. ruber* abundance during high salinity events (LoDico et al., 2006).

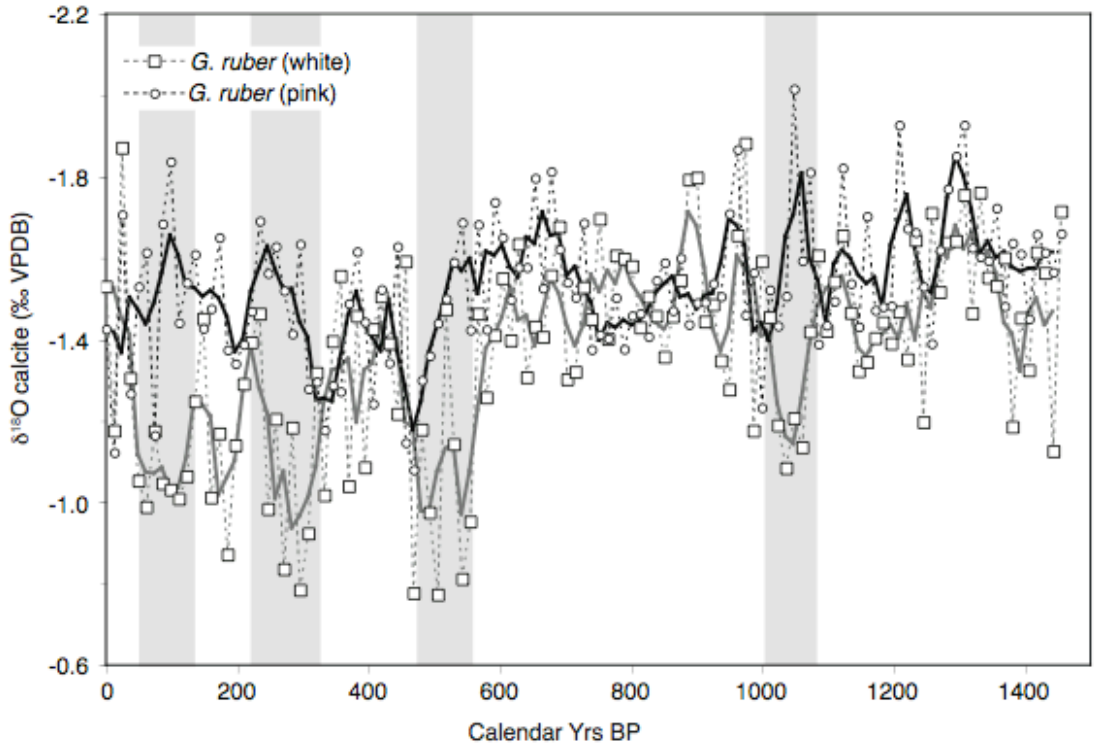

Figure 4.7. Downcore comparison of $\delta^{18}O$ data for white and pink *G. ruber*. Downcore raw Mg/Ca is indicated by dashed lines, and multi-decadal smoothed record is illustrated with solid lines. Shaded bars indicate intervals of high salinity.

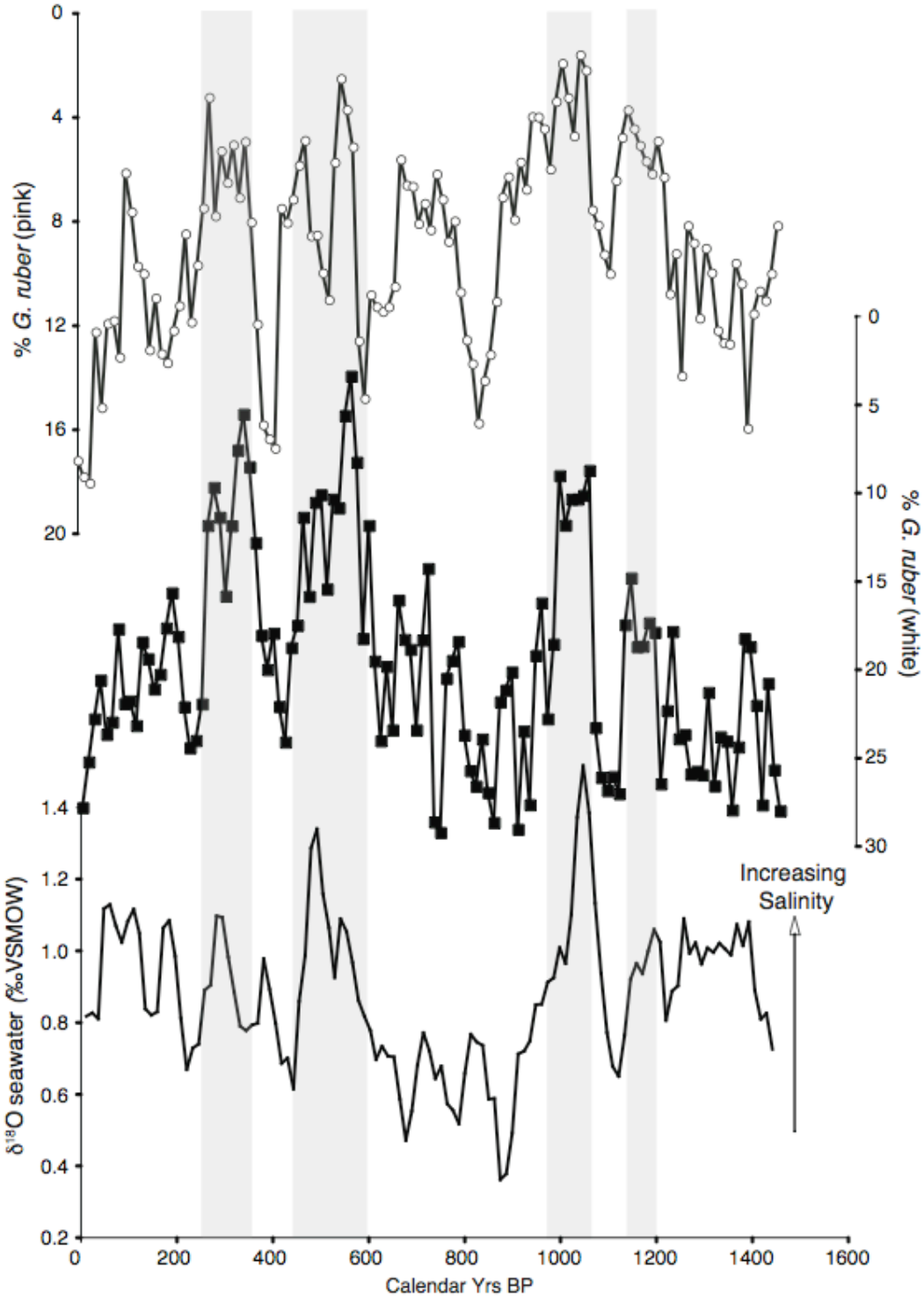

Figure 4.8. Comparison of *G. ruber* abundance with GOM salinity. A) % abundance for *G. ruber* (pink). B) % abundance for *G. ruber* (white). C) $\delta^{18}O$ seawater record for Pigmy Basin (Richey et al., 2007). $\delta^{18}O$ seawater record in panel C. was generated using paired Mg/Ca-$\delta^{18}O$ measurements on the 250-300μm size fraction of the *G. ruber* (white), and using equations (1) and (2).

4.7. Conclusions

This study presents a detailed assessment of the relationship between foraminiferal test size and geochemical parameters commonly used for paleoceanographic reconstruction (i.e. $\delta^{13}C$, $\delta^{18}O$ and Mg/Ca) in the pink and white varieties of *G. ruber*. A systematic relationship between foraminiferal test size and either $\delta^{18}O$ or Mg/Ca has not been demonstrated in previous studies. However, this study finds a significant decrease in $\delta^{18}O$, and a significant increase in Mg/Ca with increasing test size for pink and white *G. ruber*. We hypothesize that these relationships are the result of larger individuals calcifying at higher temperatures then smaller individuals. An increase in calcification temperature of 0.66ºC per 100μm increase in size is found when both Mg/Ca and $\delta^{18}O$ data are converted to temperature using their respective paleotemperature equations, providing an internally consistent explanation for these observations. The proposed increase in calcification temperature with increasing test size is likely the result of differences in the seasonal and/or depth distribution of different size fractions (i.e. white and pink *G. ruber* grow larger during the summer and/or at depths closest to the surface). The overall range of calcification temperature (~2.5ºC) over the entire range of size fractions is reasonable, given the seasonal range of temperature and/or the thermal gradients in the mixed layer for the northern Gulf of Mexico.

Although many studies suggest that ontogeny plays a role in the $\delta^{13}C$-size relationship, the enrichment in ^{13}C that we observe with increasing size is also consistent with a symbiont photosynthesis influence on the increase in $\delta^{13}C$ with size. Larger individuals living at shallower depths and/or with a warmer seasonal bias, would lead to

enhanced symbiont photosynthesis with increasing size, resulting in increasing ^{13}C enrichment with increasing size.

This study also presents a downcore comparison of a decadal resolution $\delta^{18}O$ and Mg/Ca records for white and pink *G. ruber* from co-occurring sediments in the Pigmy Basin. Results indicate an offset in the raw $\delta^{18}O$ of pink and white *G. ruber*, while the raw Mg/Ca of the two records is identical within analytical error. Using a $\delta^{18}O$-paleotemperature equation indicates that the average $\delta^{18}O$ depletion of 0.27‰ in *G. ruber* (pink) relative to the white variety corresponds to *G. ruber* (pink) having a calcification temperature that is ~1.2±0.4ºC warmer than *G. ruber* (white). Although the raw Mg/Ca values are the same for both pink and white *G. ruber*, using their respective Mg/Ca-paleotemperature equations results in the pink variety being offset by 1.8±0.8ºC warmer than the white variety. This supports the hypothesis that pink *G. ruber* is consistently calcifying in warmer waters than white *G. ruber*, either due to a more summer-weighted seasonal distribution, or a shallower depth habitat.

Chapter 5

Summary

5.1. Conclusions

The Little Ice Age and Medieval Warm Period are two of the most prominent climatic events of the past millennium, recorded in climate proxy records throughout the mid-to high latitude Northern Hemisphere. However, there are still gaps in our knowledge of the magnitude and spatial extent of these events, the low latitude oceans being an area from which there are very few proxy records. In this thesis I contribute to the understanding of sub-tropical Atlantic Ocean variability by presenting multiproxy records of sea surface temperature variability from three different sites in the Gulf of Mexico (GOM). Data from the GOM indicate a significant Little Ice Age cooling of 2ºC. This cooling is observed in the foraminiferal Mg/Ca records from three different GOM basins, in the Mg/Ca records of two different planktonic foraminifers in the same basin (pink and white *Globigerinoides ruber*), and among the SST signals recorded in an inorganic and molecular organic proxy from the same GOM basin (Mg/Ca and TEX_{86}). The similarities in the timing and magnitude of the Little Ice Age cooling among the three different GOM Basins suggests that the Mg/Ca proxy is recording a robust, reproducible regional climate signal in these basins.

Comparison of the Mg/Ca-SST record with the TEX_{86}-SST record from Pigmy Basin reveals significant similarities between the two proxy records. For instance, the timing and magnitude of Little Ice Age cooling are similar for the two proxy records.

There are also important differences between the two records, which I hypothesize result from differences in the seasonal/depth distribution of Foraminifera and marine Crenarchaeota. These offsets are exploited to make inferences about changing seasonality/mixed layer depth over the past 1,000 years. For example, the offset between TEX_{86} and Mg/Ca is minimal during the medieval Warm period, suggesting that there was reduced seasonality and/or increased mixed layer depth during that time. Maximum offset between the two records during the Little Ice Age suggests enhanced seasonality and/or a shallow mixed layer during that time.

In addition to the paleoclimate records presented in this thesis, I present a detailed study on the effect of foraminiferal test size on the different geochemical parameters commonly used for paleoenvironmental reconstruction. The change in $\delta^{13}C$, $\delta^{18}O$ and Mg/Ca over the size range from 150μm to 500μm of the pink and white variety of *G. ruber* is larger than the observed variability in each of these parameters over the past 1,000 years. There is an increase in Mg/Ca and decrease in $\delta^{18}O$ with increasing size that equates to a 0.66ºC increase in calcification temperature with 100μm increase in shell size. These data suggest that larger individuals are calcifying under warmer conditions, and may be weighted toward a warmer season or shallower depth habitat than the smaller individuals. This study emphasizes the importance of using a well-constrained size range of Foraminifera for paleoenvironmental reconstruction.

5.2. Future Research Directions

The work presented in this dissertation has provided a number of important answers regarding climate variability in the subtropical Atlantic Ocean over the past

millennium, but has also led to further questions. These additional questions generate new potential research directions that could be pursued in the future. Below is a brief outline of those potential research projects that would further develop or complement the research presented in this dissertation.

In this dissertation, I make large assumptions about the ecologies of planktonic Foraminifera and Crenarchaeota in the Gulf of Mexico. These assumptions have significant implications for the paleoclimatic interpretations, and thus it is important to determine the modern depth habitat and seasonal distribution for these proxy recorders in the Gulf of Mexico. Sediment trap and water column filtration studies in the GOM are essential to better understanding the ecology of the biogenic proxies used in paleoenvironmental reconstruction.

Globally, the TEX_{86} signal corresponds to mean annual sea surface temperatures. However, the TEX_{86} data presented in this dissertation from the Pigmy Basin are summer-weighted. Due to the delivery of large amounts of terrestrial organic matter to the Pigmy Basin via the Mississippi River, it is possible that the TEX_{86} signal is being influenced by terrestrially derived isoprenoid GDGTs. In order to determine whether or not the Pigmy Basin TEX_{86} is being biased toward warmer temperatures by terrestrially derived GDGTs, I propose to analyze the GDGT composition of surface sediments across a transect of surface sediments from the Mississippi River Delta to the Pigmy Basin on the continental slope.

The molecular compounds commonly used for paleo-environmental reconstruction (e.g. alkenones, GDGTs, fatty acids, *n*-alkanes, etc.) are contained within the fine sediment fraction (<63μm), and can have different transport mechanisms to

depositional basins than Foraminifera. In order to directly compare downcore records of sea surface variability derived from both Foraminifera and molecular fossils, it is best to have an independent chronology based on compound-specific radiocarbon dating of the molecular fraction. Molecular radiocarbon dating of the isoprenoid GDGTs used for the TEX_{86} index would verify that the TEX_{86} and Mg/Ca records in the Pigmy Basin are contemporaneous. Isolation and radiocarbon dating of terrestrially derived compounds (e.g. long-chain *n*-alkanes and fatty acids) from Gulf of Mexico sediments can provide information about residence times of terrestrial carbon on the North American continent, as well as sediment transport to marine depositional basins.

There are very few records of terrestrial climate variability from the subtropical Atlantic region. Lake Tulane, located in central Florida (27.5853ºN, 81.5034ºW), is a high sedimentation rate lake with a small catchment basin. It is an ideal setting for comparing terrestrial temperature and hydrologic variability in an environment that is closely linked to the GOM. I plan to use the TEX_{86} proxy to reconstruct lake surface temperature. Additionally, the hydrogen isotopic composition (δD) of terrestrially derived fatty acids can be used to reconstruct regional hydrologic variability.

References

Ammann, C.N., F. Joos, D.S. Schimel, B.L. Otto-Bliesner, and R.A. Tomas (2007), Solar influence on climate during the past millennium: Results from transient simulations with the NCAR Climate System Model, *PNAS*, 104(10), 3713-3718, doi:10.1073/pnas0605064103.

Anand, P., H. Elderfield, and M.H. Conte (2003), Calibration of Mg/Ca thermometry in planktonic foraminifera from a sediment trap time series, *Paleoceanography*, 18, 1050, doi: 10.1029/2002PA000846.

Bard, E., G. Raisbeck, F. Yiou, and J. Jouzel (1997), Solar modulation of cosmogenic nucide production over the last millennium: comparison between ^{14}C and ^{10}Be records, *Earth and Planetary Science Letters*, 150, 453-462.

Bard, E., G. Raisbeck, F. Yiou, and J. Jouzel (2000), Solar irradiance during the last 1200 years based on cosmogenic nuclides. *Tellus* 52B: 985-992.

Barker, S., M. Greaves, and H. Elderfield (2003), A study of cleaning procedures used for foraminiferal Mg/Ca paleothermometry, *Geo-chem. Geophys. Geosyst.*, 4, doi:10.1029/2003GC000559.

Bé, A.W.H. (1982), Biology of planktonic foraminifera, in *Foraminifera: notes for a short course*, edited by T. W. Broadhead, pp. 51-92, Department of Geological Sciences, Knoxville, Tennessee.

Bé, A.W.H., and W. H.Hamlin (1967), Ecology of Recent Planktonic Foraminifera: Part 3: Distribution in the North Atlantic during the Summer of 1962, *Micropaleontology*, *13*(1), 87-106.

Berger, W.H., J.S. Killingley, and E. Vincent (1978), Stable isotopes in deep-sea carbonates: Box core ERDC-92, west equatorial Pacific, *Oceanol. Acta*, 1, 203-216.

Berger, W.H., M.C. Bonneau, and F.L. Parker (1982), Foraminifera on the deep-sea floor: Lysocline and dissolution rate, *Oceanol. Acta*, 5, 249–258.

Black, D.E., M.A. Abahazi, R.C. Thunell, A. Kaplan, E.J. Tappa, and L.C. Peterson (2007), An 8-century tropical Atlantic SST record from the Cariaco Basin: Baseline variability, twentieth-century warming, and Atlantic hurricane frequency, *Paleoceanography*, 22, PA4204, doi:10.1029/2007PA001427.

Bond, G., W. Showers, M. Cheseby, R. Lotti, P. Almasi, P. deMenocal, P. Priore, H. Cullen, I. Hajdas, and G. Bonani (1997), A Pervasive Millenial-Scale Cycle in North Atlantic Holocene and Glacial Climates, *Science*, 278, doi:10.1126/science.278.5341.1257.

Boyle, E. A. (1983), Manganese carbonate overgrowths on foraminifera tests, *Earth Planet. Sci. Lett*., 53, 11-35.

Brassell, S.C., G. Eglinton, I.T. Marlowe, U. Pflaumann, and M. Sarnthein (1986), Molecular stratigraphy: A new tool for climatic assessment, *Nature*, 320, 129–133, doi:10.1038/320129a0.

Broecker, W.S., and T.H. Peng (1982), *Tracers in the Sea*, Lamont-Doherty Geological Observatory, Palisades, N. Y.

Broecker, W.S. (2001), Was the Medieval Warm Period Global?, *Science*, 291, 1497-1499.

Brown, S.J., and H. Elderfield (1996), Variations in Mg/Ca and Sr/Ca ratios of planktonic foraminifera caused by postdepositional dissolution: Evidence of shallow Mg-dependent dissolution, *Paleoceanography*, 11, 543–551, 1996.

Brunner, C.A. (1979), Distribution of planktonic Foraminifera in surface sediments in the Gulf of Mexico, *Micropaleontology*, 25, p.325-335.

Castañeda, I.S., E. Schefuß, J. Pätzold, J.S. Sinninghe Damsté, S. Weldeab, and S. Schouten (2010), Millennial‐scale sea surface temperature changes in the eastern Mediterranean (Nile River Delta region) over the last 27,000 years, *Paleoceanography*, 25, PA1208, doi:10.1029/2009PA001740.

Cook E.R., C. Woodhouse, C.M. Eakin, D. M. Meko, and D.W. Stahle (2004), Longterm aridity changes in the western United States, *Science*, 306, 1015–1018.

Cook, E.R., R. Seager, R.R. Heim Jr., R.S. Vose, C. Herweijer, and C. Woodhouse (2010), Megadroughts in North America: placing IPCC projections of hydroclimatic change in a long-term palaeoclimate context, *J. Quaternary Sci*., 25, 48–61, ISSN 0267-8179.

Crowley, T.J, and T. Lowery (2000), How Warm was the Medieval Warm Period?, *Ambio*, v. 29, p. 51-54.

Crowley, T.J. G. Zielinski, B. Vinther, R. Udisti, K. Kreutz, J. Cole-Dai, and E. Castellano (2008), Volcanism and the Little Ice Age, *PAGES News*, 16, 22-23.

Curry, W.B., and R.K. Matthews (1981), Equilibrium ^{18}O fractionation in small size fraction planktic foraminifera: Evidence from recent Indian Ocean sediments, *Marine Micropaleontology*, 6, 327-337.

Dekens, P.S., D.W. Lea, D.K. Pak, and H.J. Spero (2002), Core top calibration of Mg/Ca in tropical foraminifera: Refining paleotemperature estimation, *Geo-chem. Geophys. Geosyst*., v. 3, doi: 10.129/2001GC000200.

deMenocal, P., J. Ortiz, T. Guilderson, and M. Sarnthein (2000), Coherent High- and Low- Latitude Climate Variability During the Holocene Warm Period, *Science*, 288(5474), 2198-2202.

Deuser, W.G., E.H. Ross, C. Hemleben, and M. Spindler (1981), Seasonal changes in species composition, numbers, mass, size, and isotopic composition of planktonic foraminifera settling into the deep Sargasso Sea, *Palaeogeography Palaeoclimatology Palaeoecology*, 33, 103– 127.

Deuser, W.G. (1987), Seasonal variations in isotopic composition and deep-water fluxes of the tests of perennially abundant planktonic Foraminifera of the Sargasso Sea: Results from sediment-trap collections and their paleoceanographic significance, *Journal of Foraminiferal Research*, 17, 14-27.

Deuser, W.G., and E.H. Ross (1989), Seasonally abundant planktonic foraminifera of the Sargasso Sea: Succession, deep-water fluxes, isotopic compositions, and paleoceanographic implications, *Journal of Foraminiferal Research*, 19, 268–293.

Dowsett, H.J., S. Verardo, and R.Z. Poore (2003), Gulf of Mexico planktonic foraminifer transfer function GOM2: Preliminary Report, *USGS Open File Report OF 03-61*.

Eggins, S.M., A.Y. Sadekov, and P. De Deckker (2004), Modulation and daily banding of Mg/Ca in *Orbulina universa* tests by symbiont photosynthesis and respiration: A complication for seawater thermometry?, *Earth Planet. Sci. Lett*., 225, 411-419.

Eglinton, T.I., and G. Eglinton (2008), Molecular proxies for paleoclimatology, *Earth and Planetary Science Letters*, 275, 1-16, doi:10.1016/j.epsl.2008.07.012.

Elderfield, H., and G. Ganssen (2000), Past temperature and $\delta^{18}O$ of surface ocean waters inferred from foraminiferal Mg/Ca ratios, *Nature*, 405, 442–445.

Elderfield, H., M. Vautravers, and M. Cooper (2002), The relationship between shell size and Mg/Ca, Sr/Ca, $d^{18}O$ and $d^{13}C$ of species of planktonic foraminifera, *Geochemistry Geophysics Geosystems*, 3, doi: 10.1029/2001GC000194.

Elderfield, H., J. Yu, P. Anand, T. Kiefer, B. Nyland, (2006), Calibrations for benthic foraminiferal Mg/Ca paleothermometry and the carbonate ion hypothesis. *Earth Planet. Sci. Lett*., 250 (3-4), 633–649.

Emiliani, C. (1954), Depth habitats of some species of pelagic foraminifera as indicated by oxygen isotope ratios, *American Journal of Science*, 252, 149–158.

Emiliani, C. (1955), Pleistocene temperatures, *Journal of Geology*, 63, 538–578.

Englebrecht, A.C., and J.P. Sachs (2005), Determination of sediment provenance at drift sites using hydrogen isotopes and unsaturation ratios in alkenones, *Geochimica et Cosmochimica Acta*, 69, 4253-4265.

Esper, J., E.R. Cook, and F.H. Schweingruber (2002), Low-frequency signals in long tree-ring chronologies for reconstructing past temperature variability, *Science*, 295, 2250–2254, doi: 10.1126/science.1066208.

Fairbanks, R.G., P.H. Wiebe, and A.W.H. Bé (1980), Vertical distribution and isotopic composition of living planktonic Foraminifera in the western North Atlantic, *Science*, 207, 61-63.

Ferguson, J.E., G.M. Henderson, M. Kucera, and R.E.M. Rickaby (2008), Systematic change of foraminiferal Mg/Ca rations across a strong salinity gradient, *Earth Planet. Sci. Lett*., 265, doi:10.1016/j.epsl.2007.10.011.

Flannery, J.A., D.J. Hollander, J.N Richey, and B.P. Flower (2008), A 1400-Year Sedimentary Record from the Pigmy Basin, Gulf of Mexico Reveals Strong Decadal-Scale Linkages Between Solar Variability, Gulf of Mexico Moisture Balance, and Hydrologic Conditions over the North American Continent, *Eos Trans. AGU, 89*(53), Fall Meet. Suppl., Abstract PP13E-06.

Flower, B.P., D.W. Hastings, H.W. Hill, and T.M. Quinn (2004), Phasing of deglacial warming and Laurentide Ice Sheet meltwater in the Gulf of Mexico: *Geology*, 32, 597–600, doi: 10.1130/G20604.1.

Fröhlich, C. and J. Lean (2004), Solar Radiative Output and its Variability: Evidence and Mechanisms, *Astron. and Astrophys. Rev.*, 12, 273--320, doi: 10.1007/s00159-004-0024-1.

Gao, C., A. Robock, and C. Ammann (2008), Volcanic forcing of climate over the past 1500 years: An improved ice corebased index for climate models, *Journal of Geophysical Research*, 113, D23111, doi:10.1029/2008JD010239.

Gischler, E., E A. Shinn, W. Oschmann, J. Fiebig, and N.A. Buster (2008), A 1500-year Holocene Caribbean climate archive from the Blue Hole, Lighthouse Reef, Belize, *Journal of Coastal Research*, 24, 1495-1505, doi: 10.2112/07-0891.1.

Goodkin, N.F., K.A. Hughen, A.L. Cohen, and S.R. Smith (2005), Record of Little Ice Age sea surface temperatures at Bermuda using a growth-dependent calibration of coral Sr/Ca, *Paleoceanography*, 20, PA4016, doi:10.1029/2005PA001140.

Haase-Schramm, A., F. Böhm, A. Eisenhauer, W.-C. Dullo, M.M. Joachimski, B. Hansen, and J. Reitner (2003), Sr/Ca ratios and oxygen isotopes from sclerosponges: Temperature history of the Caribbean mixed later and thermocline during the Little Ice Age, *Paleoceanography*,18, doi:10.1029/2002PA000830.

Haase-Schramm, A., F. Böhm, A. Eisenhauer, D. Garbe-Schönberg, W.-C. Dullo, and J. Reitner (2005), Annual to interannual temperature variability in the Caribbean during the Maunder sunspot minimum, Paleoceanography, 20, PA4015, doi: 10.1029/2005PA001137.

Hastings, D.W., A.D. Russell, and S.R. Emerson (1998), Foraminiferal magnesium in *Globeriginoides sacculifer* as a paleotemperature proxy, *Paleoceanography*, 13, 161–169.

Hegerl, G.C., T.J. Crowley, S.K. Baum, K.-Y Kim, and W.T. Hyde (2003), Detection of volcanic, solar, and greenhouse gas signals in paleo-reconstructions of Northern Hemispheric temperature. *Geophysical Reearch Letters*, 30, 1242, doi:10.1029/2002GL016635.

Hegerl, G.C., T.J. Crowley, W.T. Hyde, and D.J. Frame (2006), Climate sensitivity constrained by temperature reconstructions over the past seven centuries, *Nature*, 440, doi:10.1038/nature04679.

Hodell, D.A., M. Brenner, J.H. Curtis, R. Medina-Gonzales, E. Ildefonso-Chan Can, A. Albornaz-Pat, and T. P. Guilderson (2005), Climate change on the Yucatan Peninsula during the Little Ice Age, *Quaternary Research*, 63, 109-121, doi:10.1016/j.yqres.2004.11.004.

E.C. Hopmans, S. Schouten, R.D. Pancost, M.J.T. van der Meer, J.S. Sinninghe Damsté (2000), Analysis of intact tetraether lipids in archaeal cell material and sediments using high performance liquid chromatography/atmospheric pressure ionization mass spectrometry, *Rapid Commun. Mass Spectrom.*, 14, 585– 589.

Hopmans, E.C., J.W.H. Weijers, E. Schefuß, L. Herfort, J.S. Sinninghe Damsté, and S. Schouten (2004), A novel proxy for terrestrial organic matter in sediments based on branched and isoprenoid tetraether lipids, *Earth and Planetary Science Letters*, 224, 107-116, doi:10.1016/j.epsl.2004.05.012.

Huang, S., H.N. Pollack, and P.Y. Shen (1997), Late Quaternary temperature change seen in world-wide continental heat flow measurements, *Geophysical Research Letters*, 24, 1947-1950.

Huguet, C., J.-H. Kim, J.S.S. Damsté, and S. Schouten (2006), Reconstruction of sea surface temperature variations in the Arabian Sea over the last 23 kyr using organic proxies (TEX_{86} and $U^{K'}_{37}$), *Paleoceanography*, 21, PA3003, doi:10.1029/2005PA001215.

IPCC (Intergovernmental Panel on Climate Change) (2001), *Climate Change 2001: The Scientific Basis.* Cambridge University Press, Cambridge, UK.

Jasper, J.P. and R.B. Gagosian (1989), Alkenone molecular stratigraphy in an oceanic environment affected by glacial freshwater events, *Paleoceanography*, 4, 603-614.

Jenkyns, H., A. Forster, S. Schouten, and J.S. Sinninghe Damste (2004), High temperatures in the Late Cretaceous Arctic Ocean, *Nature*, 432, 888-891.

Jones, P.D., M. New, D.E. Parker, S. Martin, and I.G. Rigor (1999), Surface Air Temperature and its Changes Over the Past 150 Years, *Rev. Geophys.*, 37, 173-199.

Karner M., E.F. DeLong, and D.M. Karl (2001), Archaeal dominance in the mesopelagic zone of the Pacific Ocean. *Nature*, 409, 507–510.

Keigwin, L. D. (1996), The Little Ice Age and Medieval warm period in the Sargasso Sea, *Science*, 274, 1504– 1508.

Kennett, J.P., K. Elmstrom, and N. Penrose (1985), The last deglaciation in Orca Basin, Gulf of Mexico: High-resolution planktonic foraminiferal changes, *Paleogeography Paleoclimatology Paleoecology*, 50, 189-216.

Kilbourne, K.H., T.M. Quinn, R. Webb, T. Guilderson, J. Nyberg, and A. Winter (2008), Paleoclimate proxy perspective on Caribbean climate since the year 1751: Evidence of cooler temperatures and multidecadal variability, *Paleoceanography*, 23, PA3220, doi: 10.1029/2008PA001598.

Kim, J-H., S. Schouten, E.C. Hopmans, B. Donner, and J.S. Sinninghe Damsté (2008), Global sediment core-top calibration of the TEX_{86} paleothermometer in the ocean, *Geochimica et Cosmochimica Acta*, 72, 1154–1173, doi:10.1016/j.gca.2007.12.010.

Kisakürek, B., A. Eisenhauer, F. Böhm, D. Garbe-Schönberg, and J. Erez (2008), Controls on shell Mg/Ca and Sr/Ca in cultured planktonic foraminiferan, *Globigerinoides ruber* (white), *Earth Planet. Sci. Lett.* 273**,** 260-269.

Lea, D.W., T.A. Mashiotta, and H.J. Spero (1999), Controls on magnesium and strontium uptake in planktonic foraminifera determined by live culturing, *Geochem. Cosmochim. Acta*, 63, 2369–2379.

Lea, D.W. (2003), Elemental and isotopic proxies of past ocean temperatures. In: Elderfield, H. (Ed.), *The Oceans and Marine Geochemistry*. Elsevier, New York, NY, pp. 365–390.

Levitus, S. (2003), National Oceanographic Data Center World Ocean Atlas 1994, at http://www.cdc.noaa.gov/, Clim. Data Cent., Boulder, Colo.

Lipp, J.S., Y. Morono, F. Inagaki, and K-U. Hinrichs (2008), Significant contribution of Archaea to extant biomass in marine subsurface sediments, *Nature*, 454, 991-994, doi:10.1038/nature07174.

LoDico, J.M., B.P. Flower, and T.M. Quinn (2006), Subcentennial-scale climatic and hydrologic variability in the Gulf of Mexico during the early Holocene: *Paleoceanography*, 21, PA3015, doi: 10.1029/2005PA001243.

Lund, D.C., and W.B. Curry (2004), Late Holocene variability in Florida Current surface density: Patterns and possible causes, *Paleoceanography*, 19, PA4001, doi:10.1029/2004PA001008.

Lund, D.C., and W. Curry (2006), Florida current surface temperature and salinity variability during the last millennium, *Paleoceanography*, 21, PA2009, doi: 10.1029/2005PA001218.

Lund, D.C., J. Lynch-Stieglitz, and W. Curry (2006), Gulf Stream density structure and transport during the past millennium, *Nature*, 444, doi:10.1038/nature05277.

Maash, K.A., P.A. Mayewski, E.J. Rohling, J.C. Stager, W. Kalén, L.D. Meeker, and E.A. Meyerson (2005), A 2000-year context for modern climate change, *Geogr. Ann., Ser. A, Phys. Geogr*., 87, 7-15, doi:10.1111/j.0435-3676.2005.00241.x.

Mann, M.E., R.S. Bradley, and M.K. Hughes (1998), Global-scale temperature patterns and climate forcing over the past six centuries, *Nature*, 392, 779-787.

Mann, M.E., R.S. Bradley, and M.K. Hughes (1999), Northern Hemisphere temperatures during the past millennium: Interferences, uncertainties, and limitations, *Geophysical Research Letters*, 26, 759-762.

Mann, M.E. and P.D. Jones (2003), Global surface temperatures over the past two millennia. *Geophysical Research Letters*, 30, 1820.

Marshall, J., Y. Kushnir, D.S. Battisti, P. Chang, A. Czaja, R. Dickson, J. Hurrell, M. McCartney, R. Saravanan, and M. Visbeck (2001), North Atlantic climate variability: Phenomena impacts and mechanisms, *Int. J. Climatol*., 21, 1863-1898. doi:10.1002/ioc.693.

Meeker, L.D., and P. A. Mayewski (2002), A 1400-year high-resolution record of atmospheric circulation over the North Atlantic and Asia, *Holocene*, 12, 257–266, doi:10.1191/0959683602hl542ft.

Moberg, A., D.M. Sonechkin, K. Holmgren, N.M. Datsenko, and W. Karlén (2005), Highly variable Northern Hemisphere temperatures reconstructed from low-and high-resolution proxy data, *Nature*, 433, 613–617, doi:10.1038/nature03265.

Mollenhauer G., M. Kienast, F. Lamy, H. Meggers, R.R. Schneider, J.M. Hayes, and T.I. Eglinton (2005), An evaluation of C-14 age relationships between co-occurring foraminifera, alkenones, and total organic carbon in continental margin sediments. *Paleoceanography*, 20, doi:10.1029/2004PA001103.

Mollenhauer G., M. Inthorn, T. Vogt, M. Zabel, J.S. Sinninghe Damsté, and T.I. Eglinton (2007), Aging of marine organic matter during cross-shelf lateral transport in the Benguela upwelling system revealed by compound-specific radiocarbon dating, *Geo-chem. Geophys. Geosyst.,* 8, doi:10.1029/2007GC001603.

National Research Council. Surface Temperature Reconstructions for the Last 2,000 Years (National Academy Press, 2006); available at <http://www.nap.edu/catalog.php? record_id51167>.

Newton, A., R. Thunell, and L. Stott (2006), Climate and hydrographic variability in the Indo-Pacific Warm Pool during the last millennium: *Geophysical Research Letters,* 33, L19710, doi: 10.1029/2006GL027234.

Ni, Y., G.L. Foster, T. Bailey, T. Elliott, D.N. Schmidt, P. Pearson, B. Haley, and C. Coath (2007), A core top assessment of proxies for the ocean carbonate system in surface-dwelling foraminifers, *Paleoceanography*, 22, PA3212, doi:10.1029/2006PA001337.

Nürnberg, D., J. Bijma, and C. Hemleben (1996), Assessing the reliability of magnesium in foraminiferal calcite as a proxy for water mass temperatures, *Geochimica et cosmochimica Acta*, 60, 803-814.

Nyberg, J., B.A. Malmgren, A. Kuijpers, and A. Winter (2002), A centennial-scale variability of tropical North Atlantic surface hydrography during the late Holocene, *Palaeogeography Palaeoclimatology Palaeoecology*, 183, 25–41.

Ohkouchi N., T.I. Eglinton, L.D. Keigwin, and J.M. Hayes (2002), Spatial and temporal offsets between proxy records in a sediment drift, *Science*, 298, 1224–1227.

Ohkouchi, N., L. Xu, C.M. Reddy, D. Montluçon, and T.I. Eglinton (2005), Radiocarbon dating of alkenones from marine sediments: I. Isolation Protocol, *Radiocarbon*, 47, 401-412.

Oppo, D.W., and R.G. Fairbanks (1989), Carbon isotope composition of tropical surface water during the past 22,000 years, *Paleoceanography*, 4, 333-351.

Oppo, D.W., Y. Rosenthal, and B.K. Linsley (2009), 2,000-year-long temperature and hydrology reconstructions from the Indo-Pacific warm pool, *Nature*, 460, 1113-1116, doi:10.1038/nature08233.

Overpeck, J.T., K. Hughen, D. Hardy, R. Bradley, R. Case, M. Douglas, B. Finney, K. Gajewski, G. Jacoby, A. Jennings, S. Lamoureux, A. Lasca, G. MacDonald, J. Moore, M. Retelle, S. Smith, A. Wolfe, G. Zielinski (1997), Artic environmental change of the last four centuries, *Science*, 278, 1251-1256, doi:10.1126/science.278.5341.1251.

Pelejero, C., and E. Calvo (2003), The upper end of the $U^{K'}_{37}$ temperature calibration revisited, *Geochem. Geophys. Geosyst*., 4(2)1014, doi:10.1029/2002GC000431.

Pena, L.D., E. Calvo, I. Cacho, S. Eggins, and C. Pelejero (2005), Identification and removal of Mn-Mg-rich contaminent phases on foraminiferal tests: Implications for Mg/Ca past temperature reconstructions, *Geo-chem. Geophys. Geosyst*., 6, doi:10.1029/2005GC000930.

Prahl F. G. and S.G. Wakeham (1987), Calibration of unsaturation patterns in long-chain ketone compositions for paleotemperature assessment, *Nature,* 330, 367–369.

Ravelo, C.A., and R.G. Fairbanks (1992), Reconstructing the photic zone temperature range using $\delta^{18}O$ measured on multiple species of planktonic foraminifera. *Paleoceanography*, 7, 815-832.

Ravelo, A.C., and R.G. Fairbanks (1995), Carbon isotope fractionation in multiple species of planktonic foraminifera from coretops in the tropical Atlantic, *Journal of Foraminiferal Research*, 25, 53–74.

Richey, J.N., R.Z. Poore, B.P. Flower, and T.M. Quinn (2007), 1400 yr multiproxy record of climate variability from the northern Gulf of Mexico, *Geology*, 35, 423-426, doi:10.1130/G23507A.1.

Richey, J.N., R.Z. Poore, B.P. Flower, and T.M. Quinn, and D.J. Hollander (2009), Regionally coherent Little Ice Age cooling in the Atlantic Warm Pool, *Geophys. Res.Lett.,* 36, L21703, doi:10.1029/2009GL040445.

Robock, A., (2000), Volcanic eruptions and their impact on climate, *Earth in Space*, 12, 9-10.

Rosenheim, B.E., P.K. Swart, S.R. Thurrold, P. Willenz, L. Berry, and C. Latkoczy (2004), High resolution Sr/Ca records in sclerosponges calibrated to temperature in situ, *Geology*, 32, 145– 148.

Rosenthal, Y., and E.A. Boyle (1993), Factors controlling the fluoride content of planktonic foraminifera: An evaluation of its paleoceanographic applicability, *Geochim. Cosmochim. Acta*, 57, 335–346.

Rosenthal, Y., E.A. Boyle, and N. Slowey (1997), Temperature control on the incorporation of magnesium, strontium, fluorine, and cadmium into benthic foraminiferal shells from Little Bahama Bank: Prospects for thermocline paleoceanography, *Geochem. Cosmochim. Acta*, 61, 3633–3643.

Rosenthal, Y., et al. (2004), Interlaboratory comparison study of Mg/Ca and Sr/Ca measurements in planktonic foraminifera for paleoceanographic research, *Geochem. Geophys. Geosyst*., 5, Q04D09, doi:10.1029/2003GC000650.

Russell, A.D., S. Emerson, B.K. Nelson, J. Erez, and D.W. Lea (1994), Uranium in foraminiferal calcite as a recorder of seawater uranium concentrations, *Geochim. Cosmochim. Acta*, 58, 671–681.

Russell, A., B. Hönisch, H. Spero, D. Lea (2004), Effects of seawater carbonate ion concentration and temperature on shell U, Mg, and Sr in cultured planktonic foraminifera. *Geochim. Cosmochim. Acta*, 68, 4347–4361.

Sadekov, A., S.M. Eggins, P. De Deckker, and D. Kroon (2008), Uncertainties in seawater thermometry deriving from intratest and intertest Mg/Ca variability in *Globigerinoides ruber*, *Paleoceanography*, 23, PA1215, doi:10.1029/2007PA001452.

Saenger, C., A.L. Cohen, D.W. Oppo, R.B. Halley, and J.E. Carilli (2009), Surface-temperature trends and variability in the low-latitude North Atlantic since 1552, *Nature Geoscience*, 2, 492-495, doi: 10.1038/NGEO552.

Schouten, S., E.C. Hopmans, E. Schefuß, and J.S. Sinninghe Damsté (2002), Distributional variations in marine crenarchaeotal membrane lipids: A new tool for reconstructing ancient sea water temperatures?, *Earth Planet. Sci. Lett*., 204, 265– 274.

Shah, S.R., G. Mollenhauer, N. Ohkouchi, T.I. Eglinton, and A. Pearson (2008), Origins of archaeal tetraether lipids in sediments: Insights from radiocarbon analysis, *Geochimica et cosmochimica Acta*, 72, 4577–4594, doi:10.1016/j.gca.2008.06.021.

Shindell, D.T., G. Faluvegi, R.L. Miller, G.A. Schmidt, J.E. Hansen, and S. Sun (2006), Solar and anthropogenic forcing of tropical hydrology, *Geophys. Res. Lett.*, 33, L24706, doi:10.1029/2006GL027468.

Sluijs, A., S. Schouten, T.H. Donders, P.L. Schoon, U. Röhl, G.J. Reichart, F. Sangiorgi, J.-H. Kim, J.S. Sinninghe Damsté and H. Brinkhuis (2009), Warm and wet conditions in the Arctic region during Eocene Thermal Maximum 2, *Nature Geosciences* 2, 777–780, doi:10.1038/NGEO668.

Spero, H.J., and D.W. Lea (1993), Intraspecific stable isotope variability in the planktic foraminifera Globigerinoides sacculifer: Results from laboratory experiments, *Marine Micropaleontology*, 22, 221-234.

Spero, H.J., and S.L. Parker (1985), Photosynthesis in the symbiotic planktonic foraminifer *Orbulina universa*, and its potential contribution to oceanic primary productivity, *Journal of Foraminiferal Research*, 15, p. 273-281, doi: 10.2113/gsjfr.15.4.273.

Spero, H.J., and D.F. Williams (1998), Extracting environmental information from planktonic foraminiferal $\delta^{13}C$ data, *Nature*, 375, 717–719.

Stuiver, M., P.J. Reimer, E. Bard, J.W. Beck, G.S. Burr, K.A. Hughen, B. Kromer, F. G. McCormac, J. Van Der Plicht, and M. Spurk (1998), INTCAL98 radiocarbon age calibration 24,000–0 cal BP, *Radiocarbon*, v. 40, p. 1041–1083.

Tedesco, K. A., J.W. Spear, E. Tappa, and R.Z. Poore (2009), Seasonal flux and assemblage composition of planktic foraminifera from the northern Gulf of Mexico: *U.S. Geological Survey Open-File Report 2009-1293*, 19 p.

Tedesco, K.A, and R.C. Thunell (2003), Seasonal and interannual variations in planktonic foraminiferal flux and assemblage composition in the Cariaco Basin, Venezuela, *Journal of Foraminiferal Research*, 33, 192-210.

Thunell, R., E. Tappa, C. Pride, and E. Kincaid (1999), Sea-surface temperature anomalies associated with the 1997-1998 El Nino recorded in the oxygen isotope composition of planktonic foraminifera, *Geology*, 27, 843-846.

Tierney, J.E., J.M. Russell, Y. Huang, J.S. Sinninghe Damsté, E.C. Hopmans, and A.S. Cohen (2008), Northern Hemisphere controls of tropical Southeast African climate during the past 60,000 years, *Science*, 322, 252-255.

Tolderlund, D.S., and A.W.H. Bé (1971), Seasonal distribution of Foraminifera in the western North Atlantic, *Micropaleontology*, 17, 297-329.

Trouet, V., J. Esper, N.E. Graham, A. Baker, J.D. Scourse, and D.C. Frank (2009), Persistent Positive North Atlantic Oscillation Mode Dominated the Medieval Climate Anomaly, *Science*, 324, doi: 10.1126/science.1166349.

Urey, H.C., (1947), The thermodynamic properties of isotopic substances, *Journal of the Chemical Society,* 562–581.

Wang, C., D.B. Enfield, S.-K. Lee, and C.W. Landsea (2006), Influences of the Atlantic warm pool on Western Hemisphere summer rainfall and Atlantic hurricanes, *J. Clim*., 19, 3011-3028, doi:10.1175/JCLI3770.1.

Wang, C., S.-K. Lee, and D.B. Enfield (2008a), Climate response to anomalously large and small Atlantic warm pools during the summer, *J. Clim.*, 21, 2437-2450, doi: 10.1175/2007JCLI2029.1.

Wang, C., S.-K. Lee, and D.B. Enfield (2008b), Atlantic Warm Pool acting as a link between Atlantic Multidecadal Oscillation and Atlantic tropical cyclone activity, *Geochem. Geophys. Geosyst.*, 9, Q05V03, doi:10.1029/2007GC001809.

Watanabe, T., A. Winter, and T. Oba (2001), Seasonal changes in sea surface temperature and salinity during the Little Ice Age in the Caribbean Sea deduced from Mg/Ca and $^{18}O/^{16}O$ rations in corals, *Marine Geology*, 173, 21–35, doi: 10.1016/S0025-3227(00)00166-3.

Weijers, J.W.H., S. Schouten, O.C. Spaargaren, and J.S. Sinninghe Damsté (2006), Occurrence and distribution of tetraether membrane lipids in soils: Implications for the use of the TEX_{86} proxy and the BIT index, *Org. Geochem*., 37, 1680-1693, doi:10.1016/j.orggeochem.2006.07.018.

Williams, C., B.P. Flower, D.W. Hastings, T.P. Guilderson, and A.C. Hine (2009), Meltwater and Abrupt Climate Change During the Last Deglaciation: A Gulf of Mexico Perspective, Master's thesis, University of South Florida.

Winter, A., H. Ishioroshi, T. Watanabe, T Oba, and J. Christy (2000), Caribbean Sea surface temperatures: Two-to-three degrees cooler than present during the Little Ice Age, *Geophys. Res. Lett.*, 27, 3365–3368, doi: 10.1029/2000GL011426.

Wuchter, C., S. Schouten, M.J.L. Coolen, and J.S. Sinninghe Damsté (2004), Temperature- dependent variation in the distribution of tetraether membrane lipids of marine Crenarchaeota: Implications for TEX_{86} paleothermometry, *Paleoceanography*, 19, PA4028, doi:10.1029/2004PA001041.

Wuchter, C., S. Schouten, S.G. Wakeham, and J.S. Sinninghe Damsté (2005), Temporal and spatial variation in tetraether membrane lipids of marine Crenarchaeota in particulate organic matter: Implications for TEX_{86} paleothermometry, *Paleoceanography*, 20, PA3013, doi:10.1029/2004PA001110.

Wuchter, C., S. Schouten, S.G. Wakeham, and J.S. Sinninghe Damsté (2006), Archaeal tetraether membrane lipid fluxes in the northeastern Pacific and the Arabian Sea: Implications for TEX_{86} paleothermometry, *Paleoceanography*, 21, PA4208, doi:10.1029/2006PA001279.

Žarić, S., B. Donner, G. Fischer, S. Mulitza, and G. Wefer (2005), Sensitivity of planktic foraminifera to sea surface temperature and export production as derived from sediment trap data, *Marine Micropaleontology*, *55*, 75-105.

Appendices

Appendix I: Fisk Basin (PE07-5) Data

AI.1. Fisk Basin Downcore Mg/Ca Data

Core Depth (mm)	Calendar Age (Yrs BP)	Mg/Ca (mmol/mol)	SST (ºC)
0	0.0	4.75	26.2
5	18.8	4.37	25.3
10	37.6	4.13	24.7
15	56.4	4.16	24.7
20	75.2	4.29	25.1
25	94.0	4.28	25.0
30	112.8	3.72	23.5
35	131.6	3.77	23.6
40	150.4	3.88	24.0
45	169.2	3.61	23.1
50	188.0	3.75	23.6
55	206.8	3.69	23.4
60	225.6	3.60	23.1
65	244.4	3.69	23.4
70	263.2	3.82	23.8
75	282.0	3.90	24.0
80	300.8	3.89	24.0
85	319.6	3.95	24.1
90	338.4	3.88	24.0
95	357.2	3.94	24.1
100	376.0	3.72	23.5
105	394.8	4.08	24.5
110	413.6	3.95	24.2
115	432.4	4.26	25.0
120	451.2	3.69	23.4
125	470.0	4.18	24.8
130	488.8	4.28	25.0
135	507.6	3.92	24.1
140	526.4	4.05	24.4
145	545.2	4.53	25.7
150	564.0	4.20	24.9
155	582.8	4.03	24.4
160	601.6	4.25	25.0
165	620.4	4.04	24.4
170	639.2	4.14	24.7
175	658.0	4.10	24.6
180	676.8	4.24	25.0
185	695.6	4.09	24.5
190	714.4	4.22	24.9

195	733.2	4.48	25.6
200	752.0	4.63	25.9
205	not calibrated	4.45	25.5
210	not calibrated	4.24	25.0
215	not calibrated	4.37	25.3
220	not calibrated	4.46	25.5
225	not calibrated	4.50	25.6
230	not calibrated	4.34	25.2
235	not calibrated	4.42	25.4
240	not calibrated	4.73	26.2
245	not calibrated	4.52	25.7
250	not calibrated	4.28	25.1
255	not calibrated	4.24	24.9
260	not calibrated	4.37	25.3

AI.1. Fisk Basin Downcore Mg/Ca Data. Each Mg/Ca measurement is based on 60 *G. ruber* (white) from the 250-300μm size fraction. Shaded rows represent the interval of the core for which there are large uncertainties in the age model, and therefore a calibration to calendar age was not made.

AI.2. Fisk Basin Radiocarbon Data

Sample Depth (mm)	AMS ^{14}C Date	error	1 sigma (low)	1 sigma (high)	Cal yrs BP	STDEV
0-5	-215	30	0	0	0	0
150-155	925	35	494	552	523	41
160-165	1090	30	628	676	652	34
200-205	1210	30	703	782	743	56
220-225	1675	35	1201	1276	1239	53
230-235	1610	35	1135	1230	1183	67

AI.2. Fisk Basin Radiocarbon Data. Raw radiocarbon dates were made on mixed assemblages of planktonic Foraminifera, and measured via Accelerator Mass Spectrometer at Lawrence Livermore National Laboratory AMS facility. Raw AMS ^{14}C dates are reported in the second column with instrumental ^{14}C error in the third column. Radiocarbon ages were converted to calendar years using the CALIB 5.0 program, with an assumed constant 400-year reservoir correction. 1 sigma (high and low) range is reported.

Appendix II. Garrison Basin (PE07-2) Data

AII.1. Garrison Basin Mg/Ca Data

Core Depth (mm)	Calendar Age (Yrs BP)	Mg/Ca (mmol/mol)	SST (ºC)
0	0	4.43	25.4
5	11.8	4.29	25.1
10	24.7	4.42	25.4
15	38.6	4.26	25.0
20	53.6	4.13	24.7
25	69.6	4.06	24.5
30	86.6	4.21	24.9
35	104.5	3.81	23.8
40	123.5	3.96	24.2
45	143.3	4.33	25.2
50	164.2	3.95	24.2
55	185.9	4.00	24.3
60	208.6	3.80	23.7
65	232.1	4.01	24.3
70	256.6	3.73	23.5
75	281.9	3.78	23.7
80	308.0	4.02	24.4
85	335.0	3.91	24.1
90	362.8	3.90	24.0
95	391.4	4.51	25.6
100	420.8	4.19	24.8
105	451.0	3.79	23.7
110	481.9	4.07	24.5
115	513.6	3.78	23.7
120	546.0	3.76	23.6
125	579.2	3.88	23.9
130	data not used	3.52	22.9
135	data not used	3.27	22.1
140	data not used	3.49	22.8
145	data not used	3.84	23.9
150	data not used	3.36	22.3
155	data not used	3.15	21.6
160	data not used		
165	data not used	3.66	23.33
170	data not used	3.40	22.48
175	data not used	4.13	24.64
180	data not used		
185	data not used	4.32	25.2
190	data not used	4.11	24.6
195	data not used	3.49	22.8
200	data not used	3.80	23.7
205	data not used	3.51	22.9

210	data not used	3.19	21.8
215	data not used	4.08	24.5
220	data not used	3.80	23.7
225	data not used	3.86	23.9
230	data not used	3.84	23.8
235	data not used	3.81	23.8
240	data not used	3.76	23.6
245	data not used	3.62	23.2
250	data not used	3.97	24.2
255	data not used	3.93	24.1
260	data not used	3.90	24.0
265	data not used	4.13	24.7
270	data not used	4.27	25.0
275	data not used	4.02	24.4
280	data not used	3.83	23.8
285	data not used	4.26	25.0
290	data not used	4.05	24.4
295	data not used	4.46	25.5
300	data not used	4.32	25.2
305	data not used	4.51	25.6
310	data not used	4.35	25.2
315	data not used	4.24	25.0
320	data not used	4.50	25.6
325	data not used	4.35	25.2
330	data not used	4.05	24.4
335	data not used	4.09	24.5
340	data not used	4.30	25.1
345	data not used	4.15	24.7
350	data not used	4.04	24.4
355	data not used	4.00	24.3
360	data not used	3.95	24.2
365	data not used	3.98	24.2
370	data not used	4.35	25.2
375	data not used	3.92	24.1
380	data not used	4.06	24.5
385	data not used	3.99	24.3
390	data not used	3.88	24.0
395	data not used	3.74	23.6
400	data not used	4.17	24.8
405	data not used	3.85	23.9
410	data not used	4.11	24.6
415	data not used	3.90	24.0
420	data not used	3.83	23.8
425	data not used	4.11	24.6
430	data not used	4.05	24.4

AII.1. Garrison Basin Mg/Ca Data. Each Mg/Ca measurement is based on 60 *G. ruber* (white) from the 250-300μm size fraction. Shaded rows represent data that were not used for climatic interpretation due to indications of diagenetic alteration of the foraminiferal calcite (i.e. low weight per foram and visual evidence of manganese coatings).

AII.2. Garrison Basin Radiocarbon Data

Core Depth (mm)	AMS ^{14}C age	error	1 sigma (high)	1 sigma (low)	Cal Yr BP
0-5	140	35	n/a	n/a	0
10-15	455	25	0	81	41
70-75	935	35	127	244	186
120-125	1435	45	563	645	604
200-205	2080	20	1221	1274	1248
270-275	2495	35	1610	1722	1666
340-345	3300	35	2655	2735	2695
390-395	3640	30	3002	3125	3064

AII.2. Garrison Basin Radiocarbon Data. Raw radiocarbon dates were made on mixed assemblages of planktonic Foraminifera, and measured via Accelerator Mass Spectrometer at Lawrence Livermore National Laboratory AMS facility. Raw AMS ^{14}C dates are reported in the second column with instrumental ^{14}C error in the third column. Radiocarbon ages were converted to calendar years using the CALIB 5.0 program, with an assumed constant 400-year reservoir correction. 1 sigma (high and low) range is reported**.**

Appendix III. Pigmy Basin GDGT Data

AIII.1. TEX_{86} Data for Pigmy Basin (PBBC-1F)

Core Depth (mm)	Calendar Yrs BP	TEX_{86} Index	SST (°C)	STDEV (°C)
0	0	0.70	28.6	0.59
5	12	0.69	28.1	0.26
10	25	0.70	28.5	0.88
15	37			
20	49	0.69	28.1	0.28
25	62	0.68	27.4	0.39
30	74	0.69	28.0	0.36
35	86	0.70	28.3	0.75
40	98	0.69	27.8	0.33
45	111	0.68	27.7	0.43
50	123	0.69	27.7	0.36
55	135	0.67	26.9	0.79
60	148	0.67	26.9	0.28
65	160	0.68	26.8	0.50
70	172	0.69	27.4	0.42
75	185	0.67	26.7	0.47
80	197	0.68	27.6	0.18
85	209	0.68	27.5	0.60
90	221	0.68	27.3	0.32
95	234	0.68	27.4	0.19
100	246	0.68	27.2	0.50
105	258	0.67	26.8	1.11
110	271	0.69	27.6	0.43
115	283	0.68	27.3	0.29
120	295	0.68	27.2	0.33
125	308	0.68	27.5	0.66
130	320	0.67	27.2	0.18
135	332	0.68	27.4	0.34
140	344	0.68	27.3	0.38
145	357	0.67	26.9	0.41
150	369	0.69	28.0	0.14
155	381	0.68	27.5	0.69
160	394	0.69	27.8	0.44
165	406	0.68	27.5	0.22
170	418	0.69	27.7	0.56
175	431	0.67	27.1	1.09
180	443	0.68	27.5	0.71
185	455	0.69	28.0	1.43
190	467	0.68	27.6	0.58
195	480	0.68	27.4	0.54

200	492	0.68	27.7	0.56
205	504	0.69	27.7	0.47
210	517	0.68	27.5	0.45
215	529	0.68	27.7	0.46
220	541	0.68	27.6	0.26
225	554	0.68	27.3	0.32
230	566	0.68	27.2	0.49
235	578	0.68	27.5	0.34
240	590			
245	603	0.68	27.4	0.92
250	615	0.67	27.1	0.14
255	627	0.66	26.1	0.21
260	640	0.67	26.8	0.25
265	652	0.67	27.0	0.37
270	664	0.66	26.6	0.79
275	677	0.68	27.6	0.86
280	689	0.67	26.6	0.48
285	701	0.68	27.1	0.34
290	713	0.68	27.3	0.20
295	726	0.67	27.1	0.53
300	738	0.68	27.3	0.87
305	750	0.67	27.0	0.40
310	763	0.66	26.5	0.12
315	775	0.68	27.3	0.30
320	787	0.67	26.7	0.73
325	800	0.68	27.3	1.19
330	812	0.68	27.4	0.25
335	824	0.66	26.5	0.59
340	836	0.68	27.6	1.17
345	849	0.67	26.7	0.24
350	861	0.68	27.2	0.44
355	873	0.67	27.0	0.22
360	886	0.66	26.1	0.74
365	898	0.66	26.5	0.27
370	910	0.67	26.6	0.46
375	923	0.65	26.0	0.53
380	935	0.66	26.2	0.91
385	947	0.65	25.9	0.15
390	959	0.65	25.7	0.11
395	972	0.67	27.0	0.55
400	984	0.66	26.5	0.38
405	996	0.67	27.0	0.40
410	1009	0.67	26.6	0.40
415	1021	0.68	27.5	0.35
420	1033	0.67	27.1	0.51
425	1046	0.67	27.0	0.68

430	1058	0.67	26.6	0.26
435	1070	0.67	26.8	0.15
440	1082	0.66	26.5	0.02

AII.1. TEX_{86} Index Data for Pigmy Basin (PBBC-1F). The TetraEther indeX of 86-carbon GDGTs (TEX_{86}) was calculated using the equation ([II]+[III]+[IV'])/ ([I]+[II]+[III]+[IV']) (see Figure 3.2. for compound structures). SST was calculated using $T=-1078 + 56.2*TEX_{86}$ (from Kim et al., 2008). STDEV listed in the fifth column represents the standard deviation of the SST (ºC) of six replicate injections for each sample.

AIII.2. BIT Index Data for Pigmy Basin (PBBC-1F)

Core Depth (mm)	Calendar Yrs BP	BIT Index	STDEV
0	0	0.144	0.002
5	12	0.149	0.003
10	25	0.181	0.003
15	37		
20	49	0.206	0.011
25	62	0.264	0.003
30	74	0.237	0.006
35	86	0.147	0.006
40	98	0.272	0.004
45	111	0.293	0.005
50	123	0.276	0.008
55	135	0.347	0.007
60	148	0.305	0.003
65	160	0.268	0.005
70	172	0.270	0.015
75	185	0.269	0.004
80	197	0.257	0.002
85	209	0.269	0.012
90	221	0.278	0.006
95	234	0.295	0.007
100	246	0.308	0.002
105	258	0.313	0.005
110	271	0.313	0.004
115	283	0.317	0.007
120	295	0.321	0.005
125	308	0.329	0.009
130	320	0.338	0.003
135	332	0.308	0.002
140	344	0.265	0.006
145	357	0.263	0.004
150	369	0.238	0.013
155	381	0.194	0.003

160	394	0.199	0.003
165	406	0.202	0.002
170	418	0.213	0.002
175	431	0.218	0.001
180	443	0.220	0.004
185	455	0.228	0.003
190	467	0.199	0.008
195	480	0.208	0.012
200	492	0.219	0.004
205	504	0.216	0.001
210	517	0.226	0.008
215	529	0.236	0.002
220	541	0.176	0.005
225	554	0.230	0.003
230	566	0.214	0.007
235	578	0.227	0.015
240	590		
245	603	0.202	0.004
250	615	0.217	0.008
255	627	0.245	0.009
260	640	0.243	0.002
265	652	0.227	0.007
270	664	0.287	0.001
275	677	0.345	0.008
280	689	0.298	0.010
285	701	0.211	0.007
290	713	0.178	0.003
295	726	0.155	0.002
300	738	0.167	0.003
305	750	0.215	0.004
310	763	0.251	0.005
315	775	0.237	0.000
320	787	0.229	0.020
325	800	0.212	0.003
330	812	0.230	0.008
335	824	0.255	0.011
340	836	0.255	0.006
345	849	0.338	0.016
350	861	0.368	0.029
355	873	0.266	0.007
360	886	0.256	0.008
365	898	0.269	0.011
370	910	0.262	0.008
375	923	0.306	0.008
380	935	0.324	0.010
385	947	0.288	0.011

390	959	0.271	0.006
395	972	0.239	0.001
400	984	0.160	0.007
405	996	0.146	0.004
410	1009	0.171	0.006
415	1021	0.196	0.007
420	1033	0.212	0.008
425	1046	0.212	0.006
430	1058	0.215	0.007
435	1070	0.192	0.006
440	1082	0.201	0.005

AII.2. BIT Index Data for Pigmy Basin (PBBC-1F). The branched to isoprenoid tetraether (BIT) index was calculated using the equation ([V]+[VI]+[VII])/ ([V]+[VI]+[VII]+[IV]) (see Figure 3.2. for compound structures). STDEV listed in the forth column represents the standard deviation of six replicate injections for each sample.

Appendix IV. Elemental and Isotopic Size Fraction Data

AIV.1 Size Fraction Isotope Data for *G. ruber* (white)

Size Fraction (μm)	Sediment Core-top	$\delta^{13}C$ (permille)	$\delta^{18}O$ (permille)
150-212	PBBC-1	0.32	-1.33
150-212	PBBC-1	0.39	-1.35
150-212	PBBC-1	0.26	-1.24
150-212	PE07-2	0.21	-0.93
150-212	PE07-2	0.12	-0.99
212-250	PBBC-1	0.60	-0.92
212-250	PBBC-1	0.60	-1.09
212-250	PBBC-1	0.59	-1.25
212-250	PBBC-1	0.51	-1.39
212-250	PE07-2	0.47	-1.26
212-250	PE07-2	0.55	-1.46
212-250	PE07-2	0.61	-1.15
250-300	PBBC-1	1.03	-1.30
250-300	PBBC-1	0.84	-1.53
250-300	PBBC-1	0.27	-1.42
250-300	PBBC-1	0.90	-1.62
250-300	PBBC-1	1.02	-1.05
250-300	PE07-2	1.11	-1.41
250-300	PE07-2	1.02	-1.55
250-300	PE07-2	0.72	-1.41
300-355	PBBC-1	1.12	-1.29
300-355	PBBC-1	1.30	-1.38
300-355	PBBC-1	1.19	-1.31
300-355	PBBC-1	0.98	-1.54
300-355	PBBC-1	1.31	-1.64
300-355	PE07-2	1.39	-1.27
300-355	PE07-2	1.39	-1.29
355-425	PBBC-1	1.52	-1.54
355-425	PBBC-1	1.33	-1.70
355-425	PE07-2	1.17	-1.87

Appendix III.1. Size Fraction Isotope Data for *G. ruber* (white). Raw carbon and oxygen isotopic data for *G. ruber* (white) represent measurements on separate aliquots of 60 individuals from the respective size fractions. Foraminifera were picked from two different box core core-top samples: Pigmy Basin (PBBC-1) and Garrison Basin (PE07-2).

AIV.2. Size Fraction Mg/Ca Data for *G. ruber* (white)

Size Fraction (μm)	Sediment Core-top	Mg/Ca (mmol/mol)
150-212	PBBC-1	4.30
150-212	PBBC-1	4.39
150-212	PE07-2	4.35
150-212	PE07-2	4.50
150-212	PE07-2	4.23
212-250	PBBC-1	4.64
212-250	PBBC-1	4.36
212-250	PE07-2	4.41
212-250	PE07-2	4.38
212-250	PE07-2	3.86
212-250	PE07-2	4.10
250-300	PBBC-1	4.40
250-300	PBBC-1	4.32
250-300	PBBC-1	4.56
250-300	PBBC-1	4.31
250-300	PE07-2	4.39
250-300	PE07-2	4.17
250-300	PE07-2	4.02
250-300	PE07-2	4.40
300-355	PBBC-1	4.22
300-355	PBBC-1	4.66
300-355	PBBC-1	4.28
300-355	PE07-2	4.05
300-355	PE07-2	4.30
355-425	PBBC-1	4.59
355-425	PE07-2	4.86

Appendix III.2. Size Fraction Mg/Ca Data for *G. ruber* (white). Raw Mg/Ca data for *G. ruber* (white) represent measurements on separate aliquots of 60 individuals from the respective size fractions. Foraminifera were picked from two different box core core-top samples: Pigmy Basin (PBBC-1) and Garrison Basin (PE07-2).

AIV.3. Size Fraction Isotope Data for *G. ruber* (pink)

Size Fraction (μm)	Sediment Core-top	$\delta^{13}C$ (permille)	$\delta^{18}O$ (permille)
150-212	PBBC-1	0.68	-1.35
150-212	PBBC-1	0.52	-1.46
150-212	PE07-2	0.56	-1.39
150-212	PE07-2	0.33	-1.32
212-250	PBBC-1	1.29	-1.46
212-250	PBBC-1	1.10	-1.62
212-250	PBBC-1	0.92	-1.76
212-250	PE07-2	0.97	-1.65
212-250	PE07-2	0.89	-1.51
212-250	PE07-2	1.00	-1.44
212-250	PE07-2	0.93	-1.64
250-300	PBBC-1	1.24	-1.58
250-300	PBBC-1	1.38	-1.57
250-300	PBBC-1	1.26	-1.57
250-300	PBBC-1	1.26	-1.64
250-300	PE07-2	1.21	-1.62
250-300	PE07-2	1.22	-1.40
250-300	PE07-2	1.05	-1.23
250-300	PE07-2	1.43	-1.46
250-300	PE07-2	1.29	-1.65
300-355	PBBC-1	1.79	-1.67
300-355	PBBC-1	1.43	-1.60
300-355	PBBC-1	1.65	-1.69
300-355	PE07-2	1.92	-1.59
300-355	PE07-2	1.81	-1.67
300-355	PE07-2	1.67	-1.82
300-355	PE07-2	1.61	-1.57
355-425	PBBC-1	1.79	-1.94
355-425	PBBC-1	1.60	-1.96
355-425	PBBC-1	2.23	-1.90
355-425	PBBC-1	1.92	-2.02
355-425	PE07-2	1.98	-1.98
355-425	PE07-2	1.66	-1.81
355-425	PE07-2	1.92	-1.97
355-425	PE07-2	1.85	-2.10
425-500	PBBC-1	1.87	-1.98
425-500	PBBC-1	1.79	-1.98
425-500	PBBC-1	1.81	-2.22
425-500	PE07-2	1.95	-2.00
425-500	PE07-2	2.36	-2.19
425-500	PE07-2	2.16	-2.18

Appendix III.3. Size Fraction Mg/Ca Data for *G. ruber* (pink). Raw carbon and oxygen isotopic data for *G. ruber* (pink) represent measurements on separate aliquots of 60 individuals from the respective size fractions. Foraminifera were picked from two different box core core-top samples: Pigmy Basin (PBBC-1) and Garrison Basin (PE07-2).

AIV.4. Size Fraction Data for Mg/Ca in *G. ruber* (pink)

Size Fraction (μm)	Sediment Core-top	Mg/Ca (mmol/mol)
150-212	PBBC-1	3.82
150-212	PBBC-1	3.77
150-212	PE07-2	4.01
150-212	PE07-2	4.54
150-212	PE07-2	3.85
212-250	PBBC-1	4.01
212-250	PBBC-1	4.46
212-250	PE07-2	4.22
212-250	PE07-2	4.00
212-250	PE07-2	4.24
250-300	PBBC-1	4.47
250-300	PBBC-1	4.55
250-300	PBBC-1	4.48
250-300	PBBC-1	3.96
250-300	PBBC-1	4.05
250-300	PE07-2	4.05
250-300	PE07-2	4.55
250-300	PE07-2	4.46
250-300	PE07-2	4.45
250-300	PE07-2	4.43
300-355	PBBC-1	4.11
300-355	PBBC-1	4.33
300-355	PBBC-1	4.55
300-355	PE07-2	4.55
300-355	PE07-2	4.41
300-355	PE07-2	4.49
300-355	PE07-2	4.11
355-425	PBBC-1	4.56
355-425	PBBC-1	4.50
355-425	PBBC-1	4.34
355-425	PE07-2	4.44
355-425	PE07-2	4.65
355-425	PE07-2	5.19
355-425	PE07-2	4.31
425-500	PBBC-1	5.00
425-500	PBBC-1	4.48
425-500	PBBC-1	4.88
425-500	PE07-2	4.77
425-500	PE07-2	4.61
425-500	PE07-2	5.23
>500	PE07-2	4.92

Appendix III.2. Size Fraction Mg/Ca Data for *G. ruber* (pink). Raw Mg/Ca data for *G. ruber* (pink) represent measurements on separate aliquots of 60 individuals from the respective size fractions. Foraminifera were picked from two different box core core-top samples: Pigmy Basin (PBBC-1) and Garrison Basin (PE07-2).

AIV.5. Summary of Size Fraction Data

AIII.5.a. Summary of Size Fraction Isotopic Data for *G. ruber* (pink)

Size Fraction (μm)	*n*	$\delta^{18}O$ (permille)	STDEV	$\delta^{13}C$ (permille)	STDEV
150-212	4	-1.38	0.06	0.52	0.14
212-250	7	-1.58	0.12	1.01	0.14
250-300	9	-1.52	0.14	1.26	0.11
300-355	7	-1.66	0.09	1.70	0.16
355-425	8	-1.96	0.08	1.87	0.20
425-500	6	-2.09	0.11	1.99	0.22

AIII.5.b. Summary of Size Fraction Isotopic Data for *G. ruber* (white)

Size Fraction (μm)	*n*	$\delta^{18}O$ (permille)	STDEV	$\delta^{13}C$ (permille)	STDEV
150-212	5	-1.17	0.20	0.26	0.10
212-250	7	-1.22	0.18	0.56	0.05
250-300	8	-1.41	0.18	0.86	0.27
300-355	7	-1.39	0.15	1.24	0.15
355-425	3	-1.70	0.16	1.34	0.17

AIII.5.c. Summary of Size Fraction Mg/Ca Data for *G. ruber* (pink)

Size Fraction (μm)	*n*	Mg/Ca (mmol/mol)	STDEV	SST (°C)
150-212	5	4.00	0.32	26.1
212-250	5	4.19	0.19	26.7
250-300	10	4.35	0.23	27.1
300-355	7	4.37	0.19	27.1
355-425	7	4.57	0.30	27.6
425-500	6	4.83	0.27	28.2
>500	1	4.92	n/a	28.5

AIII.5.d. Summary of Size Fraction Isotopic Data for *G. ruber* (white)

Size Fraction (μm)	*n*	Mg/Ca (mmol/mol)	STDEV	SST (°C)
150-212	5	4.36	0.10	25.2
212-250	6	4.29	0.27	25.1
250-300	8	4.32	0.16	25.2
300-355	5	4.30	0.22	25.1
355-425	2	4.73	0.19	26.2

AIII.5a-d. Summary of Size Fraction Data. These tables summarize the data in AIII.1-AIII.4, by presenting the mean values for all replicate measurements within each size fraction for *G. ruber* (pink) and *G. ruber* (white), respectively. *n* represents the number of measurements made in each size fraction, and the STDEV is the standard deviation of those *n* measurements.

About the Author

Julie N. Richey was born in Cincinnati, Ohio in 1981. She earned a B.S. Degree in Biological Sciences and a B.A. Degree in Geology from The Ohio State University in Columbus, Ohio in 2004. She was awarded a Presidential Doctoral Fellowship at the University of South Florida, where she began as a doctoral student in the College of Marine Science in 2004. She received her M.S. Degree from USF in 2007, and will complete her Ph.D in Marine Science in August, 2010. During her studies at USF, she has published 4 peer-reviewed papers, and presented her research findings at more than 10 international research conferences. She has participated in 3 research cruises to the Gulf of Mexico, Caribbean Sea and Tropical North Atlantic Ocean. She has been awarded a NOAA UCAR Global Climate Change Postdoctoral Research Fellowship, which she will carry out at the University of Washington's School of Oceanography in Seattle, WA, beginning in August 2010.